Thermal and Mechanical properties of Short Carbon Fiber dispersed Aluminum Composites

（短炭素繊維分散アルミニウム複合材料の熱物性および機械的性質）

Graduate School of Advanced Science and Engineering

Hiroshima University, Japan

Advisor: Prof. Gen Sasaki

2023 年 9 月

GUO YING

CONTENTS

List of Figures

List of Tables

Chapter 1

Background and Objective

1.1 Introduction

In recent years, the aerospace, automotive, and electronics industries have experienced rapid development on a global scale due to the continuous progress of science and technology and the breakthrough of several technical barriers[1-3]. Materials science, as the foundation for the development of various fields, has also undergone a technological transformation and innovative upgrades, particularly in the area of composite materials[4-7]. To meet the growing demand for comprehensive performance and increasingly complex applications, the development of high-performance composites has become an urgent issue[8-12].

In the field of composites, metal matrix composites have been developed and applied on a large scale in recent years because of their excellent mechanical and physical properties[13-16]. Among the many metal matrix composites, aluminum (Al) and its alloys are extensively utilized because of their low density, excellent wear resistance, good electrical and thermal conductivity, and abundant energy storage in the earth's crust[17-23]. However, the increasing complexity of application scenarios poses more challenges to the development of Al matrix composites. For instance, how to enhance the mechanical properties of composites without compromising their plastic deformation capacity, and how to improve the strength of composites while maintaining excellent thermal conductivity. As a result, the exploration of innovative design ideas has become a significant task in the development and application of Al matrix composites.

Various factors influence the performance of Al matrix composites, including the preparation method, the type and content of reinforcement, and the heat deformation parameters[24-27]. The solid-phase and liquid-phase preparation methods produce different microstructure characteristics in the metal matrix. Moreover, fiber-like and particle-like reinforcements employ different strengthening mechanisms, and the subsequent heat deformation parameters significantly impact the performance [28-30]. The interfacial structure and interfacial products are also widely studied. Studies

indicate that the interfacial structure is a crucial factor in determining the reinforcement's effectiveness. Additionally, harmful interface products, such as Al_4C_3, adversely affect composite performance[31,32]. Therefore, comprehensive investigations of the effects of reinforcement type, interfacial structure, and thermal deformation on the organization and properties of Al matrix composites are necessary.

1.2 Aluminum matrix composites

1.2.1 Concept of Aluminum matrix composites

The Al matrix composite comprises Al or its alloy as the matrix and inorganic or metal fiber, whisker, or particle as the reinforcement[33,34].

Due to the low specific strength and modulus of pure Al, it is challenging to utilize it in stressed structural parts or complex working conditions[18,21]. Adding high-strength reinforcements to pure Al comprehensively enhances composite performance. With a reasonable and scientific design, the reinforcement's excellent electrical and thermal conductivity can be fully utilized, providing Al matrix composites with good overall performance[25,33,35].

Al matrix composites with Al alloy as the matrix have higher specific strength and specific modulus. However, the complex elemental composition of Al alloys inevitably reacts with the reinforcement at the interface, resulting in complex interfacial products that exceed the performance expectations of Al matrix composites[36-40]. Therefore, interfacial reactions should be fully considered when utilizing Al alloys as the metal matrix.

1.2.2 Preparation of Aluminum matrix composites

The preparation methods of Al matrix composites can be categorized into two types: solid phase method and liquid phase method. The solid phase method includes powder metallurgy, vacuum hot pressing, and spark plasma sintering. The liquid phase method includes stir casting, pressure infiltration, spray deposition, etc.[24,29,41].

(1) Powder metallurgy method

The principle of powder metallurgy involves high-temperature sintering. In this method, as shown in Figure 1-1, metal powder is mixed with the reinforcement and injected into a mold for hot pressing. The resulting composite is then subjected to high-temperature sintering under a protective atmosphere to obtain a fixed shape[42-44].

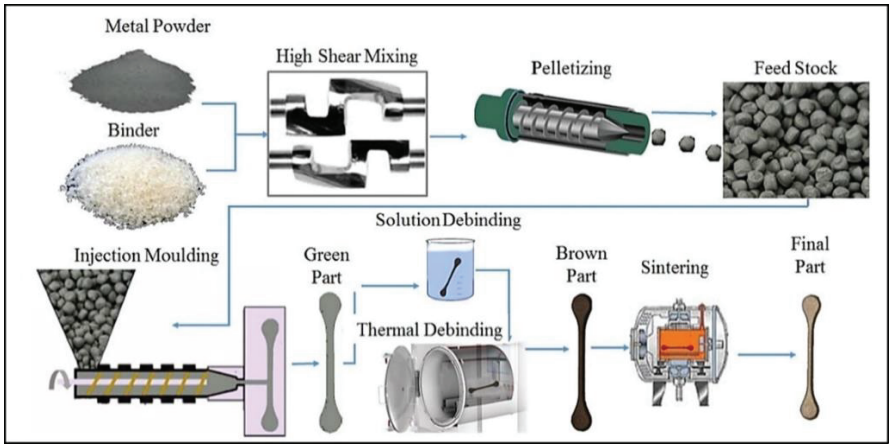

Figure 1-1 Schematic diagram of powder metallurgy method[42]

As one of the most commonly used methods in composites preparation, powder metallurgy has many advantages[43]:

1) Powder metallurgy offers strong design flexibility. The ratio of reinforcement to the metal matrix can be freely selected, and the type of reinforcement is less limited. Both fiber and particle reinforcements can be sintered using powder metallurgy.

2) Low sintering temperature, and low requirements for equipment.

3) High utilization rate of raw materials, less waste, conducive to cost control, suitable for mass production.

4) High dimensional accuracy.

At the same time, the powder metallurgy method inevitably has limitations[45]:

1) There are defects such as pores, resulting in low density, which need to be modified by subsequent thermal deformation.

2) The size of the product is limited by the limitation of mold and equipment, and it is difficult to manufacture large size samples.

(2) Vacuum hot pressing method

The vacuum hot pressing method improves the powder metallurgy process by

uniformly hot pressing the mixed powder into blocks under a load in a die and then directly sintering them[46,47]. The working schematic of the vacuum hot pressing method is shown in Figure 1-2[48]. Unlike powder metallurgy, vacuum hot pressing integrates hot pressing and sintering in one step, reducing energy consumption, and avoiding secondary heating. Furthermore, by reducing the pressure, it minimizes the gas in the powder, decreasing the porosity of the material and providing the composites with a denser texture.

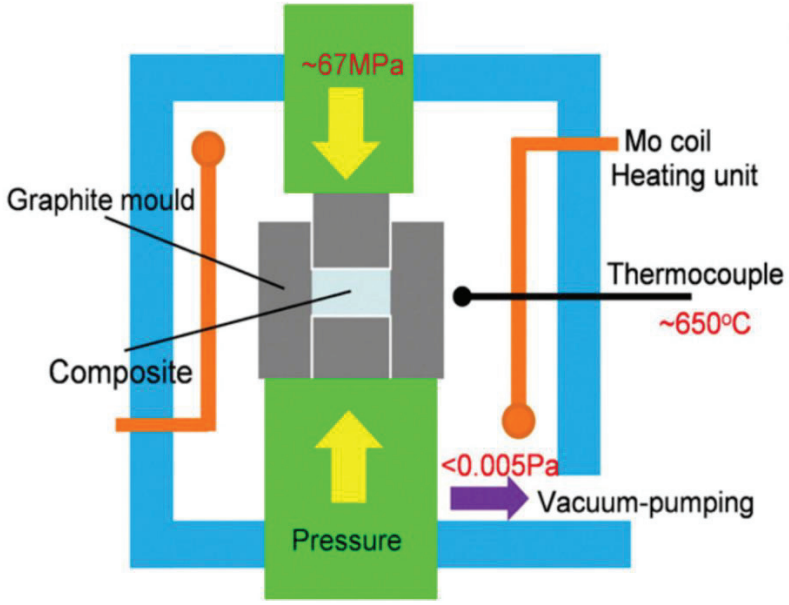

Figure 1-2 Schematic diagram of vacuum hot pressing method[48]

(3) Spark plasma sintering method

Spark plasma sintering (SPS) is a modification of the powder metallurgy method. The structure of the discharge plasma sintering equipment is shown in Figure 1-3[49]. High temperature plasma is generated between the powders by pulse discharge, and then the mold is heated to a certain temperature, and then uniaxial pressure is applied to the powder to achieve rapid densification of the powder at low temperature, which is also known as plasma activated sintering or plasma assisted sintering[50]. When the pulse current passes over the surface of the metal powder, it will scorch off the oxide film on the surface of the powder, which promotes interfacial bonding between metal and reinforcement and improves the metallurgical bonding between metal powders. Discharge plasma sintering technology combines plasma activation, resistance heating, and uniaxial hot pressing processes. It has the advantages of fast temperature rise, low

sintering temperature, short sintering time, etc., making it superior in the preparation of nanomaterials and composite materials, etc.[51,52].

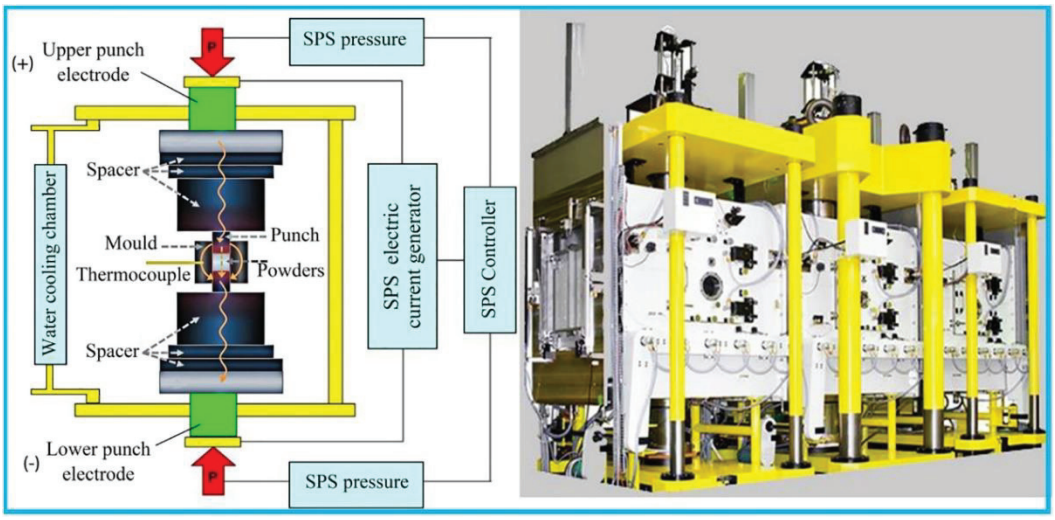

Figure 1-3 Schematic diagram of spark plasma sintering method[49]

(4) Stir casting method

The stir casting method is one of the most commonly used liquid phase methods for preparing Al matrix composites, and its specific process operation is shown in Figure 1-4[53]. After heating the metal to a liquid or semi-solid state, a set volume fraction of reinforcement is added, and the metal and reinforcement are uniformly mixed by mechanical stirring. Finally, the mixed metal liquid is cast into the mold to obtain the composite ingot. This method is widely used because of its simplicity of equipment, ease of operation, and ability to prepare composites in large quantities[54,55]. However, the poor surface wettability of the Al matrix with some reinforcements results in poor interfacial bonding. Moreover, when the density difference between the metal matrix and the reinforcement is significant, the reinforcement tends to float on the metal liquid or sink to the bottom of the metal liquid, making it challenging to be uniformly distributed in the metal matrix. Additionally, the introduction of gas into the material due to mechanical stirring also tends to create pores.

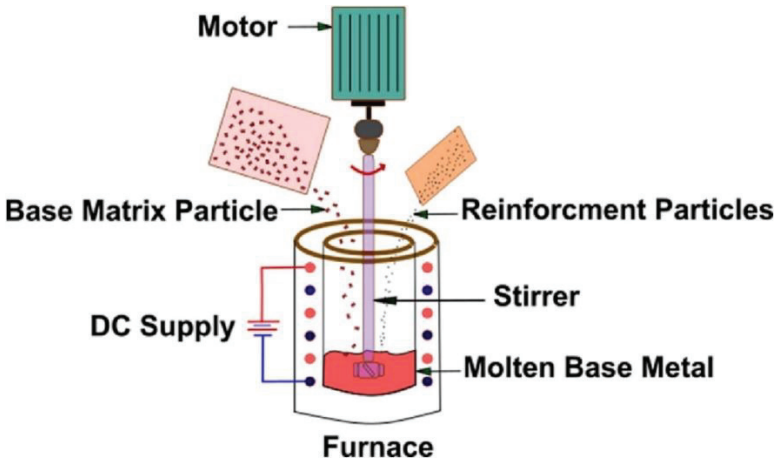

Figure 1-4 Schematic diagram of stir casting method[53]

(5) Pressure infiltration method

The preparation of Al matrix composites by pressure infiltration method involves the initial preparation of the reinforcement preform, followed by pouring the liquid metal into the mold with the reinforcement preform. The metal liquid infiltrates into the preform pores under pressure, and the composite is obtained after the metal solidifies[56,57]. The preparation method is shown in Figure 1-5[58].

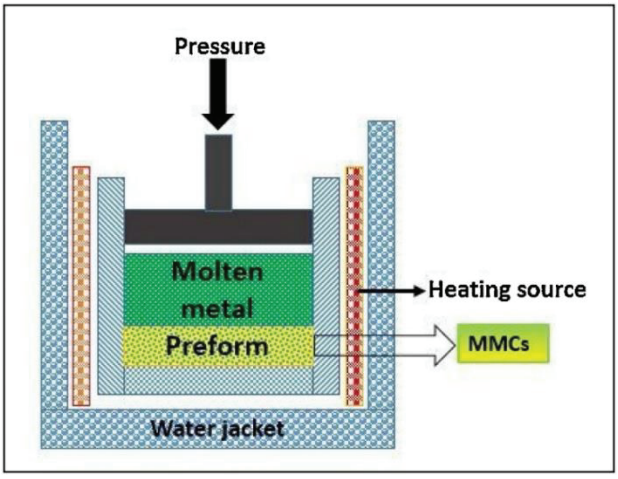

Figure 1-5 Schematic diagram of pressure infiltration method[58]

This method requires a highly precise preparation process for the reinforcement preform and has stringent requirements for molds and equipment, which need to withstand high infiltration pressure without getting damaged. However, the pressure infiltration method exhibits a high material utilization rate and involves a simple production process, enabling large-scale preparation and application.

(6) Spray deposition method

The spray deposition method utilizes a high-speed and high-pressure inert gas to impact metal liquid and reinforcement, atomize them, and finally deposit them together on the substrate for rapid solidification. The preparation process is shown in Figure 1-6[59-61]. This method allows for the preparation of composites in a very short time, and the short contact time between the reinforcement and the metal matrix prevents excessive interfacial reactions from occurring. Moreover, the atomized powder can be mixed uniformly, resulting in composites with evenly distributed reinforcement. However, the low utilization of raw materials and high preparation cost associated with the spray deposition method makes it difficult to be applied on a large scale.

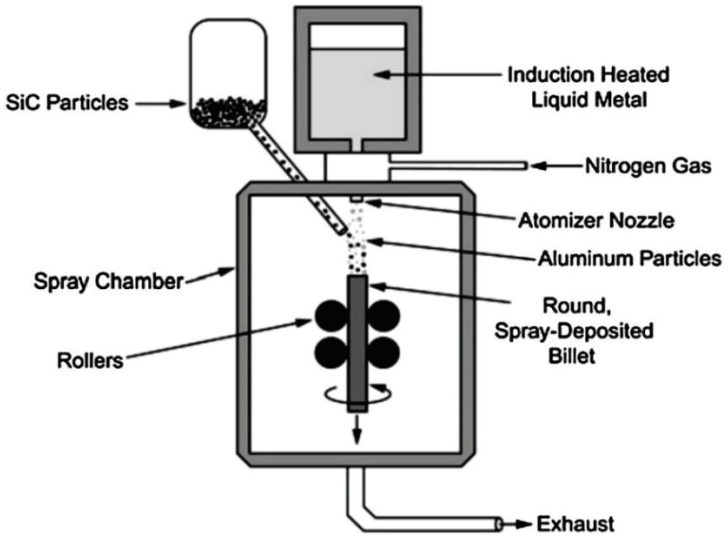

Figure 1-6 Schematic diagram of spray deposition method[59]

1.2.3 Strength mechanism of Aluminum matrix composites

In Al matrix composites, the reinforcement enhances the strength of the metal matrix mainly through the following mechanisms:

(1) Dislocation strengthening mechanism

The dislocation strengthening mechanism is one of the most common and effective strengthening mechanisms in Al matrix composites[62]. During the preparation of composites, the addition of reinforcements introduces many dislocations into the matrix, causing severe lattice distortion in the grains of the matrix metal. This distortion leads

to the generation of edge dislocations and spiral dislocations. The increase in dislocation density increases the critical kinetic value required for the opening of the slip system during plastic deformation, increasing the deformation resistance[63].

In addition, the reinforcement also plays a pinning role in the dislocations generated during the plastic deformation of composites. When the dislocation moves close to the reinforcement, it will either bend around the reinforcement or consume its energy, resulting in the dislocation forming a loop around the reinforcement[64]. Both of these effects will create a greater obstruction to the movement of subsequent dislocations, and the density of dislocations near the reinforcement will gradually increase, resulting in dislocation pinning and entanglement, eventually forming a dislocation network. The formation of dislocation networks makes the movement and annihilation of dislocations more difficult, increasing the deformation resistance of the material and thus the strength of the matrix.

(2) Grain refinement strengthening mechanism

Compared to pure metal, the preparation of composites results in a refinement of the matrix metal grain. This grain refinement is influenced by the distribution of the reinforcement, which is typically found at the grain boundaries of the matrix metal in composites. The presence of reinforcement at the grain boundaries restricts the growth of grains by limiting the movement of grain boundaries. Furthermore, the reinforcement in the composites provides a location and energy for grain nucleation during the preparation process. The increased nucleation of new grains results in smaller average grain sizes in the base metal due to smaller nucleation sizes. The energy consumed during grain nucleation competes with grain growth, resulting in smaller grain sizes.

After grain refinement, the grain boundaries in composites increase, which hinders the movement of dislocations when the material is subjected to external force or plastic deformation. This hindrance increases the energy barrier required for the movement of the slip system and dislocation, leading to an increase in the deformation resistance of the material.

(3) Load transfer enhancement mechanism

The load transfer reinforcement mechanism is widely present in various types of

composites. When external forces are applied to the composites, the load is transferred to the reinforcement through the matrix and the interface between the matrix and the reinforcement[68-70]. Particle reinforcements can withstand loads in different directions due to their greater strength and mostly equiaxed profile. Fiber and whisker-type reinforcements, on the other hand, have a certain aspect ratio and anisotropic physical properties, which limit their ability to withstand loads perpendicular to the fiber axis. In this case, short fiber reinforcements with a smaller aspect ratio and randomly distributed in the matrix have a more significant strengthening effect.

1.2.4 Development and application of Aluminum matrix composites

Since the 1950s, when Al matrix composites were first developed, decades of research and development have resulted in tremendous progress[71,72]. Initially, these composites were only used in simple structural parts such as rudders. However, with the rapid advancement of science and technology, the demand for materials with high comprehensive performance and light weight in engineering has increased, which has promoted the technical innovation and development of new materials such as Al matrix composites. Through the exploration of numerous researchers, Al matrix composites have been developed with high strength, high modulus, high thermal conductivity, and high wear resistance. These composites are now widely used in aerospace, the automotive industry, and high-end electronic devices, including aircraft fuselages, automotive engines, and heat sinks for electronic devices[73-75].

Zhu et al.[76] prepared continuous mesophase bitumen-based carbon fiber (MPCF) reinforced Al matrix composites by vacuum hot pressing and investigated the effects of process parameters and reinforcement volume fraction on the microstructure, mechanical properties, and thermal properties of the composites. The results showed that the longitudinal thermal conductivity of the composites with 20-50 vol% MPCF prepared at 650°C and held at 45 MPa for 60 min was 230.3-288.3 W/(mK), and the experimentally measured thermal conductivity values were 90% higher than those predicted based on the mixing rule. The longitudinal thermal expansion coefficient was

2.28-0.22 ppm/K and the modulus of elasticity was 147.5-324 GPa. Analysis of the interfacial structure shows that the interface between the carbon fiber and the Al matrix consists mainly of 2-5 nm thick amorphous as well as a very small amount of carbide crystals. The excellent thermal properties of this composite demonstrate its potential for thermal management material applications.

Zhai et al.[77] prepared Al matrix composites reinforced with nanodiamonds through hot-press sintering. They investigated the effect of different ball milling times on the morphology and microstructure of the composite powders of diamond and Al, as well as the effect of diamond content on the microstructure, mechanical properties, and tribological behavior of the composites. The results showed that ball milling for 15 hours produced flake Al particles with uniformly distributed nanodiamond particles. Increasing the nanodiamond content resulted in more and larger pores in the composites, leading to a decrease in relative density. The composites with 2.5% nanodiamond content exhibited the highest hardness and compressive strength, as well as the lowest coefficient of friction and wear rate.

Zhong et al.[78] used CNTs to construct interfacial transition layers for the reinforcement and toughening of carbon fiber reinforced composites. Multiscale layered CF/Al composite structures were prepared by electrophoretic deposition and pressure infiltration. The results showed that the grafting interface modified by CNTs exhibited progressive damage during the damage process, resulting in an increase in the tensile strength, fracture toughness, and fracture work of the composites by 128%, 21.6%, and 113%, respectively.

Zhang et al.[79] prepared diamond-reinforced Al matrix composites with Ti coating by gas-assisted pressure infiltration method and investigated the mechanical properties and microstructure of the composites and compared the effect of coating time on the composites. The results showed that the tensile and compressive strengths as well as the flexural strength of the composites gradually increased as the coating time increased from 15 to 180 min at 850 °C.

Mohammed et al.[80] fabricated carbon nanotube (CNT)-reinforced bimodal grain Al-Cu-Mg nanocomposites by two-step ball milling, powder metallurgy, and extrusion.

The results show that excellent strength-ductility synergy is achieved due to the presence of both ultra-fine grains (UFG) and coarse grains (CG). The monodisperse CNT and good CNT/Al interfacial bonding in UFG contribute to significantly improving the strength of the nanocomposites. The shearing effect causes the CNT to break into nanoscale fragments during the ball milling process, which induces the Orowan strengthening effect. In addition, the dislocation strengthening mechanism caused by load transfer and thermal mismatch also plays a strengthening role.

Zhu et al.[81] prepared nano-SiC particles (SiCnp) reinforced 6082 Al matrix composites by a combination of extrusion casting and stir casting and investigated the effects of SiCnp and the extrusion casting process on the microstructure and mechanical properties of the material. The results showed that stir casting resulted in a uniform distribution of SiCnp in the metal matrix. the microstructure of 6082 Al alloy was significantly improved, and the grain refinement was up to 30.55% compared with that of 6082 Al alloy without SiCnp addition. The ultimate tensile strength, yield strength, and elongation of SiCnp/Al6082 Al matrix composites were improved by 8.92%, 12.16%, and 12.60%, respectively, compared with 6082 Al alloy. After extrusion casting, the denseness of the SiCnp/Al6082 composites was significantly improved and the grains of the composites were further refined.

Zhang et al.[82] prepared graphene-reinforced Al matrix composites by friction stir processing (FSP) and discussed the effect of the preparation process on the material organization and properties. The results show that the addition of graphene leads to grain refinement and structural changes in the stirred region during the FSP process. In addition, the mechanical properties, electrical conductivity, thermal conductivity, tribological properties, and corrosion resistance of the composites are significantly affected by the graphene content and the evolution of various microstructures caused by the addition of graphene. The graphene addition method, reinforcement-matrix bonding, FSP parameters, number of channels, and path patterns are key process conditions that determine the microstructure and properties of the composites.

Akinwamide et al.[83] investigated the microstructure and mechanical properties of

discharge plasma sintered Al matrix composites with titanium-iron (TiFe) and silicon carbide (SiC) reinforcements. High-energy ball milling technique was used to effectively disperse SiC and TiFe reinforcing particles into the Al matrix, and the hybrid powder was compacted using discharge plasma sintering. The microstructural characteristics and mechanical properties of the sintered composites were investigated. The results show that the reinforcing particles are uniformly dispersed in the Al matrix due to the grinding process. In addition, the microstructural features of all sintered composites were enhanced. Higher hardness and elastic modulus were obtained in the composites reinforced with 2% SiC + 2% TiFe particles.

1.3 Reinforcement of Aluminum matrix composites

The type, size, and physical properties of reinforcements have a direct impact on the organization and properties of Al matrix composites. Therefore, in the design and preparation of these composites, it is crucial to choose the appropriate reinforcement according to the desired properties[27]. Therefore, it is necessary to evaluate the potential effects of various types of reinforcements on the properties of composites. Currently, carbon fiber, carbon nanofiber, and various ceramic particles are the most commonly used reinforcements in research on Al matrix composites[33].

1.3.1 Carbon fiber

Carbon fiber is a high-strength, high-modulus fiber with a carbon content of more than 90% and a diameter of a micron, which combines the high electrical and thermal conductivity of carbon with the softness of fiber materials[84]. Due to its excellent mechanical properties, carbon fiber is considered to be one of the most desirable reinforcements for Al matrix composites[85,86]. Carbon fiber is around 20 times stronger than iron but has a lower density. Among all fibrous materials, carbon fiber has the highest specific strength and modulus. Its physical properties are also exceptional, with high electrical and thermal conductivity, good wear and corrosion resistance, low coefficient of thermal expansion, and excellent electromagnetic shielding performance.

Furthermore, carbon fiber is the only material that can maintain its strength in environments exceeding 2000℃, which is crucial for the application of composite materials in ultra-high-temperature conditions[87].

Composites made of carbon fiber as reinforcement are widely used in the aerospace and automotive industries as well as in sports equipment. For example, a significant portion of metal parts of aircraft fuselages and landing gears have been replaced by carbon fiber reinforced composites. Car engines, heat sinks, and bodies are also heavily used with high strength, low density carbon fiber reinforced composites, which not only greatly reduce the weight of the body, but also improve the overall performance. In addition, there are also a lot of carbon fiber applications in sporting goods such as fishing rods, racquets, and racing frames, to pursue weight reduction and performance improvement[88,89]. Carbon fiber reinforced composites have also been used in the construction industry for strengthening and repairing concrete structures, due to their high strength and corrosion resistance. With the continuous development and improvement of carbon fiber technology, the application of carbon fiber reinforced composites in various fields is expected to continue to expand and promote the development of related industries.

Carbon fibers can be classified into two types: long fibers and short fibers, based on their lengths. Long fibers have lengths in the range of 10-15mm, while short fibers have lengths in the range of 0.2-1mm. Due to their multi-walled tubular structure, carbon fibers have different structures in the length and diameter directions, resulting in their anisotropic nature with high axial strength and low radial strength. As fiber-like reinforcements mainly reinforce the matrix through the load transfer mechanism, the anisotropy of carbon fiber strength affects the strength of composites with long fibers as reinforcements in different directions, depending on the fiber arrangement method. Thus, long fiber-reinforced composites are mostly utilized in workpieces subjected to loads in specific directions. Short fibers are randomly distributed after being added to the matrix as reinforcements due to their small aspect ratio. This makes the composites less significant in terms of strength orientation.

1.3.2 Carbon nanofiber

Carbon nanofiber is a kind of carbon fiber, usually at the nanometer level in diameter, which has become a hot carbon based reinforcement in recent years due to its ultra-high strength and excellent thermal conductivity[90]. Al matrix composites using carbon nanotubes as reinforcements have a wide range of applications, such as in precision thermal management devices, turbine blades, and wear-resistant cylinder blocks[91]. However, carbon nanofibers are prone to agglomeration due to their fine diameter and relatively large length-diameter characteristics. Therefore, it becomes difficult to make the carbon nanofibers uniformly dispersed in the Al matrix, and the volume fraction of carbon nanofibers is usually controlled and subjected to high-energy ball milling to promote uniform dispersion.

CNTs and vapor-phase-grown carbon nanofibers (VGCNFs) are common among carbon nanofibers[92]. Due to the high preparation cost of CNTs, it is difficult to carry out large-scale preparation applications. Therefore, VGCNFs with lower preparation costs have attracted wide attention.

1.3.3 Particles

Ceramic particles are widely used to strengthen Al matrix composites because of their high specific strength and modulus. Commonly used ceramic particles mainly include silicon carbide (SiC), alumina (Al_2O_3), silicon dioxide (SiO_2), titanium carbide (TiC), boron carbide (B_4C), and aluminum nitride (AlN), etc.[93-95].

Ceramic particles used for reinforcement are typically equiaxed or have a relatively small length and diameter to facilitate uniform distribution in the metal matrix and reduce the likelihood of agglomeration. These particles enhance the deformation resistance of Al matrix composites by refining the grain size of the base metal and impeding the movement of grain boundaries and dislocations. The reinforcing effect of the particles is primarily achieved through loading at the interface with the substrate. While higher particle hardness contributes to increased composite strength, the interfacial bonding between the particles and the metal matrix also impacts the material

properties. Excessive interfaces can negatively impact composite plasticity.

The sizes of ceramic particles currently used for reinforcement are mainly in the micron and nanoscale[96]. Uniformly distributed micron-sized particles in the metal matrix at an appropriate volume fraction have a positive impact on material properties and result in fewer interfaces. Nanoscale particles mainly enhance material strength through dispersion strengthening, but agglomeration and interfacial issues due to small size must be addressed.

1.4 Hot rolling of Aluminum matrix composites

Whether it is solid phase preparation or liquid phase preparation, the composites is inevitably prepared with defects such as high porosity and poor metallurgical bonding, which can negatively affect the organization and properties of the composite material and thus affect its application. Therefore, composite materials are usually prepared by hot rolling, hot extrusion, hot compression, and hot stretching processes for secondary processing[97-101].

Thermal deformation not only gives the composites a certain shape and size but also enhances the overall performance of the material. This is because high temperature not only improves the plastic deformation ability of the material but also improves the microstructure of the material and gives it excellent mechanical properties. However, the processing properties of the material during thermal deformation have a large impact on the production yield and product performance. For example, the relationship between stress and strain affects the filling of the material in the mold and the load required for forming. Combined with the tissue evolution can realize the reasonable selection of deformation process parameters, to achieve the synergistic control of product shape and performance[101-106]. Therefore, the study of thermal processing properties is of great importance for the processing applications and performance control of materials.

Due to the addition of reinforcements, the heat deformation behavior of Al matrix composites is more complex than that of pure Al and Al alloys. For example, during

thermal deformation, the reinforcement enhances the deformation resistance of the material through the dislocation strengthening mechanism and load transfer mechanism, which increases the rheological stress value of the material. The hindering effect of the reinforcement on the dislocation motion leads to more energy accumulation inside the material, increasing the driving force of dynamic recrystallization and promoting the occurrence of dynamic recrystallization. The effect of reinforcements on the heat deformation properties of aluminum matrix composites is a major concern of researchers[107,108].

Xu et al.[109] prepared 6061 Al matrix composites coated with SnO_2 of various thicknesses in $Al_{18}B_4O_{33}$ whiskers and carried out a hot rolling study. The mechanical properties and microstructure of Al matrix composites after hot rolling were investigated. The results show that the modification of whiskers with SnO_2 has a positive effect on the thermal deformation properties of the materials. However, the too thick coating will not only not give the material a better structure, but also cause interface failure such as hot cracking cracks, thus reducing the mechanical properties of the composites. After investigation, the mass ratio of SnO_2 to whisker is 1:40, which can give the material excellent mechanical properties.

Mokdad et al.[110] investigated the high temperature rheological behavior of CNTs/Al and showed that CNTs/Al have a higher resistance to high temperature deformation than the matrix material. The addition of CNTs increased the plastic deformation activation energy of the material from 274.5 kJ/mol to 322.3 kJ/mol, which significantly improved the high-temperature mechanical properties.

Wu et al.[111] prepared pure Al, 0.5 wt%, and 1.0 wt% nanodiamond-reinforced Al matrix composites by powder metallurgy and explored the thermal deformation properties of Al matrix composites and the effect of reinforcing particles on the microstructure evolution and properties of the material by hot extrusion. The microstructure of the material was characterized by electron backscatter diffraction(EBSD) and transmission electron microscopy, and the results indicated that the average grain size of the nanodiamond-reinforced Al matrix composites decreased rapidly after entering the extrusion deformation zone. The microstructures in simple

shear, tensile pure shear, and compressive pure shear deformation modes differ greatly. With the increase of plastic strain, the dispersed nanodiamond particles effectively promote grain refinement and improve the dislocation driving force. Besides, the mechanical test results showed that the hardness of 0.5 wt% and 1.0 wt% nanodiamond-reinforced Al matrix composites were 1.9 and 2.1 times that of pure Al, respectively, and the tensile strength of the composites were up to 205 MPa and elongation was 18%, which were 115% and 91% of that of pure Al, respectively.

Wang et al.[112] investigated the thermal deformation properties of Al matrix composites (CNTs/Al) reinforced by CNT with different contents at different loading rates and temperatures. The strengthening capacity of CNTs/Al was found to decrease with the increase in temperature and the decrease in loading rate. However, microstructure characterization shows that CNTS plays a crucial role in hindering dislocation motion and stabilizing the microstructure, so the strength of the composite increases at temperatures up to 603K regardless of loading rates. In addition, CNTs/Al showed higher strain rate sensitivity and lower activation volume than pure Al at all test temperatures.

Wu et al.[113] prepared short carbon fiber reinforced AA7075 composites by powder metallurgy extrusion. The mechanical behavior of Al matrix composites induced by reinforcement content and temperature parameters was investigated. The experimental results showed that the arrangement of carbon fibers changed after hot extrusion. High temperature tensile tests were performed on composites with different reinforcement contents to investigate the heat deformation properties. The results showed that the 8 vol% and 12 vol% carbon fiber reinforced composites have high yield strength, which is similar to that of AA7075 Al alloy at 100°C. Composites containing 12 vol% short carbon fiber have hardness up to 200 HV. The increase of high temperature strength of composites depends on the load transfer mechanism and the contribution of residual thermal stress.

1.5 Interface of Aluminum matrix composites

During the preparation of Al matrix composites, the addition of reinforcement will introduce many interfaces into the matrix. The degree of interfacial bonding, interfacial structure, and interfacial products all have important effects on the overall properties of composites[36]. Good interface bonding is not only conducive to the load transfer mechanism but also conducive to the transfer of heat and current in the composites, giving the composites well electrical and thermal conductivity. However, poor interfacial bonding can have a negative impact on the performance of the composites[37,40].

If the interfacial bonding strength is too low, it is difficult for the interface to bear the load during the deformation of the composites, and it is easy to fail due to cracking, which will cause the destruction of the composites. If the interfacial strength is too high, it indicates a serious interfacial reaction between the reinforcement and the matrix. The atomic diffusion in this process leads to the destruction of the structure of the reinforcement and a decrease in strength, which in turn makes it difficult to withstand the load, resulting in a decrease in the performance of the composites. In addition, the generation of harmful interfacial products, such as Al_4C_3 and other brittle phases, can lead to brittle fracture of the interface, which also increases the obstruction of electrical and thermal conductivity[31,32]. Therefore, interface research is an important issue in the field of Al matrix composites.

Due to the density difference and structural difference between some of the reinforcement and the Al matrix, it is difficult to produce a tight interfacial bond due to the poor wettability between the base metal and the reinforcement. The interface that only relies on molecular force bonding can hardly play the role of load transfer, and the strengthening effect on the metal matrix is very limited. To solve the problems of poor wettability, excessive interfacial reaction, and generation of harmful interfacial products between the reinforcement and the metal matrix, interfacial modification is usually used to improve the bonding of the reinforcement and the matrix. Commonly used interfacial modifications include copper and nickel coating on the reinforcement

and grafting of nanofibers on the reinforcement[37,39].

Zhu et al.[114] prepared Al_2O_3 coatings on the surface of continuous carbon fibers using the sol-gel method. The effects of immersion time, heat treatment temperature, and immersion-drying cycle on the surface morphology and mechanical properties of the coated carbon fibers were investigated. The Al_2O_3-coated carbon fiber-reinforced Al matrix composites were also prepared by pressure infiltration technique. The microstructure and mechanical properties of the composites were investigated, and the effect of the thickness of the carbon fiber coating was analyzed. The results show that the Al_2O_3 coating can improve the mechanical properties of the composites by controlling the interfacial reaction between the carbon fiber and the Al matrix. However, as the coating thickness increases, the diffusion of carbon in Al is hindered and the interfacial bond strength decreases. Therefore, the best mechanical properties of Al matrix composites can be given at a coating thickness of 100 nm.

Gao et al.[115] prepared nickel-cobalt-phosphorus coating (Ni-Co-P) by chemical plating on the surface of carbon fibers. And the carbon fiber-reinforced 7075 Al matrix composites before and after the modification of Ni-Co-P coating was prepared by vacuum hot press sintering. The reactions of interfacial elements and their effects on the mechanical properties of Al matrix composites were investigated. The results show that the Ni-Co-P coating on carbon fibers can inhibit the formation of harmful products Al_4C_3 and form Al-Co-Ni intermetallic compounds around carbon fibers, which significantly improve the interfacial bonding state of C and Al and give the composites good mechanical properties.

Zhang et al.[116] prepared a SiC transition layer between Al and CNT by careful structural design and process parameter control to enhance the composite strengthening effect. The effects of synthesizing SiC nano-transition layers of controlled thickness at the CNTs/Al interface on the microstructure, interfacial behavior, and overall properties of CNTs-SiC reinforced Al matrix composites were investigated. The results show that the wettability and interfacial bonding between CNTs and the Al matrix is improved due to the stronger covalent bonding of the SiC transition layer. The SiC transition layer

essentially inhibits the formation of the interfacial product Al_4C_3 by wrapping the CNT to keep it free from exposure. In addition, under the condition of good interfacial bonding during loading, thicker SiC transition layer consumes more energy during stripping and fracture, resulting in stronger fracture resistance of the composites.

To explore the relationship between interfacial structure and material properties, Zhu et al.[117] manufactured uncoated, W-coated, and WC-coated diamond-reinforced Al matrix composites through gas-assisted pressure penetration technology. The influence mechanism of interfacial products Al_4C_3 and Al_5W on the thermal conductivity of composites was also investigated. The results show that the W and WC coatings inhibit the formation of Al_4C_3 in the composite by forming Al_5W, reducing the size of Al_4C_3 by 70% and 94% compared with uncoated diamond/Al composites. The decrease of Al_4C_3 content and size improves the thermal conductivity of the composites, while Al_5W not only enhances the interfacial binding but also brings about additional phonon scattering. The introduction of W coating contributes to the high thermal conductivity, flexural strength, and high-performance stability of diamond/Al composites, indicating that it has great application potential in the field of electronic packaging and thermal management.

1.6 Objective of this thesis

Numerous studies have demonstrated that SPS technology has a series of advantages in the preparation of Al matrix composites, such as lower sintering temperature and sintering pressure, giving good density, and promoting the bonding of the reinforcement to the matrix. As the application of Al matrix composites in the field of electronic devices and engines is gradually increasing, the thermal conductivity of the material is also increasingly required. Therefore, the preparation of Al matrix composites with excellent thermal properties has become an urgent need. Carbon-based reinforcements such as carbon fibers have excellent thermal properties, and the combination of carbon-based reinforcements with an Al matrix can impart desirable thermal properties to the composite. However, the interfacial structure and interfacial

products are also major factors in determining the thermal properties of composites, so it is critical to find a suitable way to improve the wettability of the reinforcement and the Al matrix to enhance the interfacial bonding.

While paying attention to the thermal properties of composites, it is also necessary to pay attention to the mechanical properties of the materials. The addition of reinforcements inevitably introduces more interfaces into the Al matrix while cutting the integrity of the Al matrix, which in turn has a negative impact on the plasticity of the material. Therefore, how to safeguard the thermal properties and strength of Al matrix composites while enhancing the plastic deformation capacity has also become an urgent problem.

To solve the above problems, in this study, pure Al was used as the matrix, and copper-coated carbon fibers and uncoated carbon fibers were selected as the reinforcement for the preparation of composites by SPS, and the effects of copper coating on the microstructure, mechanical properties and thermal properties of Al matrix composites were analyzed. To investigate the mechanism of the influence of reinforcement diameter on the composites, short carbon fibers, and carbon nanofibers were used as reinforcements for comparison. And the design of gradient structured Al matrix composites was used to enhance the strength and plasticity of the composites. The microstructure analysis of the composites was performed using electron backscatter diffraction (EBSD), scanning electron microscopy (SEM), and transmission electron microscopy (TEM). The mechanical properties of the composites were analyzed using microhardness, nano-hardness, and room temperature tensile equipment. The thermal conductivity of the composites was also measured and analyzed.

In this study, the mechanisms of copper coating, hot rolling, reinforcement diameter, and gradient structure design on the microstructure and mechanical properties of the composites were investigated in depth, revealing the contribution of each reinforcement to the strengthening mechanism, providing a theoretical reference for the application and development of Al matrix composites.

1.7 Outline of this thesis

Chapter 1 Background and Objective

This chapter introduced the preparation methods, reinforcement mechanisms, and the current development status of Al matrix composites. The factors that determine the performance of Al matrix composites, such as the type of reinforcement, the size, and the interfacial structure of the reinforcement, are investigated and analyzed. And the research objectives of this study are refined.

Chapter 2 Effect of copper coating on interfacial properties, interfacial thermal resistance, microstructure evolution and mechanical properties of aluminum matrix composites

In this chapter, uncoated and copper-coated short carbon fiber reinforced aluminum matrix composites were prepared by spark plasma sintering. The arrangement of the short carbon fibers was changed by hot rolling. The effects of copper coating and carbon fiber arrangement on the microstructure, interfacial structure, thermal conductivity, and mechanical properties of aluminum matrix composites were investigated. The influence of the copper coating on the interfacial reaction and metallurgical bonding of the composites was revealed, the mechanism of carbon fiber arrangement on thermal conductivity was clarified, and the evolution of microstructure during the SPS and hot rolling process and its influence on properties were investigated in depth.

Chapter 3 Effect of short carbon fiber and nano carbon fiber as reinforcement on microstructure and properties of hot-rolled aluminum matrix composites

In this chapter, short carbon fiber (SCF) and VGCNF reinforced Al matrix composites were prepared by spark plasma sintering (SPS). The effects of different reinforcements on the microstructure evolution and properties of the hot-rolled

composites were investigated. The mechanism of the effect of different diameter reinforcements on the microstructure and mechanical properties was revealed.

Chapter 4 Microstructure evolution, property analysis, and interface study of 3%CF-3%SiC-10%SiC functional gradient aluminum matrix composites

To overcome the limitations of the low strength and plasticity in the application of aluminum (Al)-based composites, a functional gradient Al matrix composites of 3 vol.% carbon fiber (CF)-3 vol.% SiC-10 vol.% SiC, with excellent comprehensive performance, was prepared by spark plasma sintering (SPS) technology. The microstructure of the layers and interlayer interfaces of the functional gradient composites (FGC) was analyzed in depth, and the mechanical properties and thermal conductivity were investigated.

Chapter 5 Conclusions

The results from the studies mentioned above are summarized in this chapter.

1.8 References

[1]. JJ Sun, W Liu, XX Lv, J Jiao. Characterization of BN interface and its effect on the mechanical behavior of SiC_f/SiC composites[J]. Vacuum. 2023, 211:111918.

[2]. XM Xu, XG Luan, JH Zhang, XX Cao, DL Zhao et al. Significant improvement of ultra-high temperature oxidation resistance of C/SiC composites upon matrix modification by SiHfBCN ceramics[J]. Composites Part B. 2023, 253:110553.

[3]. X You, QQ Zhang, JS Yang, SM Dong. Review on 3D-printed graphene-reinforced composites for structural applications[J]. Composites Part A. 2023, 167:107420.

[4]. ZJ Ye, ZH Su, KL Zhao, XL Wang, WX Cao et al. Preparation of high thermal conductivity shaped diamond/copper composites by isostatic pressing[J]. Materials Letters. 2023, 336:133894.

[5]. G Wang, YM Zhang, BK Zou, Y Liu, SQ Zheng et al. Enhanced plasticity due to melt pool flow induced uniform dispersion of reinforcing particles in additively manufactured metallic composite[J]. International Journal of Plasticity. 2023, 164:103591.

[6]. XW Guo, S Lin, FH Dai. A metal hybrid bistable composite tube for multifunctional and reconfigurable antenna[J]. Composites Science and Technology. 2023, 233:109887.

[7]. Y Li, Y Xiao, L Yu, K Ji, DS Li. A review on the tooling technologies for composites manufacturing of aerospace structures: materials, structures and processes[J]. Composites Part A. 2022, 154:106762.

[8]. ZC Lin, YS Su, CH Qiu, JY Yang, XS Chai et al. Configuration effect and mechanical behavior of particle reinforced aluminum matrix composites[J]. Scripta Materialia. 2023, 224:115135.

[9]. DP Mohanty, BJ Arnold, S Baruah, S Chandrasekar, JB Mann. A new class of high performance metal-fiber thermoplastic composites for additive manufacturing[J]. Composites Part A. 2023, 169:107519.

[10]. YQ Fu, YL Zhang, H Chen, LY Han, XM Yin et al. Ultra-high temperature performance of carbon fiber composite reinforced by H_fC nanowires: A promising lightweight composites for aerospace engineering[J]. Composites Part B. 2023, 250:

110453.

[11]. S Olhan, V Khatkar, BK Behera. Novel high-performance textile fibre-reinforced aluminum matrix structural composites fabricated by FSP[J]. Materials Science & Engineering B. 2023, 289:116265.

[12]. XL Wu, YJ Liao, L Yao, YF Zha, RJ Li et al. A non-percolative rGO/XLPE composite with high electrothermal performance at high voltage and effective de/anti-icing for transmission-lines[J]. Composites Science and Technology. 2022, 230:109772.

[13]. SM Khazaal, NSM Nimer, S Szabolcs, ISA Ansar, HJ Abdulsamad. Study of manufacturing and material properties of the hybrid composites with metal matrix as tool materials[J]. Results in Engineering. 2022, 16: 100647.

[14]. M Chinababu, EB Rao, K Sivaprasad. Fabrication, microstructure, and mechanical properties of Al-based metal matrix-TiB_2-HEA hybrid composite[J]. Journal of Alloys and Compounds. 2023, 947:169700.

[15]. M Ostolaza, JI Arrizubieta, A Queguineur, K Valtonen, A Lamikiz, IF Ituarte. Influence of process parameters on the particle-matrix interaction of WC-Co metal matrix composites produced by laser-directed energy deposition[J]. Materials & Design. 2022, 223:111172.

[16]. J Huang, WG Li, Y He, Y Li, XY Zhang et al. Temperature dependent ultimate tensile strength model for short fiber reinforced metal matrix composites[J]. Composite Structures. 2021, 267:113890.

[17]. BZ Wang, ZY Zhang, GC Xu, XL Zeng, WT Hu et al. Wrought and cast aluminum flows in China in the context of electric vehicle diffusion and automotive lightweighting[J]. Resources, Conservation & Recycling. 2023, 191:106877.

[18]. JV Christy, AHI Mourad, MM Sherif, B Shivamurthy. Review of recent trends in friction stir welding process of aluminum alloys and aluminum metal matrix composites[J]. Transactions of Nonferrous Metals Society of China. 2021, 31:3281-3309.

[19]. SL Quaireau, K Colas, B Kapusta, B Verhaeghe, M Loyer-Prost et al. Impact of ion and neutron irradiation on the corrosion of the 6061-T6 aluminium alloy[J]. Journal

of Nuclear Materials. 2021, 553:153051.

[20]. TY Xu, SW Zhou, H Wu, XQ Ma, HL Liu, M Li. Dissimilar joining of low-carbon steel to aluminum alloy with TiC particles added in a zero-gap lap joint configuration by laser welding[J]. Materials Characterization. 2021, 182:111574.

[21]. B Gungor, E Kaluc, E Taban, A Sik. Mechanical, fatigue and microstructural properties of friction stir welded 5083-H111 and 6082-T651 aluminum alloys[J]. Materials & Design. 2014, 56:84-90.

[22]. K Elangovan, V Balasubramanian. Influences of tool pin profile and tool shoulder diameter on the formation of friction stir processing zone in AA6061 aluminium alloy[J]. Materials & Design. 2008, 29:362-373.

[23]. A Beggas, AE Kabeel, M Abdelgaied, MEH Attia, AS Abdulla, MM Abdel-Aziz. Improving the freshwater productivity of hemispherical solar distillers using waste aluminum as store materials[J]. Journal of Energy Storage. 2023, 60:106692.

[24]. PL Kumar, A Lombardi, G Byczynski, SVS Narayana Murty, BS Murty, L Bichler. Recent advances in aluminium matrix composites reinforced with graphene-based nanomaterial: A critical review[J]. Progress in Materials Science. 2022, 128: 100948.

[25]. B Chen, X Xi, CW Tan, XG Song. Recent progress in laser additive manufacturing of aluminum matrix composites[J]. Current Opinion in Chemical Engineering. 2020, 28:28-35.

[26]. N Idusuyi, JI Olayinka. Dry sliding wear characteristics of aluminium metal matrix composites: a brief overview[J]. Journal of Materials Research and Technology. 2019, 8:3338-3346.

[27]. M Jagannatham, P Chandran, S Sankaran, P Haridoss, N Nayan, SR Bakshi. Tensile properties of carbon nanotubes reinforced aluminum matrix composites: A review[J]. Carbon. 2020, 160:14-44.

[28]. J Singh, A Chauhan. Overview of wear performance of aluminium matrix composites reinforced with ceramic materials under the influence of controllable variable[J]. Ceramics International. 2016, 42:56-81.

[29]. M Cabeza, I Feijoo, P Merino, G Pena, MC Pérez, S Cruz, P Rey. Effect of high energy ball milling on the morphology, microstructure and properties of nano-sized TiC

particle-reinforced 6005A aluminium alloy matrix composite[J]. Powder Technology. 2017, 321:31-43.

[30]. P Maji, RK Nath, R Karmakar, P Pual, RK Bhogendro Meitei et al. Effect of post processing heat treatment on friction stir welded/processed aluminum based alloys and composites[J]. CIRP Journal of Manufacturing Science and Technology. 2021, 35:96-105.

[31]. ZW Yuan, WB Tian, FG Li, QQ Fu, XG Wang et al. Effect of heat treatment on the interface of high-entropy alloy particles reinforced aluminum matrix composites[J]. Journal of Alloys and Compounds. 2020, 822:153658.

[32]. TL Han, EZ Liu, JJ Li, NQ Zhao, CN He. A bottom-up strategy toward metal nano-particles modified graphene nanoplates for fabricating aluminum matrix composites and interface study[J]. Journal of Materials Science & Technology. 2020, 46:21-32.

[33]. WW Zhou, SR Bang, H Kurita, T Miyazaki, YC Fan et al. Interface and interfacial reactions in multi-walled carbon nanotube-reinforced aluminum matrix composites[J]. Carbon. 2016, 96:919-928.

[34]. BS Guo, M Song, JH Yi, S Ni, T Shen, Y Du. Improving the mechanical properties of carbon nanotubes reinforced pure aluminum matrix composites by achieving non-equilibrium interface[J]. Materials and Design. 2017, 120:56-65.

[35]. ZQ Yu, GH Wu, LT Jiang, DL Sun. Effect of coating Al_2O_3 reinforcing particles on the interface and mechanical properties of 6061 alloy aluminium matrix composite[J]. Materials Letters. 2005, 59:2281-2284.

[36]. JT Huang, MW Li, JY Chen, Y Cheng, ZH Lai et al. Insights into the diffusion migration behavior of alloy atoms at the graphene/aluminum interface: First-principles calculations[J]. Surfaces and Interfaces. 2023, 38:102825.

[37]. WJ Wang, H Wang, XF Liu, ZC Liu. Interface evolution and strengthening of two-step roll bonded copper/aluminum clad composites[J]. Materials Characterization. 2023, 199:112778.

[38]. WF Wei, QH Liao, ZF Yang, XB Li, ZL Huang et al. Interfacial modification and

performance enhancement of carbon matrix/aluminum composites[J]. Journal of Alloys and Compounds. 2022, 903:163877.

[39]. HL Si, QW Zhou, S Zhou, J Zhang, WJ Liu et al. Effect of interfacial stability on microstructure and properties of carbon fiber reinforced aluminum matrix composites[J]. Surfaces and Interfaces. 2023, 38:102816.

[40]. YC Jiang, N Li, ZH Liu, CL Yi, HM Zhou et al. Exceptionally strong boron nitride nanotube aluminum composite interfaces[J]. Extreme Mechanics Letters. 2023, 59:101952.

[41]. F Ogawa, C Masuda. Fabrication and the mechanical and physical properties of nanocarbon-reinforced light metal matrix composites: A review and future directions[J]. Materials Science & Engineering A. 2021, 820:141542.

[42]. S Parvizi, SM Hashemi, F Asgarinia, M Nematollahi, M Elahinia. Effective parameters on the final properties of NiTi-based alloys manufactured by powder metallurgy methods: A review[J]. Progress in Materials Science. 2021, 117:100739.

[43]. NABN Zamani, AA Iqbal, DM Nuruzzaman. ribo-mechanical characterisation of self-lubricating aluminum based hybrid metal matrix composite fabricated via powder metallurgy[J]. Materialia. 2020, 14:100936.

[44]. NA Bunakov, DV Kozlov, VN Golovanov, ES Klimov, EE Grebchuk, MS Efimov, BB Kostishko. Fabrication of multi-walled carbon nanotubes-aluminum matrix composite by powder metallurgy technique[J]. Results in Physic. 2016, 6:231-232.

[45]. PL Kumar, A Lombardi, G Byczynski, SVS Narayana Murty, BS Murty, L Bichle. Recent advances in aluminium matrix composites reinforced with graphene-based nanomaterial: A critical review[J]. Progress in Materials Science. 2022, 128:100948.

[46]. J Kesapradist, K Ono, K Fukaura. Producing Ni_3A1 matrix composite material by vacuum hot pressing and heat treatment of nickel-plated aluminum sheets with $A1_2O_3$ fiber[J]. Materials Science & Engineering A. 1992, 153:641-645.

[47]. Z Ma, ZW Yuan, XK Ma, K Wang, SR Li, XM Zhang. Interface characteristics and mechanical properties of $Al_{0.6}$CoCrFeNi/5052Al matrix composites fabricated via vacuum hot-pressing sintering and annealing[J]. Materials Science & Engineering A. 2022, 859:144234.

[48]. ZQ Tan, ZQ Li, GL Fan, XZ Kai, G Ji, LT Zhang, D Zhang. Diamond/aluminum composites processed by vacuum hot pressing: Microstructure characteristics and thermal properties[J]. Diamond & Related Materials. 2013, 31:1-5.

[49]. ZY Hu, ZH Zhang, XW Cheng, FC Wang, YF Zhang, SL Li. A review of multi-physical fields induced phenomena and effects in spark plasma sintering: Fundamentals and applications[J]. Materials and Design. 2020, 191:108662.

[50]. Y Sun, C Zhou, ZM Zhao, CH Wu. High plasticity achieved by spark plasma sintering method in aluminum matrix composites reinforced with Ti_2AlC particles[J]. Materials Characterization. 2021, 177:111204.

[51]. ZW Yuan, WB Tian, FG Li, QQ Fu, YB Hu, XG Wang. Microstructure and properties of high-entropy alloy reinforced aluminum matrix composites by spark plasma sintering[J]. Journal of Alloys and Compounds. 2019, 806:901-908.

[52]. E Ghasali, AH Pakseresht, M Alizadeh, K Shirvanimoghaddam, T Ebadzadeh. Vanadium carbide reinforced aluminum matrix composite prepared by conventional, microwave and spark plasma sintering[J]. Journal of Alloys and Compounds. 2016, 688:527-533.

[53]. KK Sadhu, N Mandal, RR Sahoo. SiC/graphene reinforced aluminum metal matrix composites prepared by powder metallurgy: A review[J]. Journal of Manufacturing Processes. 2023, 91:10-43.

[54]. S Dinesh Kumar, M Ravichandran, A Jeevika, B Stalin, C Kailasanathan, A Karthick. Effect of ZrB_2 on microstructural, mechanical and corrosion behaviour of aluminium (AA7178) alloy matrix composite prepared by the stir casting route[J]. Ceramics International. 2021, 47:12951-12962.

[55]. JV Christy, R Arunachalam, AHI Mourad, P Kumar Krishnan, S Piya, MA Maharbi. Processing, Properties, and Microstructure of Recycled Aluminum Alloy Composites Produced Through an Optimized Stir and Squeeze Casting Processes[J]. Journal of Manufacturing Processes. 2020, 59:287-301.

[56]. JJ Sha, ZZ Lu, RY Sha, YF Zu, JX Dai et al. Improved wettability and mechanical properties of metal coated carbon fiber-reinforced aluminum matrix composites by

squeeze melt infiltration technique[J]. Transactions of Nonferrous Metals Society of China. 2021, 31:317-330.

[57]. V Pandian, S Kannan. Effect of high entropy particle on aerospace-grade aluminium composite developed through combined mechanical supersonic vibration and squeeze infiltration technique[J]. Journal of Manufacturing Processes. 2022, 74:383-399.

[58]. P Samal, PR Vundavilli, A Meher, MM Mahapatra. Recent progress in aluminum metal matrix composites: A review on processing, mechanical and wear properties[J]. Journal of Manufacturing Processes. 2020, 59:131-152.

[59]. P Garg, A Jamwal, D Kumar, K Kumar Sadasivuni, C Mustansar Hussain, P Gupta. Advance research progresses in aluminium matrix composites: manufacturing & applications[J]. Journal of Materials Research and Technology. 2019, 8:4924-4939.

[60]. A Sivkov, Y Shanenkova, Y Vympina, D Nikitin, I Shanenkov. Deposition of copper coatings on internal aluminum contact surfaces by high-energy plasma spraying[J]. Surface & Coatings Technology. 2022, 440:128484.

[61]. DJ Woo, FC Heer, LN Brewer, JP Hooper, S Osswald. Synthesis of nanodiamond-reinforced aluminum metal matrix composites using cold-spray deposition[J]. Carbon. 2015, 86:15-25.

[62]. B Chen, X Xi, CW Tan, XG Song. Recent progress in laser additive manufacturing of aluminum matrix composites[J]. Current Opinion in Chemical Engineering. 2020, 28:28-35

[63]. R George, KT Kashyap, R Rahul, S Yamdagni. Strengthening in carbon nanotube/aluminium (CNT/Al) composites[J]. Scripta Materialia. 2005, 53:1159-1163.

[64]. B Chen, J Shen, X Ye, L Jia, S Li et al. Length effect of carbon nanotubes on the strengthening mechanisms in metal matrix composites[J]. Acta Materialia. 2017, 140:317-325.

[65]. DH Nam, SI Cha, BK Lim, HM Park, DS Han, SH Hong. Synergistic strengthening by load transfer mechanism and grain refinement of CNT/Al-Cu composites[J]. Carbon. 2012, 50:2417-2423.

[66]. RE Stoller, SJ Zinkle. On the relationship between uniaxial yield strength and

resolved shear stress in polycrystalline materials[J]. Journal of Nuclear Materials. 2000:349-352.

[67]. M Wang, Y Li, B Chen, D Shi, J Umeda, K Kondoh, J Shen. The rate-dependent mechanical behavior of CNT-reinforced aluminum matrix composites under tensile loading[J]. Materials Science & Engineering A. 2021, 808:140893.

[68]. B Chen, SF Li, H Imai, L Jia, J Umeda et al. An approach for homogeneous carbon nanotube dispersion in Al matrix composites[J]. Materials and Design. 2015, 72:1-8.

[69]. SI Ghazanlou, B Eghbali, R Petrov. Microstructural evolution and strengthening mechanisms in Al7075/graphene nano-plates/ carbon nano-tubes composite processed through accumulative roll bonding[J]. Materials Science & Engineering A. 2021, 807:140877.

[70]. BS Guo, YQ Chen, ZW Wang, JH Yi, S Ni et al. Enhancement of strength and ductility by interfacial nano-decoration in carbon nanotube/aluminum matrix composites[J]. Carbon. 2020, 159:201-212.

[71]. SN Patankar, V Gopinathan, P Ramakrishnan. Studies on Carbon Fibre Reinforced Aluminium Composite Processed Using Pre-Treated Carbon Fibers[J]. Journal of Materials Science. 1991, 26:4196-4202.

[72]. MK Surappa. Aluminium Matrix Composites: Challenges and Opportunities[J]. Sadhana. 2003, 28:319-334.

[73]. M Ebrahimi, QD Wang. Accumulative roll-bonding of aluminum alloys and composites: An overview of properties and performance[J]. Journal of Materials Research and Technology. 2022, 19:4381-4403.

[74]. KR Ravi, RM Pillai, KR Amaranathan, BC Pai, M Chakraborty. Fluidity of aluminum alloys and composites: A review[J]. Journal of Alloys and Compounds. 2008, 456:201-210.

[75]. R Martınez-Sanchez, J Reyes-Gasga, R Caudillo, DI Garcıa-Gutierrez, A Marquez-Lucero, I Estrada-Guel, DC Mendoza-Ruiz, M Jose-Yacaman. Mechanical and microstructural characterization of aluminum reinforced with carbon-coated silver nanoparticles[J]. Journal of Alloys and Compounds. 2007, 438:195-201.

[76]. CN Zhu, YS Su, XS Wang, HC Sun, QB Ouyang, D Zhang. Process optimization, microstructure characterization and thermal properties of mesophase pitch-based carbon fiber reinforced aluminum matrix composites fabricated by vacuum hot pressing[J]. Composites Part B. 2021, 215:108746.

[77]. MJ Zhai, FL Zhang, XS Chen, YB Lin, MX Zhu, HQ Tang, YM Zhou. Preparation and characterization of nanodiamond reinforced aluminum matrix composites by hot-press sintering[J]. Diamond & Related Materials. 2021, 120:108664.

[78]. KD Zhong, JM Zhou, CT Zhao, K Yun, LH Qi. Effect of interfacial transition layer with CNTs on fracture toughness and failure mode of carbon fiber reinforced aluminum matrix composites[J]. Composites Part A. 2022, 163:107201.

[79]. HL Zhang, JH Wu, Y Zhang, JW Li, XT Wang, YH Sun. Mechanical properties of diamond/Al composites with Ti-coated diamond particles produced by gas-assisted pressure infiltration[J]. Materials Science & Engineering A. 2015, 626:362-268.

[80]. SMAK Mohammed, DL Chen, ZY Liu, DR Ni, QZ Wang, BL Xiao, ZY Ma. Deformation behavior and strengthening mechanisms in a CNT-reinforced bimodal-grained aluminum matrix nanocomposite[J]. Materials Science & Engineering A. 2021, 817:141370.

[81]. JW Zhu, WM Jiang, GY Li, F Guan, Y Yu, ZT Fan. Microstructure and mechanical properties of SiC np /Al6082 aluminum matrix composites prepared by squeeze casting combined with stir casting[J]. Journal of Materials Processing Tech. 2020, 283:116699.

[82]. HJ Zhang, BX Zhang, QZ Gao, JL Song, GL Han. A review on microstructures and properties of graphene-reinforced aluminum matrix composites fabricated by friction stir processing[J]. Journal of Manufacturing Processes. 2021, 68:126-135.

[83]. SO Akinwamide, M Lesufi, O Jeremiah Akinribide, P Mpolo, P Apata Olubambi. Evaluation of microstructural and nanomechanical performance of spark plasma sintered TiFe-SiC reinforced aluminum matrix composites[J]. Journal of Materials Research and Technology. 2020, 9:12137-12148.

[84]. A Treviso, B Van Genechten, D Mundo, M Tournour. Damping in composite materials: Properties and models[J]. Composites Part B. 2015, 78:144-152.

[85]. XF Liu, W Sun, XF Yan, DX Du, HH Liu, H Li. Nonlinear vibration analysis of

carbon fiber-reinforced composites with frequency-dependence and strain-dependence: Experimental and theoretical studies[J]. Thin-Walled Structure. 2023, 183:110369.

[86]. M Amine Bennaceur, YM Xu. Application of the natural element method for the analysis of composite laminated plates[J]. Aerospace Science and Technology. 2019, 87:244-253.

[87]. O Ahmed, X Wang, MV Tran, MZ Ismadi. Advancements in fiber-reinforced polymer composite materials damage detection methods: Towards achieving energy-efficient SHM systems[J]. Composites Part B. 2021, 223:109136.

[88]. SK Bhudolia, G Gohel, J Kantipudi, KF Leong, P Gerard. Mechanical performance and damage mechanisms of thin rectangular carbon/Elium® tubular thermoplastic composites under flexure and low-velocity impact[J]. Thin-Walled Structures. 2021, 165:107971.

[89]. SE Arevalo, LA Pruitt. Nanomechanical analysis of medical grade PEEK and carbon fiber-reinforced PEEK composites[J]. Journal of the Mechanical Behavior of Biomedical Material. 2020, 111:104008.

[90]. TS He, XY Li, YF Wang, TJ Bai, X Weng, B Zhang. Carbon nano-fibers/ribbons with meso/macro pores structures for supercapacitor[J]. Journal of Electroanalytical Chemistry. 2020, 878:114597.

[91]. S Kumar P, K Jayanarayanan, M Balachandran. High-performance thermoplastic polyaryletherketone/carbon fiber composites: Comparison of plasma, carbon nanotubes/graphene nano-anchoring, surface oxidation techniques for enhanced interface adhesion and properties[J]. Composites Part B. 2023, 253:110560.

[92]. JL Rife, P Kung, RJ Hooper, J Allen, GB Thompson. Structural and mechanical characterization of carbon fibers grown by laser induced chemical vapor deposition at hyperbaric pressures[J]. Carbon. 2020, 162:95-105.

[93]. J Xu, LJ Guo, HH Wang. Compression and thermophysical properties of carbon fiber-reinforced high textured pyrocarbon and SiC dual matrix composites[J]. Ceramics Internationa. 2023, 49:12903-12911.

[94]. MA Awotunde, AO Adegbenjo, BA Obadele, MOBM Shongwe, PA Olubambi.

Influence of sintering methods on the mechanical properties of aluminium nanocomposites reinforced with carbonaceous compounds: A review[J]. Journal of Materials Research and Technology. 2019, 8:2432-2449.

[95]. M Habibur Rahman, HM Mamun Al Rashed. Characterization of silicon carbide reinforced aluminum matrix composites[J]. Procedia Engineering. 2014, 90:103-109.

[96]. L Jia, K Kondoh, H Imai, M Onishi, B Chen, SF Li. Nano-scale AlN powders and AlN/Al composites by full and partial direct nitridation of aluminum in solid-state[J]. Journal of Alloys and Compounds. 2015, 629:184-187.

[97]. C Nie, H Wang, J He. Evaluation of the effect of adding carbon nanotubes on the effective mechanical properties of ceramic particulate aluminum matrix composites[J]. Mechanics of Materials. 2020, 142:103276.

[98]. S Lakra, TK Bandyopadhyay, S Das, K Das. Thermal conductivity of in-situ dual matrix aluminum composites with segregated morphology[J]. Materials Research Bulletin. 2021, 144:111515.

[99]. M Jagannatham, P Chandran, S Sankaran, P Haridoss, N Nayan, SR Bakshi. Tensile properties of carbon nanotubes reinforced aluminum matrix composites: A review[J]. Carbon. 2020, 160:14-44.

[100]. C Zhu, Y Su, X Wang, H Sun, Q Ouyang, D Zhang. Process optimization, microstructure characterization and thermal properties of mesophase pitch-based carbon fiber reinforced aluminum matrix composites fabricated by vacuum hot pressing[J]. Composites Part B. 2021, 215:108746.

[101]. JJ Sha, ZZ LÜ, RY Sha, YF Zu, JX Dai, YQ Xian et al. Improved wettability and mechanical properties of metal coated carbon fiber-reinforced aluminum matrix composites by squeeze melt infiltration technique[J]. Transactions of Nonferrous Metals Society of China. 2021, 31:317-330.

[102]. S Bahl. Fiber reinforced metal matrix composites-a review[J]. Mater. Today: Proc. 2021, 39:317-323.

[103]. R Pei, G Chen, Y Wang, M Zhao, G Wu. Effect of interfacial microstructure on the thermal-mechanical properties of mesophase pitch-based carbon fiber reinforced aluminum composites[J]. Journal of Alloys and Compounds. 2018, 756:8-18.

[104]. B Guo, S Ni, J Yi, R Shen, Z Tang, Y Du, M Song. Microstructures and mechanical properties of carbon nanotubes reinforced pure aluminum composites synthesized by spark plasma sintering and hot rolling[J]. Materials Science and Engineering: A. 2017, 698:282-288.

[105]. B Guo, S Luo, Y Wu, M Song, B Chen, Z Yu, W Li. Regulating the interfacial reaction between carbon nanotubes and aluminum via copper nano decoration[J]. Materials Science and Engineering: A. 2021, 820.

[106]. WD Fei, ZJ Li, YB Li. Effects of T4 treatment on hot rolling behavior and tensile strength of aluminum matrix composite reinforced by aluminum borate whisker with NiO coating[J]. Materials Chemistry and Physics. 2006, 97:402-409.

[107]. L Jiang, P Wang, Z Xiu, G Chen, X Lin, C Dai et al. Interfacial characteristics of diamond/aluminum composites with high thermal conductivity fabricated by squeeze-casting method[J]. Materials Characterization. 2015, 106:346-351.

[108]. A Maqbool, MA Hussain, FA Khalid, N Bakhsh, A Hussain, MH Kim. Mechanical characterization of copper coated carbon nanotubes reinforced aluminum matrix composites[J]. Materials Characterization. 2013, 86:39-48.

[109]. SC Xu, LD Wang, PT Zhao, WL L, WD Fei. A study of hot rolling of 6061 aluminum alloy matrix composite reinforced with SnO_2-coated $Al_{18}B_4O_{33}$ whisker[J]. Materials Science and Engineering A. 2012, 550:146-151.

[110]. F Mokdad, DL Chen, ZY Liu, DR Ni, BL Xiao, ZY Ma. Hot deformation and activation energy of a CNT-reinforced aluminum matrix nanocomposite[J]. Materials Science and Engineering A. 2017, 695:322-331,

[111]. BL Wu, YC Peng, HQ Tang, YZ Zhan, FL Zhang. Microstructural evolution of nanodiamond-reinforced aluminum matrix composites during the process of hot extrusion[J]. Ceramics International. 2023, 49:9355-9370.

[112]. MJ Wang, JH Shen, B Chen, YF Wang, J Umeda, K Kondohd, YL Li. Compressive behavior of CNT-reinforced aluminum matrix composites under various strain rates and temperatures[J]. Ceramics International. 2022, 48:10299-10310.

[113]. JH Wu, C Zhang, QN Meng, BC Liu, YH Sun, M Wen et al. Study on tensile

properties of carbon fiber reinforced AA7075 composite at high temperatures[J]. Materials Science & Engineering A. 2021, 825:141931.

[114]. CN Zhu, YS Su, D Zhang, QB Ouyang. Effect of Al_2O_3 coating thickness on microstructural characterization and mechanical properties of continuous carbon fiber reinforced aluminum matrix composites[J]. Materials Science & Engineering A. 2020, 793:139839.

[115]. CQ Gao, MY Wei, QB Wang, JX Tian, LB Zhao et al. Interface microstructure and mechanical properties of Ni-Co-P alloy coatings modified carbon fibres reinforced 7075Al matrix composites[J]. Ceramics International. 2022, 48:36748-36757.

[116]. X Zhang, XD Ho, D Pan, B Pan, L Liu et al. Designable interfacial structure and its influence on interface reaction and performance of MWCNTs reinforced aluminum matrix composites[J]. Materials Science & Engineering A. 2020, 793:139783.

[117]. P Zhu, Q Zhang, S Qu, ZJ Wang, HS Gou et al. Effect of interface structure on thermal conductivity and stability of diamond/aluminum composites[J]. Composites Part A. 2022, 162:107161.

Chapter 2

Effect of copper coating on interfacial properties, interfacial thermal resistance, microstructure evolution and mechanical properties of aluminum matrix composites

2.1 Introduction

With the rapid iteration of the semiconductor industry, portable microelectronic devices used in aerospace and other fields require the high thermal conductivity of lightweight materials[1,2]. Because of their excellent comprehensive properties, aluminum (Al) matrix composites are more and more widely used[2-4]. Reinforcements with high strength and thermal conductivity can give the composites excellent performance. Carbon-based reinforcements such as carbon nanotubes (CNTs), graphite, and carbon fibers (CFs) are considered to be the most promising reinforcing materials[5,6]. However, considering the high price of CNTs and graphite and their drawback of being challenging to distribute uniformly in the matrix, the thermal structural materials prepared by CFs reinforced Al matrix composites have a broader application space[5,7-9].

The interface influences the microstructural evolution and mechanical properties of the composites[3,10,11]. For example, the formation of harmful interfacial products may weaken the mechanical properties and reduce the thermal conductivity. However, the weak interfacial bonding may affect stress transfer, become the crack source, and lead to severe failures in complex service environments[12,13]. Coating the reinforcement surface is one of the most effective and economical methods[8,13-15]. Guo et al.[11] effectively improved weak interfacial bonding by decorating the surface of CNTs with copper (Cu). Maqbool et al.[15] improved the wettability and interfacial bonding between CNTs and Al matrix with chemical Cu-coating. CNTs were evenly distributed in the Al matrix, resulting in good mechanical properties. Fan et al.[16] coated the surface of the graphite sheet with SiC and prepared Al matrix composites, which obtained excellent thermal conductivity and mechanical properties.

The arrangement of reinforcement in the matrix also has a significant impact on the properties of the composites[17]. Non-equiaxed reinforcements such as CFs and CNTs are anisotropic. The random arrangement is limited to improving the all-around performance in one direction. The single directional arrangement of reinforcements can significantly enhance the thermal conductivity and mechanical properties. Due to the

negative effect of reinforcement on plastic deformation ability, thermal deformation such as hot rolling and hot extrusion are usually used to improve the arrangement of reinforcements[12,18-20]. Li et al.[8] adopted the hot extrusion to distribute CFs along the extrusion direction and obtained better thermal conductivity, lower thermal expansion coefficient and higher compression strength. Bi et al.[4] improved the distribution of CNTs and optimized the texture composition through hot rolling, increasing the strength and plasticity of CNT/7055Al.

In the study of thermal properties of composites, the interfacial thermal resistance is strongly affected by the interfacial products[1]. However, few studies have comprehensively investigated the effect of interfacial products and the thickness of product on thermal conductivity. In addition, the evolution of texture composition during thermal deformation can reflect the evolutionary path of microstructure. Still, the effects of CFs and Cu-coating on texture evolution have not been clearly explained. Therefore, in this study, uncoated and Cu-coated short carbon fiber (SCF) reinforced Al matrix composites were prepared by spark plasma sintering (SPS). The arrangement of SCF in the Al matrix was improved by hot rolling. The influence of Cu-coating on the interfacial properties was explored, and the relationship between interfacial products and interfacial thermal resistance was analyzed. Through the evolution of texture, the influence of Cu-coating on the evolution of microstructure was investigated.

2.2 Experimental procedure

2.2.1 Cu-coating on short carbon fiber

The reinforcement used in this study was obtained from Mitsubishi Chemical Corporation (Japan), and its physical properties are shown in Table 2-1.

Table 2-1 Physical properties of SCF

Model Number	Diameter (μm)	Thermal conductivity (W/mK)	Modulus (GPa)	Tensile strength (MPa)	Density (g/cm^3)
K223HE	11	550	900	3800	2.2

The surface of SCF was coated with Cu by an ultrasonic-assisted chemical plating process. First, SCF was immersed in acetone solution and shaken in the ultrasonic cleaner for 10 min for degreasing. After washing, the SCF was etched in the 10% HNO_3 solution to obtain a rough surface. Then the surface of SCF was sensitized and activated by deposit Palladium. Finally, the SCF was ultrasonically shaken in Cu-coating standard solution at 35°C for 2 hours. The surface morphologies of SCF before and after Cu-coating are shown in Figure 2-1. As presented in Figure 2-1b), Cu ions are densely coated on the surface of SCF.

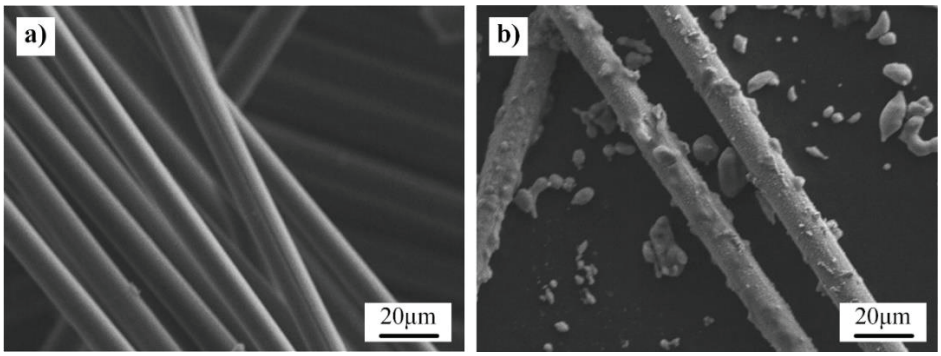

Figure 2-1 SEM morphology of SCF: a) before Cu-coating, b) after Cu-coating

2.2.2 Preparation and hot rolling of composites

The pure Al powder used in this study was purchased from Kojundo Chemical Laboratory Co., Ltd (Sakado, Saitama Pre. Japan). The model number of the Al powder is ALE11PB, the purity is 99.90%, and the diameter is 3 microns. The preparation of SCF reinforced Al matrix composites is shown in Figure 2-2. First, the SCF and pure Al powders were weighed in a ratio of 3:97 by volume and mixed evenly in the alcohol solution. The mixed solution was then injected into an Al tank and mixed with alumina balls with a diameter of 10mm on a V-type mixer for 1 hour. The mixed solution was

dried in the fuming cabinet for 24 hours, then the obtained powders were dried in a vacuum drying oven at 70°C for 24 hours. After drying, the mixed powders were sintered on the CSP-I-30201 discharge plasma sintering machine. The sintering temperature was 550°C, the pressure was 50 MPa, and the holding time was 30 min. The composites were wrapped with Al foil and rolled seven times at 450°C, with a final reduction of 70%. Uncoated and Cu-coated composites are expressed as SCF/Al and Cu-SCF/Al. For comparison, pure Al blocks were prepared under the same conditions.

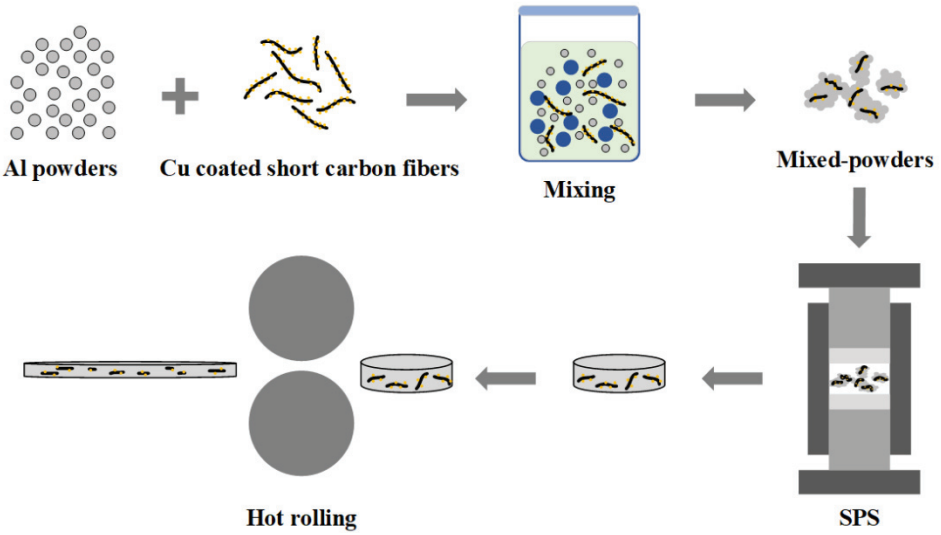

Figure 2-2 Schematic diagram of the preparation of hot-rolled SCF reinforced Al matrix composites

2.2.3 Microstructure characterization

The morphology of the composites and SCF was observed by the JXA-ISP100 scanning electron microscope (SEM). Electron backscatter diffraction (EBSD) analysis was performed by the Zeiss Sigma 300 scanning electron microscope equipped with the Oxford-SYMMETRY pattern acquisition device. The interfacial structure of the composites was observed by the JEOL transmission electron microscope (TEM). The physical phases of the composites before and after hot rolling were identified by the SmartLab type X-ray diffractometer (XRD). The interfacial strength of the composites was measured by the ELIONIX ENT-1100A nano hardness tester.

2.2.4 Mechanical and thermal conductivity tests

Tensile specimens were cut along the rolling direction and tested on the INSTRON 8801 hydraulic servo fatigue tester. The test temperature was room temperature, and the strain rate was $8.3\times10^{-4}s^{-1}$. Three samples were prepared for each material to minimize errors. The thermal conductivity of the composites was measured along the rolling direction.

2.3 Results

2.3.1 Microstructure

The SEM morphologies of SCF/Al and Cu-SCF/Al before and after hot rolling are shown in Figure 2-3. As shown in Figure 2-3 a) and c), the distribution direction of SCF in the sintered composites is random. Black bands are present in the Al matrix of SCF/Al, as presented by the blue arrows in Figure 2-3 a_1). These bands are distributed along the boundary of the Al powders. However, this phenomenon does not occur in the Al matrix of Cu-SCF/Al. In addition, as depicted in the red box in Figure 2-3 a_1), there are holes between the SCF and the Al matrix of the SCF/Al. But there are no holes observed at the interface between the SCF and the Al matrix in Figure 2-3 c_1), indicating that the interface between the Cu-coated SCF and the Al matrix is better bonded. After hot rolling, the SCF of both composites are arranged along the rolling direction, but the SCF in SCF/Al is distorted and deformed. The morphology of SCF in Cu-SCF/Al is the same as before hot rolling. The bands in the Al matrix of SCF/Al do not disappear after hot rolling, as illustrated by the arrows in Figure 2-3 b_1). Moreover, comparing Figure 2-3 b_1) and Figure 2-3 d_1), some of the interfaces in SCF/Al cracks after hot rolling, as performed in the red box in Figure 2-3 b_1). The interfacial bonding between SCF and Al matrix in Cu-SCF/Al is well.

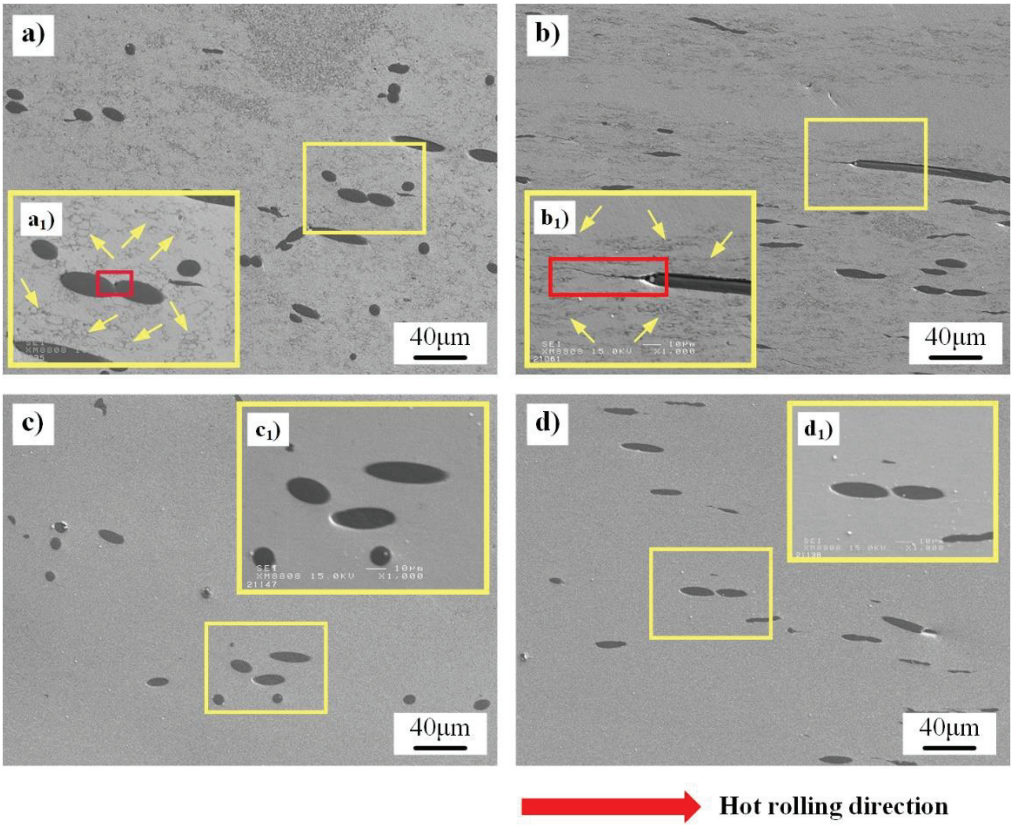

Figure 2-3 SEM morphology and local enlargement of the composites: a) Sintered SCF/Al, b) Hot-rolled SCF/Al, c) Sintered Cu-SCF/Al, d) Hot-rolled Cu-SCF/Al

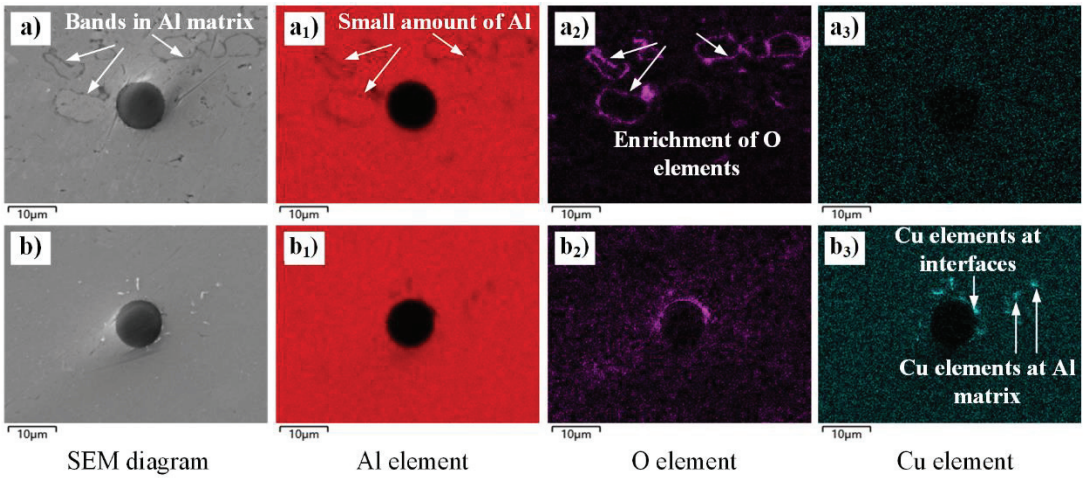

Figure 2-4 EDS analysis of sintered composites: a) SCF/Al, b) Cu-SCF/Al, a_1)-a_3) Distribution of Al element, oxygen(O) element and Cu element in SCF/Al, b_1)-b_3) Distribution of Al element, O element and Cu element in Cu-SCF/Al

EDS analysis was carried out on sintered SCF/Al and Cu-SCF/Al to investigate the composition of bands in the Al matrix of SCF/Al, respectively. The results are shown in Figure 2-4. The black bands in SCF/Al are enriched with high concentrations

of O elements and small amounts of Al elements, as illustrated in Figure 2-4 a_1) and Figure 2-4 a_2). The result shows alumina film on the surface of Al powder was not completely removed during the sintering process of SCF/Al. From the principle of SPS, one of the main reasons for setting up the discharge device is to remove the oxide from the surface of the powder by pulsing the current. Therefore, high requirements are placed on the electrical conductivity of the sintered powders[21]. The mixed powders of un-coated SCF and Al powders had poor electrical conductivity. Comparing the elemental distribution of Cu-SCF/Al, there is no O enrichment in the Al matrix. The results show that the combination of SCF and Al powders is well due to the Cu-coating. The well electrical conductivity of the mixed powders led to better interfacial bonding and metallurgical bonding of Cu-SCF/Al. In addition, as shown in Figure 2-4 b_3), there is a significant enrichment of Cu elements at and near the interface of Cu-SCF/Al, which indicates that the coating was shed or diffused into the Al matrix during the process of mixing and sintering.

The EBSD Maps of SCF/Al and Cu-SCF/Al before and after hot rolling are illustrated in Figure 2-5. The defects exist near the sintered SCF/Al interface region, where the grains near SCF are smaller and have more equiaxed grains, as performed by arrows and white dashed lines in Figure 2-5a). This is caused by the fine Al particles produced during the ball-mill mixing process and the newly formed grains during the sintering. The grain size of SCF/Al decreases obviously after hot rolling. However, the defects in the Al matrix are not eliminated. Many equiaxed grains appear near SCF, as demonstrated in Figure 2-5 b). The degree of deformation in these regions during thermal deformation was more significant. The stress concentration led to energy accumulation, which promotes the transformation from dislocations and low-angle grain boundaries to high-angle grain boundaries, forming continuous dynamic recrystallization grains[21].

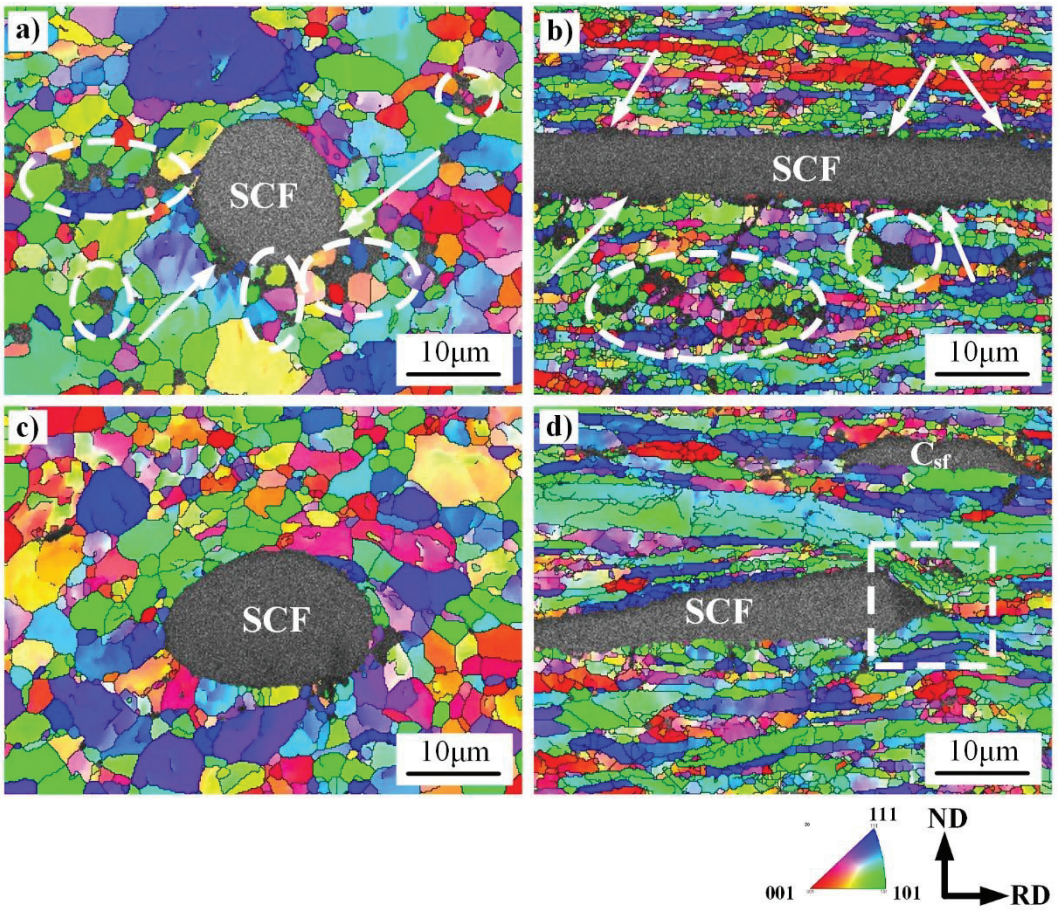

Figure 2-5 EBSD Maps of composites: a) Sintered SCF/Al, b) Hot-rolled SCF/Al, c) Sintered Cu-SCF/Al, d) Hot-rolled Cu-SCF/Al

Comparing Figure 2-5 a) with Figure 2-5 c), there are no apparent defects in the Al matrix of Cu-SCF/Al, and the interface is well bonded. The grain size decreases significantly after hot rolling, and the degree of grain deformation near SCF is more extensive, as pointed out in the white box in Figure 2-5 d). Even in the region with large deformation, no interfacial cracking occurred, indicating that Cu-SCF/Al has good interfacial consistency and plastic deformation ability.

2.3.2 Interfacial structure and strength

The XRD results of SCF/Al and Cu-SCF/Al before and after hot rolling are shown in Figure 2-6. Since the contents of other elements and structures are too small to be detected, only the XRD could identify the SCF and pure Al phases.

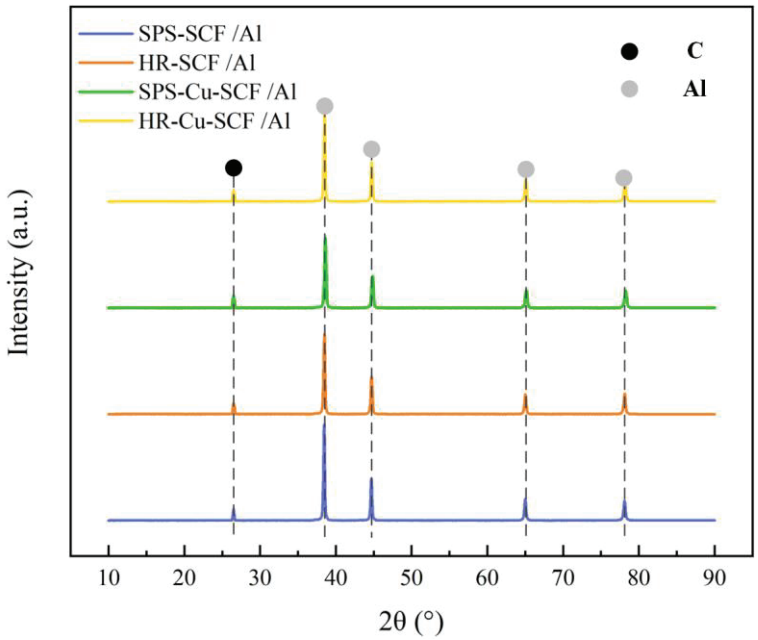

Figure 2-6 XRD results of SCF/Al and Cu-SCF/Al before and after hot rolling

TEM observations at the interface of the composites were performed to investigate the generation of interfacial products and the interfacial structure. The high-resolution morphologies at the interface of SCF/Al and Cu-SCF/Al before and after hot rolling are presented in Figure 2-7. The white dashed lines in the figure outline the interfacial region, and the fast Fourier transformations (FFT) analysis is performed in the red dashed box region. Cu-rich layer is observed at the interface of Cu-SCF/Al as shown in Figure 2-7 c). Due to the Cu-coating, there is no contact between the C atom and Al atom; no interfacial products were generated. However, the shedding and diffusion of the Cu-coating led to the generation of interfacial products, as depicted in Figure 2-7d). Amorphous Al-C compounds are generated at the interfaces of sintered SCF/Al and Cu-SCF/Al, as illustrated in Figure 2-7 a) and d). Nevertheless, the thickness of the interfacial product of SCF/Al is significantly greater than that of Cu-SCF/Al. The interfacial reaction between the uncoated SCF and the Al matrix was more severe.

The crystalline Al_4C_3 phase was generated at the interface of SCF/Al after hot rolling, as described in Figure 2-7 b). Research showed that Al_4C_3 phase is a kind of harmful phase[22]. The interfacial product of Cu-SCF/Al after hot rolling is amorphous, as shown in Figure 2-7 e). The Cu-coating reduced the interfacial reaction between the SCF and Al matrix during thermal deformation, which protected the structure of SCF and avoided the formation of harmful phase Al_4C_3.

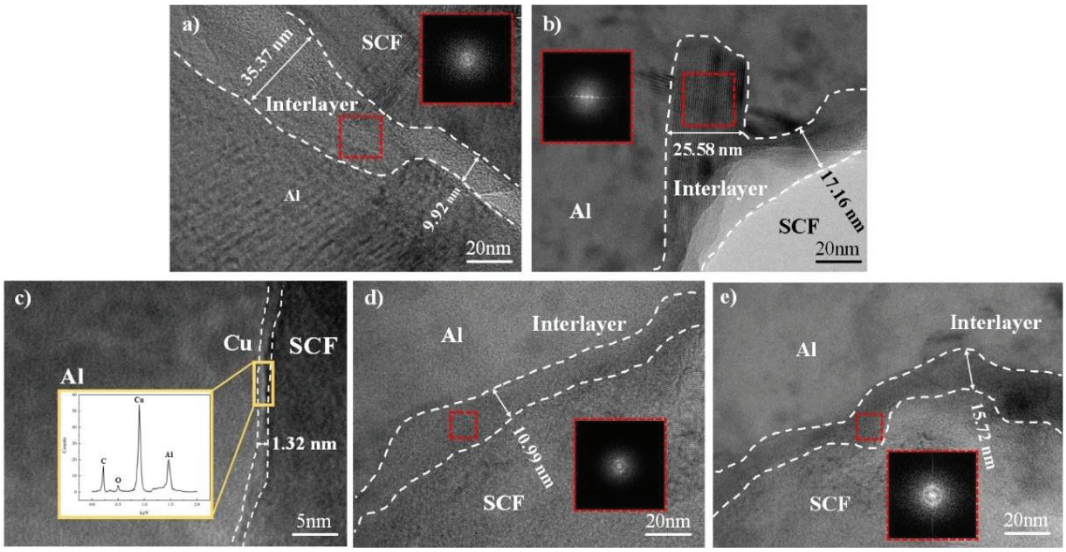

Figure 2-7 High-resolution morphology at the interface of composites: a) Sintered SCF/Al, b) Hot-rolled SCF/Al, c) Cu-rich interface of Cu-SCF/Al, d) Sintered Cu-SCF/Al, e) Hot-rolled Cu-SCF/Al

The distribution of nano-hardness values at the interfaces of SCF/Al and Cu-SCF/Al before and after hot rolling is performed in Figure 2-8. The 1st and 2nd points are at the surface of short carbon fiber, the 3rd point is at the interface, and the 4th-7th points are at the Al matrix. The hardness values of SCF in the sintered SCF/Al and Cu-SCF/Al are both high. The interfacial strength of sintered Cu-SCF/Al is higher than that of SCF/Al, indicating that the Cu-coating improved the interfacial bonding and enhanced the interfacial strength. The hardness values of SCF in SCF/Al decrease considerably, and the interfacial strength increase significantly after hot rolling. Combined with Figure 2-7b), lots of C atoms migrated to the Al matrix during thermal deformation without coating protection. The structure of SCF was destroyed, leading to a significant decline in strength[23]. In contrast, the hardness values of SCF in Cu-

SCF/Al after hot rolling only show a small decrease and a slight increase in interfacial strength. This is due to the inhibition of interfacial reactions by Cu-coating that protects the structure of SCF.

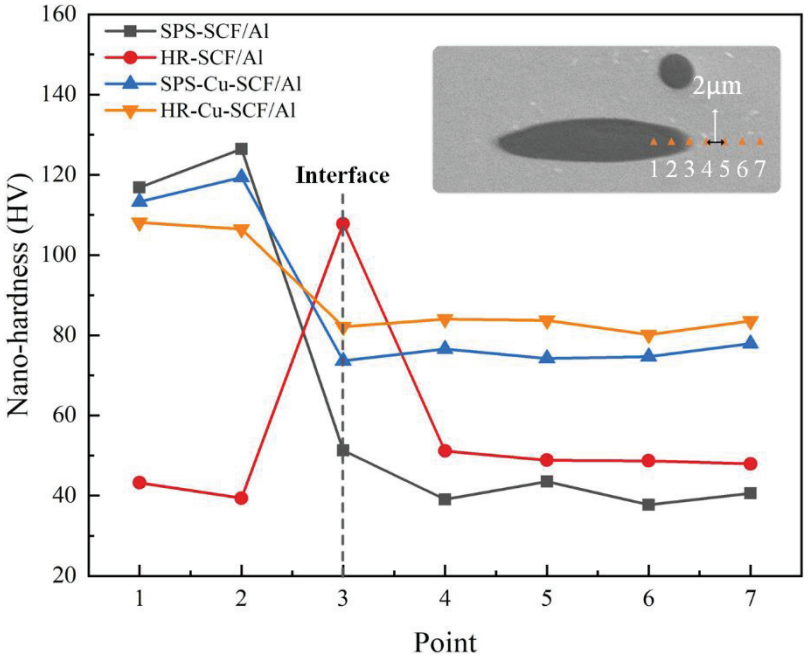

Figure 2-8 Nano-hardness values at the interface of composites before and after hot rolling

2.3.3 Mechanical properties

Tensile tests of SCF/Al and Cu-SCF/Al before and after hot rolling were carried out at room temperature, and the stress-strain curves obtained are shown in Figure 2-9.

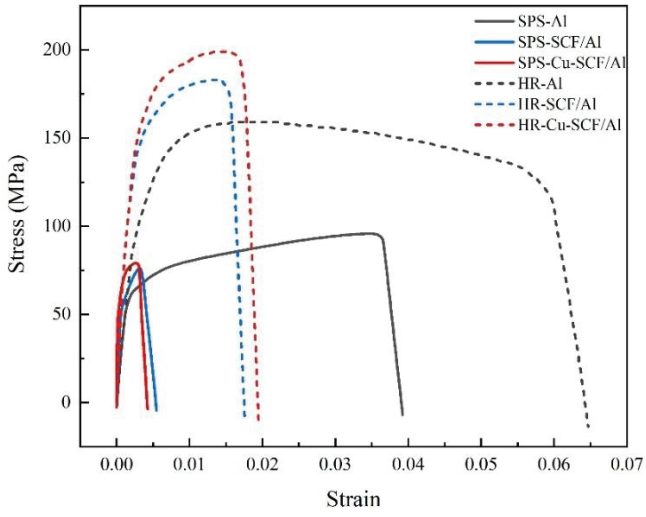

Figure 2-9 Stress-strain curves of the composites before and after hot rolling

Compared with pure Al, the plasticity of the composites with the addition of SCF is substantially reduced, but the yield strength is improved. The yield strengths of sintered SCF/Al and Cu-SCF/Al are 75.34 MPa and 78.37 MPa, respectively, higher than pure Al of 67.05 MPa. It can be seen from Figure 2-5 a) and Figure 2-5 c) that there are defects in the Al matrix of sintered SCF/Al, while no defects are observed in Cu-SCF/Al. Defects have a negative impact on mechanical properties, resulting in lower yield strength of SCF/Al than Cu-SCF/Al, as shown by the red solid line with the blue solid line in Figure 2-9. The yield strengths of all three materials are both improved after hot rolling. The yield strength of Cu-SCF/Al is 173.93MPa; the increase rate is up to 121.93%.

Moreover, the plasticity of SCF/Al and Cu-SCF/Al increases obviously after hot rolling, but the plasticity of Cu-SCF/Al is better. This is due to holes at the interface of SCF/Al and defects in the Al matrix after hot rolling, as shown in Figure 2-5b). The existence of the defects causes the yield strength and plasticity of SCF/Al to be lower than that of Cu-SCF/Al, as shown by the red dashed line and the blue dashed line in Figure 2-9.

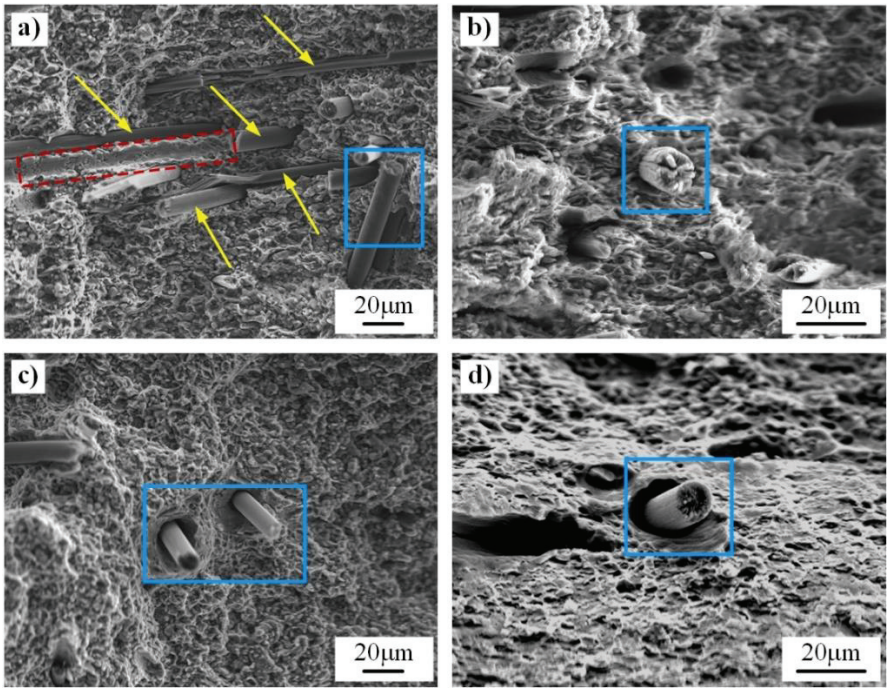

Figure 2-10 Tensile fracture images of composites: a) Sintered SCF/Al, b) Hot-rolled SCF/Al, c) Sintered Cu-SCF/Al, d) Hot-rolled Cu-SCF/Al

The SEM images of the tensile fracture of SCF/Al and Cu-SCF/Al before and after hot rolling are depicted in Figure 2-10. The cross-sectional morphology of SCF is relatively rough, a non-brittle fracture resulting in a smooth section, indicating that the SCF plays a role in bearing the load. However, from Figure 2-10 a) we could see that the aggregation of SCF in SCF/Al negatively affects plasticity. There are pores in the Al matrix after the shedding of SCF, as performed in the red box in Figure 2-10 a). The pores at the interface are also a factor contributing to the poor plasticity of SCF/Al. Since the arrangement of SCF in the sintered SCF/Al is random, the SCF is prone to cracking with the Al matrix during the tensile process, as shown in the yellow arrow. After hot rolling, SCF is arranged along the rolling direction, which plays a role in bearing the load and improving the tensile strength. In addition, as demonstrated in the blue box in Figure 2-10 b), the surface of SCF in SCF/Al is rough and cracks after hot rolling. Combined with Figure 2-7 b), hot rolling leads to a severe reaction between the uncoated SCF and the Al matrix, forming the crystal interfacial product Al_4C_3. Whereas by comparing the blue boxes in Figure 2-10 c) and Figure 2-10 d), the morphology of SCF in Cu-SCF/Al is not changed much before and after hot rolling, which is attributed to the protective effect of Cu-coating on the structure of SCF.

2.3.4 Thermal conductivity

The thermal conductivity of pure Al, SCF/Al, and Cu-SCF/Al before and after hot rolling are shown in Figure 2-11. In this study, the volume fraction of the reinforcement is 3%. According to the layered parallel model[24], the thermal conductivity of the composites under ideal conditions is:

$$K_C = fK_L + (1-f)K_M \quad (1)$$

Where K_C represents the thermal conductivity of composites, f represents the volume fraction of SCF, K_L represents the thermal conductivity of SCF in the length direction, and K_M represents the thermal conductivity of the Al matrix. According to Equation (1), the thermal conductivity of SCF/Al should be 245.42W/mK under ideal conditions. However, as shown in Figure 2-11, the thermal conductivities of SCF/Al

before and after hot rolling are lower than this value. Combined with SEM morphology and fracture morphology, there are two reasons for the low thermal conductivity of SCF/Al. One aspect is the negative effect of the pores at the interface and the oxides in the Al matrix; another aspect is that the structure of SCF is destroyed, the thermal conductivity is reduced due to the severe interfacial reaction. In addition, the thermal conductivity of sintered Cu-SCF/Al is lower than the ideal value of 245.42W /mK but much higher than the value of SCF/Al. It indicated that good interfacial and metallurgical bonding facilitate heat transfer. After hot rolling, the thermal conductivity of Cu-SCF/Al increases significantly and approaches the ideal value. It's due to the positive effect of the change in SCF arrangement on the thermal conductivity network after hot rolling[8,25].

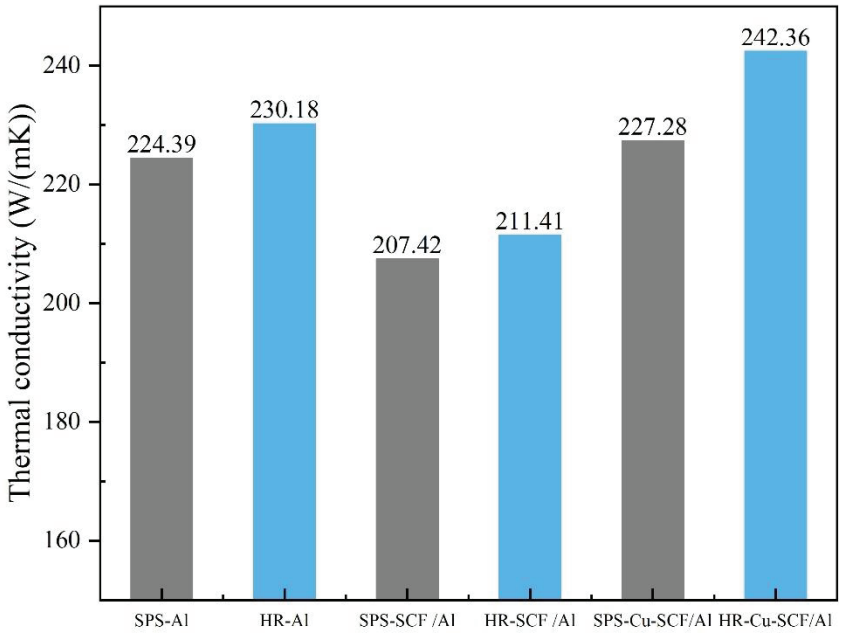

Figure 2-11 Thermal conductivity values of pure Al, SCF/Al and Cu-SCF/Al before and after hot rolling

The effects of different arrangements of SCF on the heat transfer network of the composites are illustrated in Figure 2-12. The blue dashed lines represent the effective transfer path of SCF in the heat transfer direction. SCF is anisotropic material with much higher thermal conductivity in the axial direction than in the radial direction; the arrangement of SCF in the sintered composites is random, as shown in Figure 2-12 a). The effective transfer path along the heat transfer direction is short, and part of the heat

is transferred along the radial direction of SCF, resulting in low thermal efficiency. After hot rolling, the SCF mainly is arranged along the rolling direction, leading to a longer effective transfer path. And most of the heat is transferred along the axial direction of the SCF, as presented in Figure 2-12 b). Since the axial thermal conductivity of SCF is more than twice that of the pure Al matrix, the longer the effective transfer path of SCF, the higher the thermal conductivity of the composites.

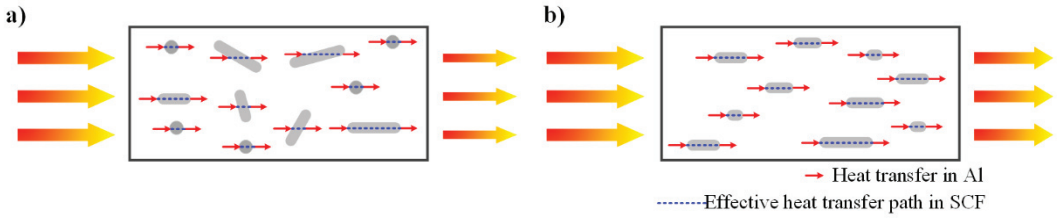

Figure 2-12 Effect of different arrangements of SCF on the thermal conductivity network: a) before hot rolling, b) after hot rolling

2.4 Discussion

2.4.1 Interfacial thermal resistance

Interfacial thermal resistance has always been a critical concern for researchers in studies on the thermal conductivity of composites. The development of numerous theoretical models has facilitated the calculation of interfacial thermal resistance[9,24,26]. However, few studies explored the effect of the interfacial product and product thickness on interfacial thermal resistance. In this study, the interfacial thermal resistance of the composites will be investigated using the interfacial product identified by high-resolution TEM.

For SCF/Al, the interfacial products are mainly amorphous Al-C compounds and Al_4C_3 crystals. Since the physical properties of amorphous Al-C compounds are not yet clear, the parameters related to Al_4C_3 are used in this study to calculate the interfacial thermal resistance. The interface of Cu-SCF/Al is composed of the amorphous Al-C compounds and part of Cu-coating. Thus there are two interfaces for Cu-SCF/Al: Al/Cu/SCF and Al/Al-C/SCF. According to the effective medium calculation model (EMA)[8,27], the interfacial thermal resistance of SCF/Al is:

$$R_{C_{sf}/Al} = R_{Al/Al-C} + R_{Al-C} + R_{Al-C/C_{sf}} \quad (2)$$

The interfacial thermal resistances of Cu-SCF/Al are:

$$R_{Cu-C_{sf}/Al} = xR_i + yR_{ii} \quad (3)$$

$$R_i = R_{Al/Al-C} + R_{Al-C} + R_{Al-C/C_{cf}} \quad (4)$$

$$R_{ii} = R_{Al/Cu} + R_{Cu} + R_{Cu/C_{sf}} \quad (5)$$

$$x + y = 1 \quad (6)$$

In the above equations, $R_{Al/Al-C}$, $R_{Al-C,}$ and $R_{Al-C/SCF}$ are the interfacial thermal resistances of Al/Al-C, Al-C and Al-C/SCF; $R_{Al/Cu}$, $R_{Cu,}$ and $R_{Cu/SCF}$ are the interfacial thermal resistances of Al/Cu, Cu-coating, and Cu/SCF. The x and y are estimated based on EDS analysis at the interface before and after hot rolling. Take x_1=0.25 before hot rolling and x_2=0.10 after hot rolling. For R_{Al-C} and R_{Cu}:

$$R_{Al-C} = t/K_{Al-C} \quad (7)$$

$$R_{Cu} = t/K_{Cu} \quad (8)$$

t represents the thickness of the interface, K_{Al-C} and K_{Cu} represent the thermal conductivity of Al-C and Cu, respectively. $R_{Al/Al-C}$, $R_{Al-C/\ SCF}$, $R_{Al/Cu,}$ and $R_{Cu/SCF}$ are calculated by the acoustic mismatch model:

$$R = \frac{2(\rho_m v_m + \rho_{re} v_{re})^2}{C_m \times {\rho_m}^2 \times {v_m}^2 \times \rho_{re} \times v_{re}} \times \left(\frac{v_{re}}{v_m}\right)^2 \quad (9)$$

In the above equations, ρ, v and C represent density, phonon velocity, and specific heat capacity. The respective parameters of pure Al, Al-C, SCF, and Cu are shown in Table 2-2.

Table 2-2 Thermal conductivity, specific heat capacity, phonon velocity and density of pure Al, Al-C, SCF, and Cu[28]

Materials	Thermal conductivity (W/mK)	Specific heat capacity C (J/kg K)	Phonon velocity-*v* (m/s)	Density-ρ (kg/m^3)
Al	236	895	3620	2700
Al-C	140	800	8160	2360
SCF	550	710	6972	2200
Cu	397	390	3810	8960

Substituting each parameter into Equation (2)-Equation (9), the interfacial thermal resistance of sintered SCF/Al is 5.73×10^{-9} m^2KW^{-1}. The interfacial thermal resistance of hot-rolled SCF/Al is 5.75×10^{-9} m^2KW^{-1}. The interfacial thermal resistance of sintered Cu-SCF/Al is 4.92×10^{-9} m^2KW^{-1}. The interfacial thermal resistance of hot-rolled Cu-SCF/Al is 5.25×10^{-9} m^2KW^{-1}. Therefore, when the thermal conductivity of the interfacial product is low (140 W/mK for Al-C), the product thickness is proportional to the interfacial thermal resistance. For SCF/Al, the severe reaction of SCF with the matrix generated a thicker Al-C interface, resulting in higher interfacial thermal resistance and lower interfacial thermal conductivity. The Cu-coating inhibits the interfacial reaction between SCF and the Al matrix, leading to lower interfacial thermal resistance.

2.4.2 Texture evolution and dynamic recrystallization mechanism

Orientation distribution functions (ODF) of texture evolution of pure Al, SCF/Al, and Cu-SCF/Al before and after hot rolling are shown in Figure 2-13. Sections were made at φ2=0°, 45°, and 90° to show the typical texture of face-centered cubic (FCC) metals. There is a high content of rotated cube (Rot-C) component in the pure Al before hot rolling, as performed in Figure 2-13 a), b), c). While the content of Copper (φ1=90°, Φ=35°, φ2=45°) component in SCF/Al and Cu-SCF/Al is higher. The cube component is a typical recrystallization texture[29,30], so the microstructure evolution of pure Al

blocks during sintering is dominated by recrystallization. The copper component is a characteristic β fiber texture[30], and the higher content of the Copper component in composites is attributed to the deformation of Al matrix grains caused by the addition of SCF. The cube component in the pure Al disappears after hot rolling, and the P (φ1=70°, Φ=45°, φ2=90°) component is dominant, as illustrated in Figure 2-13 d), e), f). P component and rotated-Gauss (Rot-G) (φ1=0°, Φ=90°, φ2=45°) component are formed in SCF/Al and Cu-SCF/Al after hot rolling.

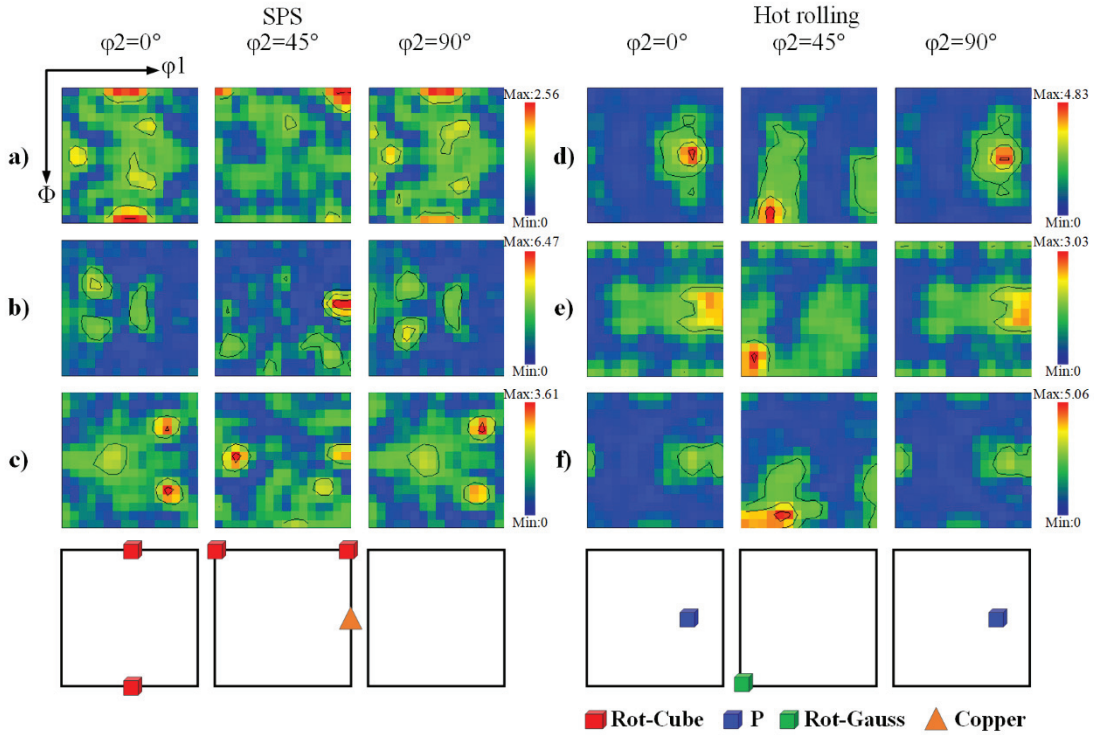

Figure 2-13 ODF diagrams and the typical component of composites: a) Sintered pure Al, b) Sintered SCF/Al, c) Sintered Cu-SCF/Al, d) Hot-rolled pure Al, e) Hot-rolled SCF/Al, f) Hot-rolled Cu-SCF/Al

The orientation strengths of each texture along the α and β orientation lines are calculated to deeply analyze the evolution of textures, as indicated in Figure 2-14. In the α orientation line, the pure Al, SCF/Al and Cu-SCF/Al after hot rolling have prominent P components. P component is a kind of recrystallization texture, which is commonly found in Al alloys' rolling deformation or annealing process, evolving from further deformation of grains in the shear band (SB)[31,32]. The orientation strength of the P component in pure Al is 6.11, while that in SCF/Al and Cu-SCF/Al is 2.35 and

3.30, respectively. It reveals that the recrystallized grains formed by SB in hot-rolled pure Al are more than SCF/Al and Cu-SCF/Al. This phenomenon is attributed to the good metallurgical bonding of pure Al. The strain instability led to SBs along the rolling direction of (RD) ±35°[33] during enormous strain rolling deformation. Pure Al is a metal undergoing plastic deformation through dislocation slip. Since there are no defects such as holes, the SB could cross the grain boundaries without deviation. This process would promote the formation of recrystallized grains by nucleation of grains of specific orientation within the SB.

For SCF/Al and Cu-SCF/Al, the movement of the SB is hindered by the addition of SCF so that fewer recrystallized grains are generated through the SB. We also note that the strength of the P component in Cu-SCF/Al is slightly higher than that of SCF/Al and has a higher strength of Gauss (φ1=0°, Φ=45°, φ2=90°) component. They are presumably related to the enhanced interfacial coherence of the Al matrix and SCF by the Cu-coating. The high interfacial coherence improves the deformation coordination, so the interfacial mismatch energy in Cu-SCF/Al is lower than that in SCF/Al, which is more favourable for the motion of SBs and nucleation recrystallized grains.

In the β orientation line, the hot-rolled SCF/Al and Cu-SCF/Al have higher strength of Rot-G components, while the content of the Rot-G component in pure Al is extremely low. The Rot-G component is generally produced during the hot rolling of FCC metals and is transformed from the Copper component or Brass component. The Rot-G component is more resistant to plane strain compression than other orientations. Therefore, it could be retained during the hot rolling[34]. It has been shown that the Rot-G component facilitates the generation of 35°-45° SBs. The recrystallized grains are generated in SBs with higher storage energy than the matrix. Consequently, the Rot-G component promotes the formation of cubically oriented recrystallized grains by facilitating the formation of SBs[35,36]. There is a higher content of copper components in SCF/Al and Cu-SCF/Al before hot rolling, as shown in Figure 2-13, which facilitates the generation of the Rot-G component during rolling. In addition, certain content of Cube (φ1=0°, Φ=0°, φ2=0°) components is observed in SCF/Al.

On the one hand, the Cube grains are further transformed from Rot-G. On the other hand, deformation bands also promote the nucleation of Cube grains. Due to the defects in the Al matrix, the deformation degree of nearby grains is large during the thermal deformation, which promoted the nucleation of recrystallized grains, as described in Figure 2-5 d).

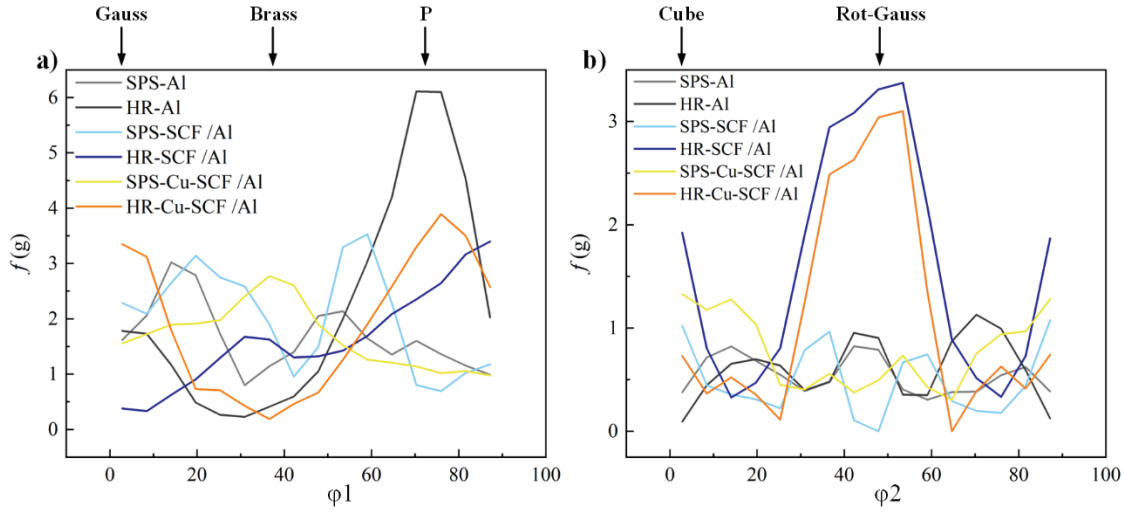

Figure 2-14 a) Texture orientation strength of the composites along the α orientation line, b) texture orientation strength of the composites along the β orientation line

The texture distribution in pure Al, SCF/Al, and Cu-SCF/Al before and after hot rolling, as illustrated in Figure 2-15. Comparison of the distribution of Copper components before and after hot rolling in SCF/Al and Cu-SCF/Al could more visually confirm the transition of Copper components to the recrystallized component during the hot rolling. The P-oriented grains strongly depended on the Rot-G-oriented grains, as depicted in Figure 2-15, b), d), f). Comparing Figure 2-15 d) and f), the grain size of the P-oriented grains and Rot-G-oriented grains of the Cu-coated composites are larger, the grains are in the growth stage. In Cu-coated composites, the Cu-coated SCF has strong interfacial coherence with the Al matrix. There are fewer defects such as oxides and pores in the Al matrix; therefore, the continuity of the Al matrix is better. These factors are conducive to the movement of SBs and provide energy for the nucleation and growth of grains of P-oriented grains and Rot-G-oriented grains.

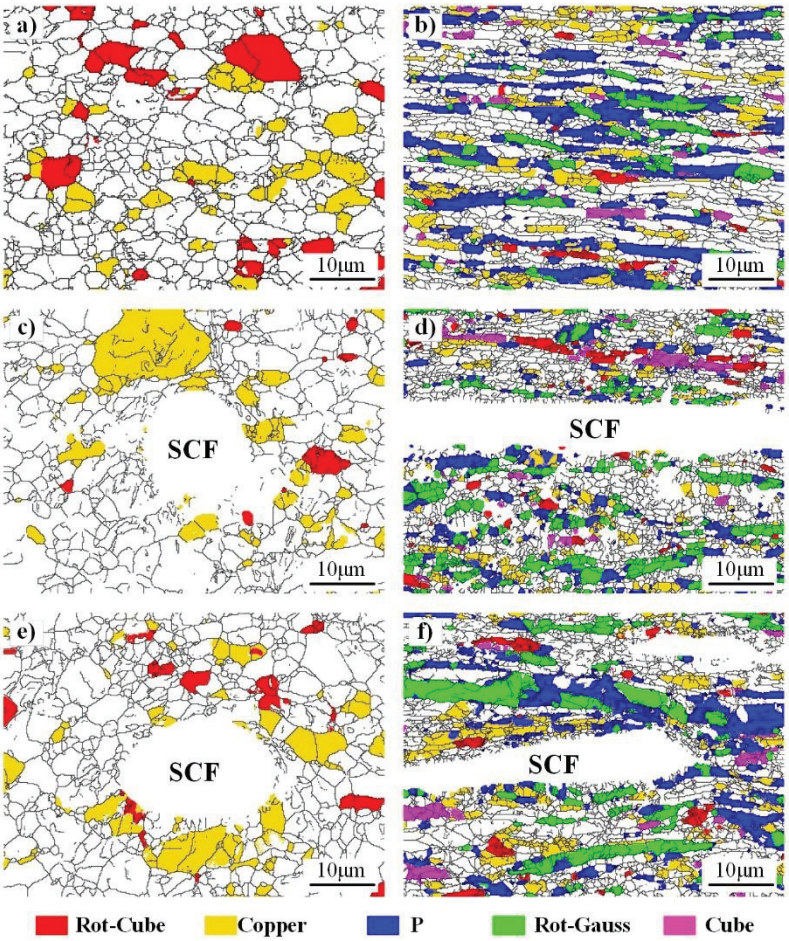

Figure 2-15 Distribution of different textures: a) Sintered pure Al, b) Hot-rolled pure Al, c) Sintered SCF/Al, d) Hot-rolledSCF/Al, e) Sintered Cu-SCF/Al, f) Hot-rolled Cu-SCF/Al

2.5 Summary

This study investigated the effects of Cu-coating on the microstructure evolution, interfacial properties, thermal properties, and texture evolution of SCF-reinforced Al matrix composites. After the analysis and discussion, the main conclusions were obtained as follows:

(1) The Cu-coating increases interfacial coherence, promotes interfacial bonding, and enhances interfacial strength. The protection of the SCF structure by the Cu-coating leads to higher yield strength and thermal conductivity.

(2) During the hot rolling, the uncoated SCF reacted severely with the Al matrix and generated the harmful phase Al_4C_3. Hot rolling promotes the arrangement of SCF along the rolling direction, and the yield strength of Cu-SCF/Al increases by 121.93%.

(3) The thermal conductivity is improved by 6.64%, close to the ideal value calculated by the layered parallel model.

(4) The analysis of the texture evolution clarifies three dynamic recrystallization mechanisms of SCF/Al and Cu-SCF/Al before and after hot rolling. In this study, Cu-coating on the surface of SCF was used to adjust the interface of the composites, which inspires the coordinated improvement of thermal and mechanical properties.

2.6 References

[1]. S Lakra, TK Bandyopadhyay, S Das, K Das. Thermal conductivity of in-situ dual matrix aluminum composites with segregated morphology[J]. Mater. Res. Bull. 2021, 144:111515.

[2]. H Cao, YS Su, D Zhang, QB Ouyang. Fabrication, mechanical and thermal behaviors of antiperovskite manganese nitride $Mn_{3.1}Zn_{0.5}Sn_{0.4}N$ reinforced aluminum matrix composites[J]. Compos Part B-Eng. 2021, 223:109080.

[3]. QB Liu, GL Fan, ZQ Tan, Q Guo, DB Xiong, et al. Reinforcement with intragranular dispersion of carbon nanotubes in aluminum matrix composites[J]. Compos Part B-Eng. 2021, 217:108915.

[4]. S Bi, ZY Liu, BL Xiao, YN Zan, D Wang, QZ Wang, et al. Enhancing strength-ductility synergy of carbon nanotube/7055Al composite via a texture design by hot-rolling[J]. Mater. Sci. Eng. A. 2021, 806: 140830.

[5]. H Naji, SM Zebarjad, SA Sajjadi. The effects of volume percent and aspect ratio of carbon fiber on fracture toughness of reinforced aluminum matrix composites[J]. Mater. Sci. Eng. A. 2008, 486:413-420.

[6]. M Jagannatham, P Chandran, S Sankaran, P Haridoss, N Nayan, et al. Tensile properties of carbon nanotubes reinforced aluminum matrix composites: A review[J]. Carbon. 2020, 160:14-44.

[7]. Zhu C, Su Y, Wang X, Sun H, Ouyang Q, Zhang D. Process optimization, microstructure characterization and thermal properties of mesophase pitch-based carbon fiber reinforced aluminum matrix composites fabricated by vacuum hot pressing[J]. Compos Part B-Eng. 2021;215: 108746.

[8]. LF Yi, T Yamamoto, T Onda, ZC Chen. Orientation control of carbon fibers and enhanced thermal/mechanical properties of hot-extruded carbon fibers/aluminum composites[J]. Diam. Relat. Mater. 2021, 116: 108432.

[9]. R Pei, G Chen, Y Wang, M Zhao, G Wu. Effect of interfacial microstructure on the thermal-mechanical properties of mesophase pitch-based carbon fiber reinforced aluminum composites[J]. J. Alloy. Compd. 2018, 756:8-18.

[10]. B Guo, S N, J Yi, R Shen, Z Tan, et al. Microstructures and mechanical properties of carbon nanotubes reinforced pure aluminum composites synthesized by spark plasma sintering and hot rolling[J]. Mater. Sci. Eng. A. 2017, 698:282-288.

[11]. B Guo, S Luo, Y Wu, M Song, B Chen, Yu Z, et al. Regulating the interfacial reaction between carbon nanotubes and aluminum via copper nano decoration[J]. Mater. Sci. Eng. A. 2021, 820:141576.

[12]. WD Fei, ZJ Li, YB Li. Effects of T4 treatment on hot rolling behavior and tensile strength of aluminum matrix composite reinforced by aluminum borate whisker with NiO coating[J]. Mater. Chem. Phys. 2006, 97:402-409.

[13]. L Jiang, P Wang, Z Xiu, G Chen, X Lin, et al. Interfacial characteristics of diamond/aluminum composites with high thermal conductivity fabricated by squeeze-

casting method[J]. Mater. Charact. 2015, 106:346-351.

[14]. JJ Sha, ZZ LÜ, RY Sha, TF Zu, JX Dai JX, et al. Improved wettability and mechanical properties of metal coated carbon fiber-reinforced aluminum matrix composites by squeeze melt infiltration technique[J]. Trans. Nonferrous Met. Soc. China. 2021, 31:317-330.

[15]. A Maqbool, MA Hussain, FA Khalid, N Bakhsh, A Hussain, MH Kim. Mechanical characterization of copper coated carbon nanotubes reinforced aluminum matrix composites[J]. Mater. Charact. 2013, 86: 39-48.

[16]. R Fan, Y Huang, XP Han, XY Peng. High thermal conductivity and mechanical properties of Si@Graphite/Aluminum nitride/aluminum composites for high-efficiency thermal management[J]. J. Alloy. Compd. 2021, 858:157630.

[17]. BS Guo, Y Chen, Z Wang, J Yi, S Ni, et al. Enhancement of strength and ductility by interfacial nano-decoration in carbon nanotube/aluminum matrix composites[J]. Carbon. 2020, 159:201-212.

[18]. SI Ghazanlou, B Eghbali, R Petrov. Study on the microstructural and texture evolution of Hot Rolled Al7075/ graphene/ carbon nanotubes reinforced composites[J]. Mater. Chem. Phys. 2021, 257:123766.

[19]. CY Huang, SP Hu, K Chen. Influence of rolling temperature on the interfaces and mechanical performance of graphene-reinforced aluminum-matrix composites[J]. Int. J. Min. Met. Mater. 2019, 26:752-759.

[20]. C Yuan, Z Tan, G Fan, M Chen, Q Zheng, Z Li. Fabrication and mechanical properties of CNT/Al composites via shift-speed ball milling and hot-rolling[J]. J. Mater. Res. 2019, 34:2609-2619.

[21]. Y Guo, XG Liu, ZF Xu, WQ Li, G Sasaki. Effect of VGCNF on high-temperature deformation performance and softening mechanism of aluminum matrix[J]. J. Alloy. Compd. 2020, 818:152923.

[22]. B Sadeghi, P Cavaliere, GA Roeen, M Nosko, M Shamanian, et al. Hot rolling of MWCNTs reinforced Al matrix composites produced via spark plasma sintering[J]. Adv. Compos. Hybrid Mater. 2019, 2:549-570.

[23]. C Zhu, Y Su, D Zhang, QB Ouyang. Effect of Al_2O_3 coating thickness on microstructural characterization and mechanical properties of continuous carbon fiber reinforced aluminum matrix composites[J]. Mater. Sci. Eng. A. 2020, 793:139839.

[24]. C Zhou, G Ji, Z Chen, M Wang, A Addad, D Schryvers,et al. Fabrication, interface characterization and modeling of oriented graphite flakes/Si/Al composites for thermal management applications[J]. Mater. Des. 2014, 63:719-728.

[25]. Z Li, C Wang, L Xia, H Yang, C Qin, B Zhong, et al. Significant improvement of thermal conductivity for AlN/LAS composite with low thermal expansion[J]. Ceram. Int. 2020, 46:28668-28675.

[26]. AT Miranda, L Bolzoni, N Barekar, Y Huang, J Shin, SH Ko, et al. Processing, structure and thermal conductivity correlation in carbon fibre reinforced aluminium metal matrix composites[J]. Mater. Des. 2018, 156:329-339.

[27]. Z Shi, W Yang, J Wang, G Liu, G Qiao, Z Jin. Effect of interfacial structure on the thermal conductivity of carbon nanofibers reinforced aluminum nitride composites[J]. Ceram. Int. 2013, 39:3365-3370.

[28]. N Li, L Wang, J Dai, X Wang, J Wang, MJ Kim, et al. Interfacial products and thermal conductivity of diamond/Al composites reinforced with ZrC-coated diamond particles[J]. Diam. Relat. Mater. 2019, 100:107565.

[29]. S Attarilar, M Ebrahimi, TH Hsieh, JY Uan, C Göde. An insight into the vibration-assisted rolling of AA5052 aluminum alloy: Tensile strength, deformation microstructure, and texture evolution[J]. Mater. Sci. Eng. A. 2021, 803:140489.

[30]. MH Alvi, SW Cheong, JP Suni, H Weiland, AD Rollett. Cube texture in hot-rolled aluminum alloy 1050 (AA1050)-nucleation and growth behavior[J]. Acta. Mater. 2008, 56:3098-3108.

[31]. O Engler, K Lacke. Mechanisms of recrystallization texture formation in Aluminium alloys[J]. Scr. Metall. Mater. 1992, 27:1527-1532.

[32]. P Qu, L Zhou, VL Acoff . Deformation textures of aluminum in a multilayered Ti/Al/Nb composite severely deformed by accumulative roll bonding[J]. Mater. Charact. 2015, 107:367-375.

[33]. M Hatherl, AS Malin. Shear bands in deformed metals[J]. Scr. Metall. 1984,

18:449-454.

[34]. S Deb, SK Panigrahi, M Weiss. The effect of annealing treatment on the evolution of the microstructure, the mechanical properties and the texture of nano SiC reinforced aluminium matrix alloys with ultrafine grained structure[J]. Mater. Charact. 2019, 154:80-93.

[35]. T Nguyen-Minh, JJ Sidor, RH Petrov, LAI Kestens. Occurrence of shear bands in rotated Goss ({110}<110>) orientations of metals with bcc crystal structure[J]. Scr. Mater. 2012, 67:935-938.

[36]. M Mehdi, Y He, EJ Hilinski, LAI Kestens, A Edrisy. The evolution of cube ({001}<100>) texture in non-oriented electrical steel[J]. Acta. Mater. 2020, 185:540-554.

Chapter 3

Effect of short carbon fiber and nano carbon fiber as reinforcement on microstructure and properties of hot-rolled aluminum matrix composites

3.1 Introduction

With the rapid development of aerospace, microelectronic devices, and other fields, the demands for lightness, strength, and thermal conductivity of materials have increased[1-4]. As one of the largest reserves of light metals in the earth's crust[5,6], the aluminum (Al) is attracting considerable critical attention. The composites prepared with Al have a wide range of applications[7,8]. The size, shape, strength, wear resistance, and thermal conductivity of the reinforcement directly affect the overall performance of the composites. Therefore, the choice of reinforcement is crucial in the design of Al matrix composites[9].

Carbon fibers (CFs) and carbon nanofibers (CNFs) attract widespread attention for their high strength and excellent physical properties[10,11]. Especially in terms of thermal conductivity, carbon-based reinforcements have absolute advantages over ceramic reinforcements, making them ideal for the preparation of semiconductor and heat-dissipating components[1,3,10,12]. CFs are generally micron in diameter with high strength, excellent thermal conductivity, and easy to disperse in the Al matrix[12]. As the cost of preparing CFs gradually decreases, there are excellent prospects for large-scale applications[13,14]. The CNFs also play an essential role in electronics and optics for their ultra-high thermal conductivity[2,6,7,15,16]. However, the different diameters of CFs and CNFs led to different strengthening mechanisms, which further affect the composites' strength, interfacial properties and microstructure evolution[3,17-20]. The current studies point out that the aggregation of nanoscale reinforcements, exemplified by CNFs, in the Al matrix weakens the overall properties of the composites due to their small diameters and large aspect ratios[21-24]. On the other hand, the micron-scale reinforcement, as exemplified by CFs, produces a splitting effect on the Al matrix and damages the plastic deformability[1,13].

Researchers have conducted a series of studies on the effects of CFs and CNFs as reinforcements on the properties of composites: The experimental results of Deshpande et al.[25], Wu[26] and Eid[27] show that CF with appropriate volume fraction could be

uniformly dispersed in the matrix. However, when the fraction of CF increases to more than 5%, it will lead to a decrease in strength and plasticity due to damage to the integrity of the Al matrix. Wang et al.[28] believe that the strong interfacial reaction between CF and Al and the destruction of CF structure are the main reasons for the macroscopic failure of materials. In addition, the aggregation of CNFs leads to the degradation of material properties, which is generally regarded as an insurmountable problem[29-32]. Yadav et al.[33] pointed out that the aggregation of CNFs will lead to weak interface bonding with the metal matrix, negatively impacting the composites' strength and electrical conductivity. The results of Miranda[34] show that aggregation of nanoscale reinforcements leads to an increase in the porosity, which leads to a decrease in mechanical properties and thermal conductivity. Chung[35] compared the effects of CF with a diameter of 7-15 μm and carbon filaments with a diameter of 160 nm on the properties of the composites. The results show that the tensile strength of carbon filaments-reinforced composites was only 42% of that of CF-reinforced composites. The study of Shim et al.[36] shows that the cross-section shape and size of CF impact the composites' performance.

Existing research have only described the influence of CFs with different diameters on the properties of composites. However, the influence mechanism of reinforcement diameter on the microstructure evolution, mechanical properties and subsequent thermal deformation still needs to be further clarified. The interfacial structure and properties of the CF and CNFs with Al also need further characterization and analysis. It is important to clarify the influence mechanism of CF and CNF on the properties of composites under the same volume fraction, which is of guiding significance for the design and application of composites. So, in this paper, SCF (6-8 μm in diameter) and VGCNF (in the range of 150-200 nm in diameter) reinforced Al matrix composites were prepared by the SPS to investigate the effects on the microstructure, interfacial bonding, thermal and mechanical properties of the composites.

3.2 Materials and methods

The pure Al powders used in this study were obtained from Kojundo Chemical Laboratory Co., Ltd (Japan); the average size of the particles is 3 μm. The SCFs were obtained from Mitsubishi Chemical Corporation (Japan). The VGCNFs were obtained from Showa Denko Co., Ltd (Japan). The electron micrographs and physical properties of SCF and VGCNF are performed in Figure 3-1a), b) and Table 3-1, respectively.

Table 3-1 The physical properties of SCF and VGCNF

Reinforcement	Diameter	Density (g/cm^3)	Modulus (GPa)	Tensile strength (MPa)	Thermal conductivity (W/mK)
SCF	11 μm	2.20	900	3800	550
VGCNF	150-200 nm	2.00	240	2920	1950

When preparing composites, SCFs and VGCNFs were first weighed separately at vol.3%, cleaned in acetone solution, and then mixed thoroughly with vol.97% pure Al powders in the alcohol solution, as shown in Figure 3-1. The mixed solution was shaken in ultrasound for 10 minutes and then injected into a closed Al can with 10 mm diameter alumina spheres for ball-milling mixing. It was then dried in the vacuum environment to get uniformly mixed powders. The mixed powders were vacuum sintered in the SPS equipment for 30 minutes, the sintering temperature was 550 °C, and the pressure was 50 MPa. To avoid contamination by impurities on the rolls, the surface of sintered composites was wrapped with a layer of Al foil and hot-rolled at 450°C with a 70% roll-off. For comparison, the pure Al blocks were prepared under the same conditions.

Tensile tests were performed at room temperature (25°C) using an INSTRON 8801 hydraulic servo fatigue tester, the tensile direction was parallel to the rolling direction, and the strain rate was $8.3\times10^{-4}s^{-1}$. Three samples were prepared for each material to minimize errors. The thermal conductivity of pure Al and composites was measured parallel to the rolling direction. The nano hardness at the interface of composites was carried out using an ELIONIX ENT-1100A nano hardness tester with a load of 0.4 mN and a holding time of 15 s. The morphology of composites was

observed using a JXA-ISP100 scanning electron microscope (SEM). Electron backscatter diffraction (EBSD) characterization was analyzed using a Zeiss Sigma 300 scanning electron microscope equipped with an Oxford-SYMMETRY. The interfacial products of composites were investigated using a JEOL transmission electron microscope (TEM).

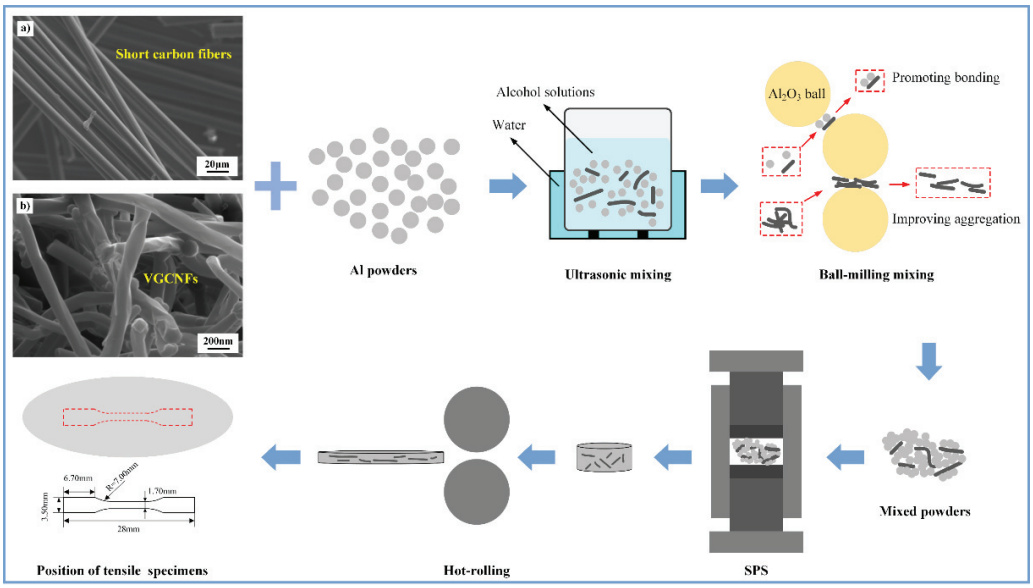

Figure 3-1 The electron micrographs of SCF and VGCNF, and the schematic diagrams of the preparation of composites

3.3 Results

3.3.1 Microstructure

The SEM morphologies of the SCF reinforced Al matrix composites (SCF/Al) and VGCNF reinforced Al matrix composites (VGCNF/Al) before and after hot rolling are shown in Figure 3-2. In the sintered SCF/Al, the SCFs are uniformly dispersed in the Al matrix, and no aggregation occurs. There are no obvious gaps at the interface, as performed in Figure 3-2 a) and a1). In the sintered VGCNF/Al, the VGCNFs agglomerate together because of their small diameter. They are dispersed in the Al matrix as clusters, as presented in Figure 3-2 c) and c_1). After hot rolling, the SCF aligned parallel to the rolling direction. Owing to the addition of SCF, cracks appeared after hot rolling, as shown in Figure 3-2 b). However, the morphology of the VGCNF

cluster changed and elongated in the rolling direction, as presented in Figure 3-2 d) and d_1).

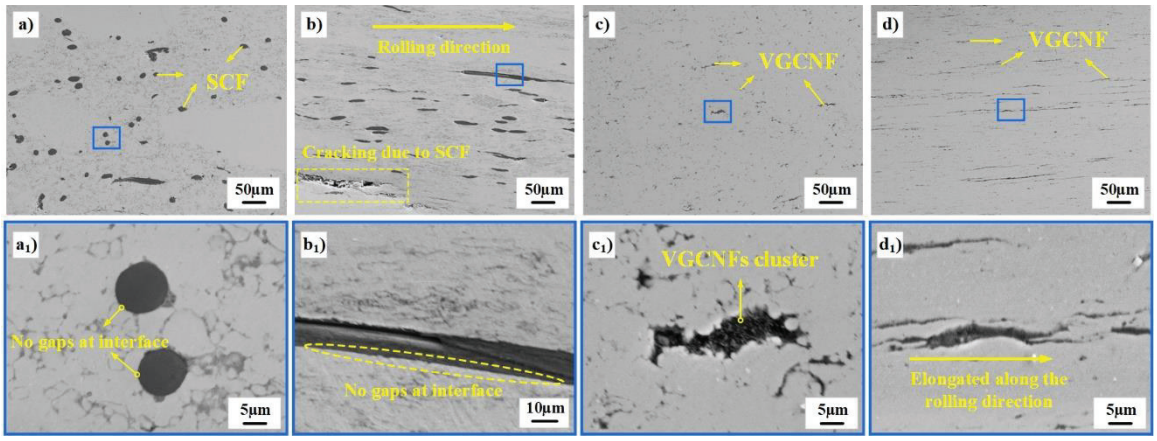

Figure 3-2 SEM morphology and local magnification of composites: a), a_1) Sintered SCF/Al; b), b_1) Hot-rolled SCF/Al; c), c_1) Sintered VGCNF/Al; d), d_1) Hot-rolled VGCNF/Al

The EBSD Map, grain boundary diagram, Local Misorientation (KAM) diagram and grain size and grain boundary distribution of pure Al, SCF/Al and VGCNF/Al before hot-rolling are demonstrated in Figure 3-3. Comparison of Figure 3-3 a), b) and c) shows that small size grains appear near the reinforcement in SCF/Al and VGCNF/Al. Indicating that the reinforcement hindered the growth of nearby grains during the sintering process. In the KAM diagram, the green lines show the region of higher stress[37]. There are more low-angle grain boundaries and higher stress at the interface of SCF/Al compared with VGCNF/Al, as shown in Figure 3-3 b_1), b_2) and c_1), c_2). Comparison of Figure 3-3 a_3), b_3) and c_3) shows more small-sized grains in the 0-1 μm range in SCF/Al. These results indicate that SCF leads to higher lattice distortion in Al matrix than VGCNF.

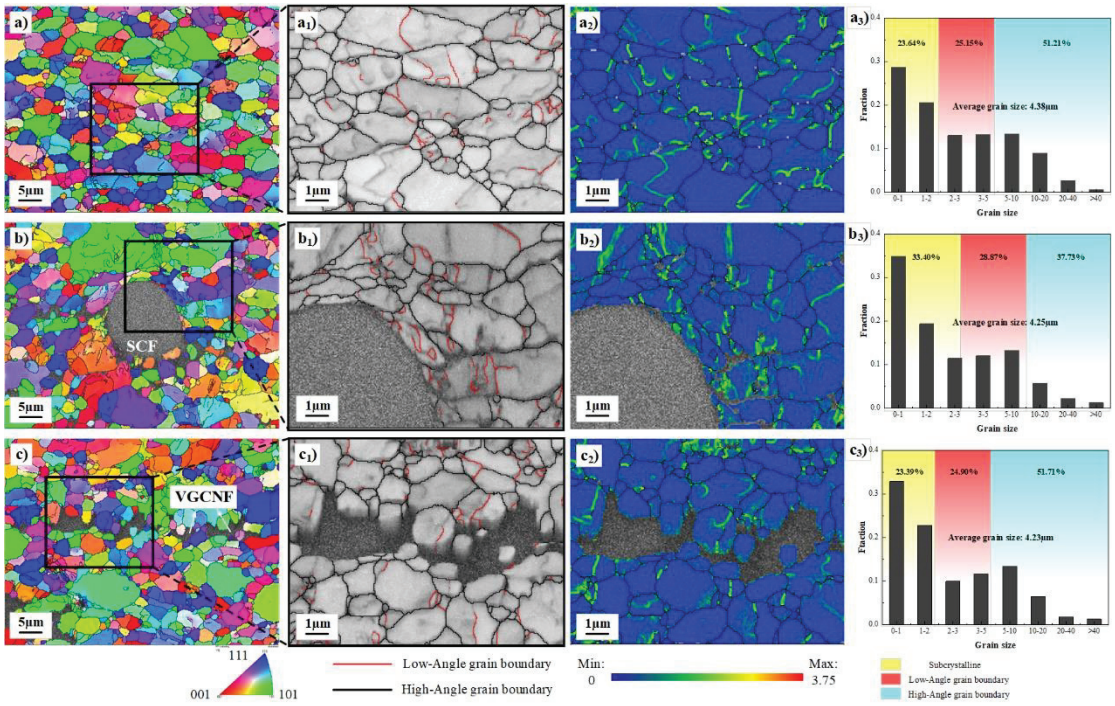

Figure 3-3 The EBSD Map, Grain boundary diagram, KAM diagram and grain size and grain boundary distribution of pure Al, SCF/Al and VGCNF/Al before hot-rolling: a), a_1), a_2), a_3) Pure Al; b), b_1), b_2), b_3) SCF/Al; c), c_1), c_2), c_3) VGCNF/Al

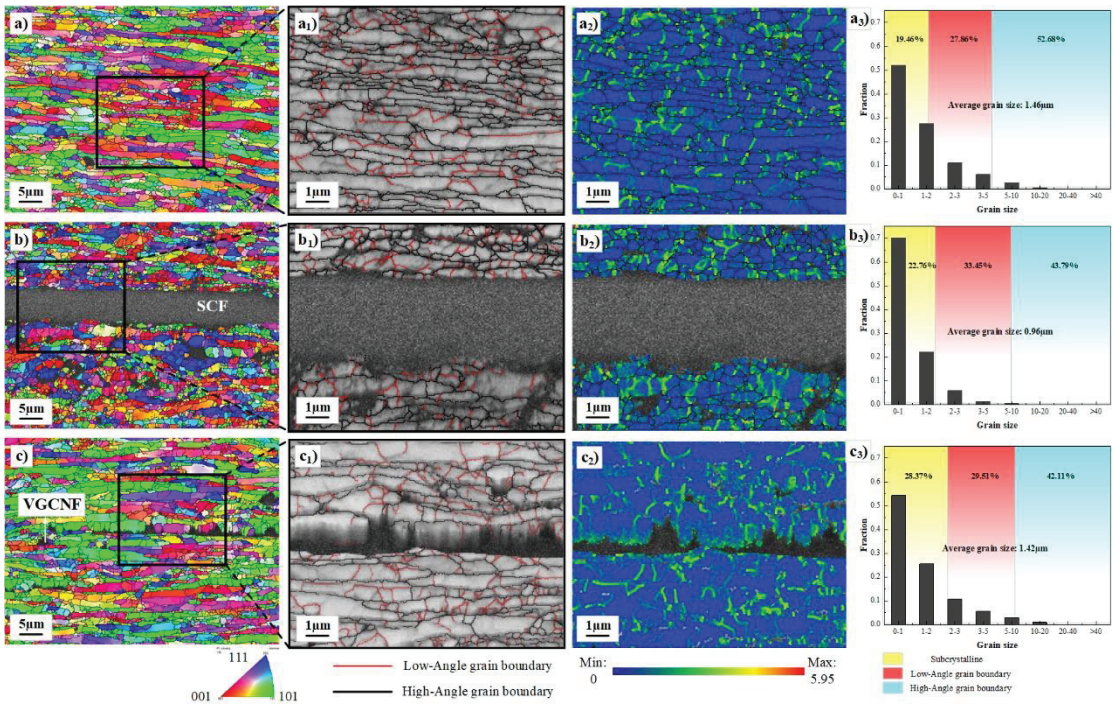

Figure 3-4 The EBSD Map, Grain boundary diagram, KAM diagram and grain size and grain boundary distribution of pure Al, SCF/Al and VGCNF/Al after hot-rolling: a), a_1), a_2), a_3) Pure Al; b), b_1), b_2), b_3) SCF/Al; c), c_1), c_2), c_3) VGCNF/Al

After hot rolling, the grains of each material are elongated along the rolling direction, and the grain size is substantially reduced, as shown in Figure 3-4. The comparison shows that the average grain size of SCF/Al after hot rolling is the smallest, with the more fine grains in the range of 0-1 μm and low angle grain boundaries. It is shown that during the hot rolling process, the SCF plays a role in hindering the grain growth and grain boundary movement due to its large size. In contrast, the small size of VGCNFs clusters has less hindering effect on grain boundary movement and grain growth.

3.3.2 Interface

To investigate the interfacial bonding of the two composites, nano-hardness tests were carried out on the interfaces of SCF/Al and VGCNF/Al before and after hot rolling, respectively. The results are concluded in Figure 3-5. In Figure 3-5 a), the hardness values at the interface of all materials are higher than those of the Al matrix. The curves in Figure 3-5 b) also show that the penetration depth of the indenter is deeper into the surface of the matrix. It shows that the phase distribution and interfacial structure of the composites are different from the matrix. Meanwhile, the interfacial hardness values of SCF/Al before and after hot-rolling are higher than those of VGCNF/Al. In particular, the interfacial hardness of SCF/Al increases substantially after hot-rolling. This indicates that the interfacial structures of SCF and VGCNF with Al are quite different.

To further investigate the interfacial structure of the two composites, high-resolution TEM observations at the interface were conducted. The high-resolution TEM morphology at the SCF/Al interface before and after hot-rolling and the FFT transitions are displayed in Figure 3-6 a), b). Continuous amorphous carbides were generated at the interface between the SCF and the Al matrix, as illustrated in Figure 3-6 a). During hot rolling, the strong plastic deformation leads to high energy at the interface, which promotes the movement of carbon and Al atoms. Finally leads to the formation of crystalline Al_4C_3 after hot rolling, as depicted in Figure 3-6 b).

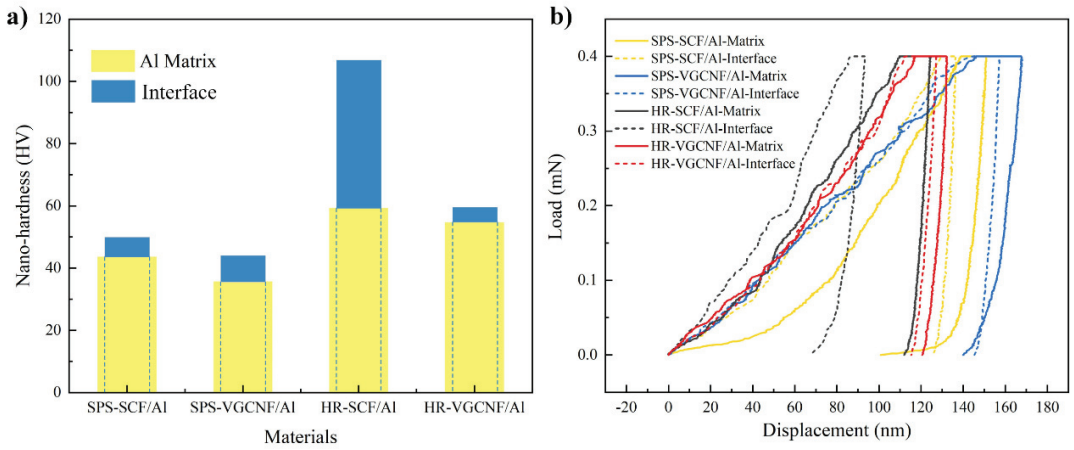

Figure 3-5 Nano hardness results at the composites interface and matrix before and after hot-rolling: a) Nano hardness values; b) Load-displacement curves

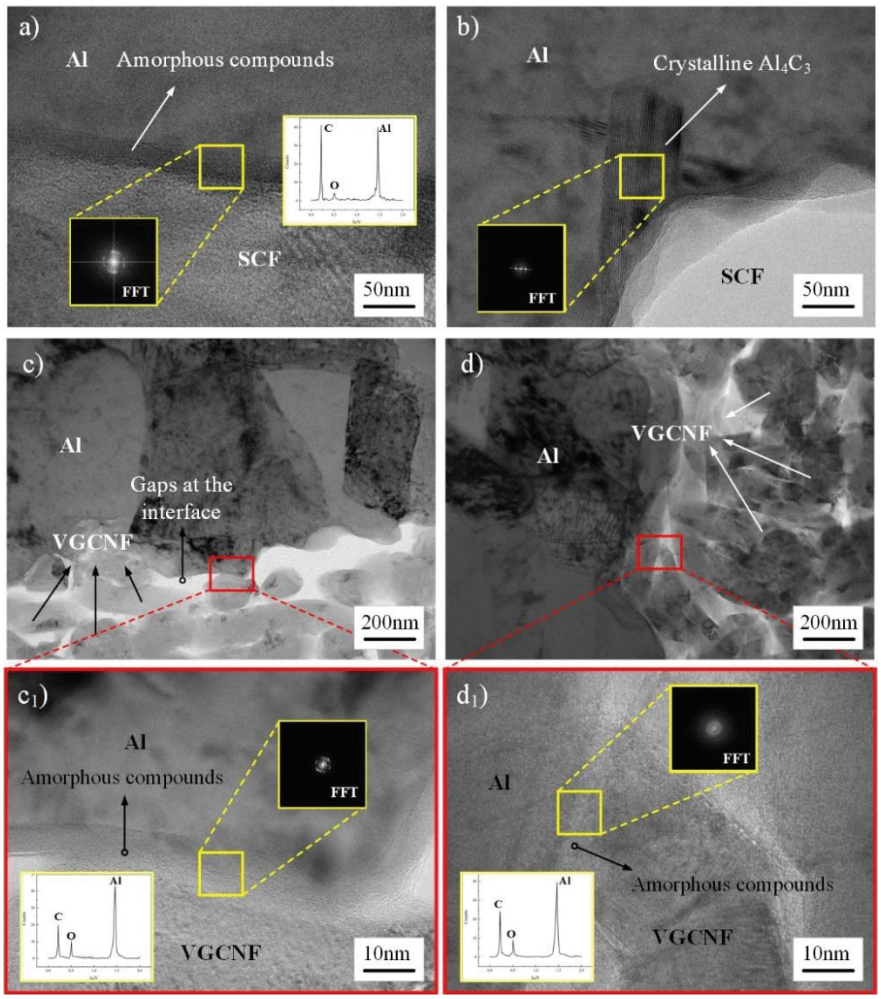

Figure 3-6 High-resolution TEM morphology of the interface in SCF/Al: a) before hot rolling, b) after hot rolling; Interfacial morphology of VGCNF/Al: c) before hot rolling, d) after hot rolling; High-resolution TEM morphology of the interface in VGCNF/Al: c_1) before hot rolling, d_1) after hot rolling

The interfacial morphology and high-resolution TEM morphology at the interface of VGCNF/Al before and after hot-rolling are provided in Figure 3-6 c), c_1), d) and d_1). As shown in Figure 3-6 c), there are some gaps between the VGCNF clusters and the Al matrix. Amorphous carbides were generated in the region where the Al matrix contacted with VGCNF, as depicted in Figure 3-6 c_1). After hot-rolling, the gaps between the VGCNF clusters and the Al matrix are reduced, and amorphous carbides are generated in the region where they are in contact, as illustrated in Figure 3-6 d) and d_1). Owing to the aggregation between VGCNFs, only some products were generated at the interface. This is also the reason for the low interfacial hardness of the VGCNF/Al.

3.3.3 Thermal conductivity

The composition of the thermal conductivity (K) of the composites can be simplified into three components: the interfacial thermal conductivity (K_I), the effective thermal conductivity of the Al matrix (K^{eff}_{Al}), and the effective thermal conductivity of the reinforcement (K^{eff}_{R}). The experimentally measured values of thermal conductivity of pure Al and composites are shown in Table 3-2. The values of K^{eff}_{R}, K_I and K^{eff}_{Al} are calculated separately.

To simplify the calculation, the VGCNF clusters are considered as a whole. According to the regular distribution model of the reinforcement, the thermal resistance of the composites is equal to the sum of the thermal resistance of each part[38,39]. The simplified equation is as follows:

$$L/K = L_{Al}/K_{Al} + L_R/K_R + L_I/K_I \quad (1)$$

where L, L_{Al}, L_R, L_I are the length of the composite, pure Al, reinforcement and interface along the heat flow transfer direction, respectively; K, K_{Al}, K_R, K_I are the thermal conductivity of the composites, Al matrix, reinforcement and interface, respectively.

The measured thermal conductivity of the composites, 238 W/(mK) for pure Al, 550 W/(mK) for SCF, and 1950 W/(mK) for VGCNF were substituted into Equation (1) to obtain the K_I of SCF/Al and VGCNF/Al before and after hot rolling, as shown in Table 3-2.

The previous studies suggest that dislocations and low-angle grain boundaries have a negative effect on the heat transfer in the Al matrix[9,40]. Therefore, the thermal conductivity of the Al matrix in the composites is lower than 100% under ideal conditions. The KAM values can represent the density of dislocations and low-angle grain boundaries. To calculate the K^{eff}_{Al} of the Al matrix, a simplified model is established based on the thermal conductivity values of pure Al and KAM values as follows:

$$y = a/x \tag{2}$$

where y is the thermal conductivity, x is the KAM value, and a is the coefficient.

The thermal conductivity and the KAM values of pure Al in the sintered state are brought into Equation (2) to obtain a_1=222.15 W/(mK); the thermal conductivity and the KAM values of pure Al after hot rolling are brought into Equation (2) to obtain a_2=267.00 W/(mK). The K^{eff}_{Al} of the Al matrix in the sintered and hot-rolled state composites are:

$$K^{eff}{}_{Al-Sintered} = V_{Al} \times (222.15/x) \tag{3}$$

$$K^{eff}{}_{Al-Hot\ rolled} = V_{Al} \times (267.00/x) \tag{4}$$

where the V_{Al} in the above equation is the volume fraction of pure Al in the composites.

The KAM values of SCF/Al and VGCNF/Al before and after hot rolling were brought into the calculation to obtain K^{eff}_{Al}, and $K^{eff}_{R} = K - K_I - K^{eff}_{Al}$, as presented in Table 3-2.

Table 3-2 Thermal conductivity parameters of composites

Materials	K (W/mK)	K_I (W/mK)	K^{eff}_{Al} (W/mK)	K^{eff}_{R} (W/mK)
Sintered-SCF/Al	207.42	0.60	195.89	12.69
Hot-rolled-SCF/Al	211.41	0.44	210.81	10.02
Sintered-VGCNF/Al	246.52	0.71	220.27	26.20
Hot-rolled-VGCNF/Al	249.87	1.09	216.40	32.38

According to the calculation results shown in Table 3-2, the contribution of the interfacial thermal conductivity to the thermal conductivity of the material is small. To compare the heat transfer efficiency of SCF and VGCNF clusters, the following

calculations are performed: the effective thermal conductivity of the reinforcement under ideal conditions, $K^{eff}_{R0} = K_R \times V_R$ (V_R denotes the volume fraction of the reinforcement, in this study, V_R is 3%), is calculated as K^{eff}_{R0} = 16.5 W/(mK) for SCF; K^{eff}_{R0}= 58.5W/(mK) for VGCNF clusters. The heat transfer efficiency of SCF in the sintered composites is further calculated to be 76.91% and 60.73% for the hot-rolled; the heat transfer efficiency of VGCNF clusters in the sintered composites is 44.79% and 55.35% for the hot-rolled. Consequently, the heat transfer efficiency of SCF is higher than that of VGCNF clusters. This is on account of the difference in reinforcement diameters leading to different dispersion patterns in the Al matrix, which ultimately has an impact on the thermal conductivity.

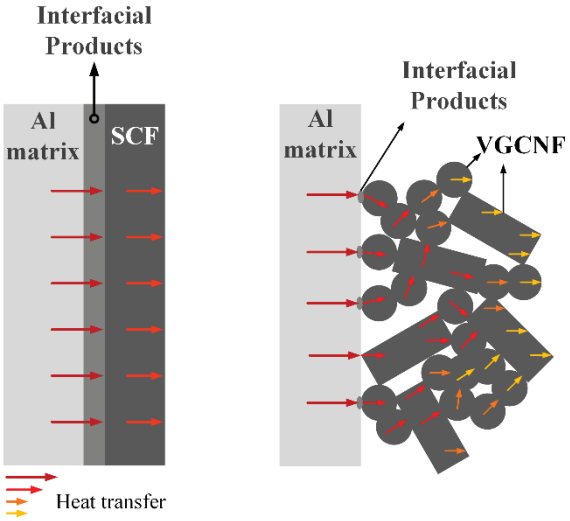

Figure 3-7 The schematic diagrams of the interfacial thermal conductivity paths of SCF/Al and VGCNF/Al

The schematic diagrams of the interfacial thermal conductivity paths of SCF/Al and VGCNF/Al are depicted in Figure 3-7. Since no aggregation occurs between the SCFs and the interface area with the Al matrix is large, the heat is directly transferred to the SCF through the interface. On the other hand, VGCNFs agglomerate due to the small diameter. The heat is transferred to the VGCNF in contact with the interface through a small portion of the interface and then to the adjacent VGCNF, leading to a decrease in thermal conductivity. Therefore, even though VGCNFs have ultra-high thermal conductivity, the aggregation between VGCNFs greatly reduces the heat transfer efficiency.

3.3.4 Mechanical properties

The tensile stress-strain curves of pure Al, SCF/Al, and VGCNF/Al before and after hot rolling are presented in Figure 3-8. Before hot rolling, the elongation of SCF/Al is lower, but the yield strength is higher than that of pure Al and VGCNF/Al. It points out that SCF enhances the strength of the composites but leads to poor plastic deformation ability. Although VGCNFs cluster with each other due to their smaller diameters, the clusters are small and uniformly distributed. Hence, the VGCNF/Al has better plasticity. However, the yield strength of VGCNF/Al is slightly lower than that of pure Al due to the poor interfacial bonding.

The yield strength of SCF/Al after hot-rolling is substantially increased and the elongation is also significantly higher. This is because of the refinement of the grain size of the Al matrix by hot rolling. Although the yield strength of VGCNF/Al is improved, it is still lower than that of pure Al, and the plasticity is reduced.

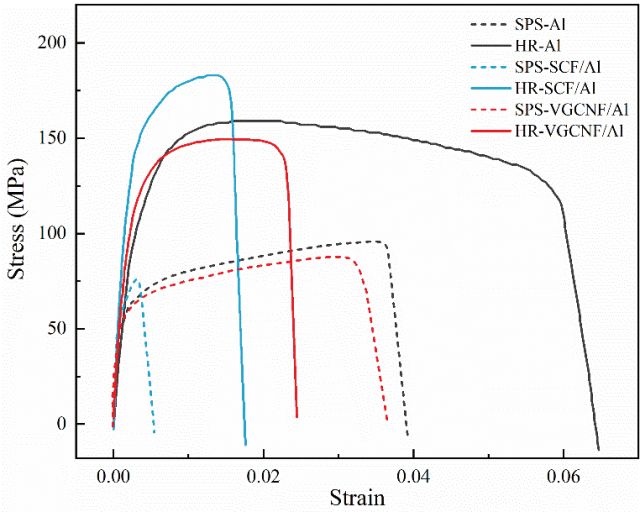

Figure 3-8 The stress-strain curves of pure Al, SCF/Al, and VGCNF/Al before and after hot rolling

The tensile fractures of pure Al, SCF/Al, and VGCNF/Al before and after hot rolling are performed in Figure 3-9. The fractures of pure Al before and after hot rolling suggest many tough nests. The fractures are flatter, and the plastic deformation capacity is improved after hot rolling, as concluded in Figure 3-9 a) and e). The fracture of sintered SCF/Al exhibits obvious brittle fracture characteristics due to the larger

diameter of the SCF and the damage of Al matrix by SCF random arrangement, as demonstrated by the arrows in Figure 3-9 b). After hot rolling, the interfacial reaction with the Al matrix leads to a decrease in the strength of the SCF, resulting in cracking during hot rolling, as described in Figure 3-9 f).

The fracture of sintered VGCNF/Al has tough nests, the VGCNF and its cluster bodies are also observed at the fracture, as suggested in Figure 3-9 c) and d). Since the deformation temperature below 2000°C does not lead to structural changes of VGCNF, thermal deformation changes the morphology of the cluster bodies by changing the arrangement between VGCNF[41]. The arrangement of VGCNF clusters is more compact and elongated along the rolling direction after hot rolling. It becomes the source of cracks during the deformation process, resulting in a decrease in the plasticity of the material, as pointed out in Figure 3-9 g) and h).

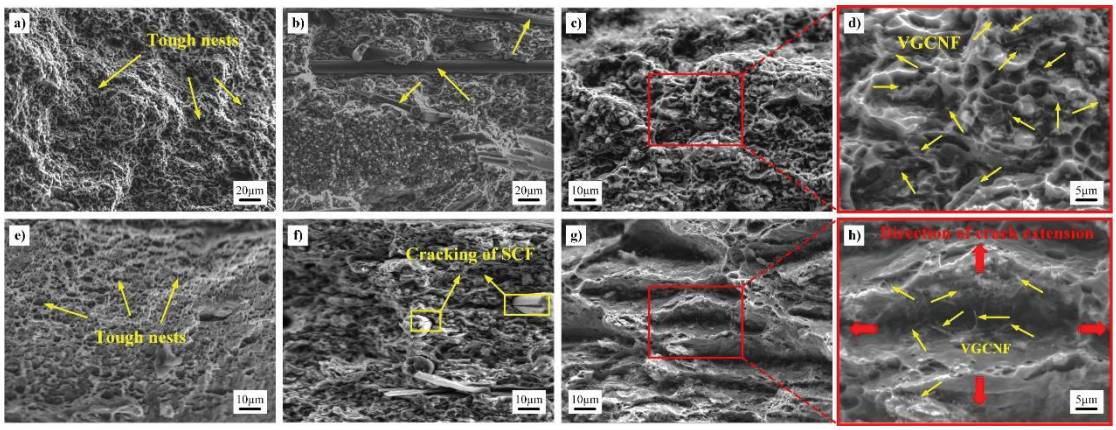

Figure 3-9 Tensile fractures of pure Al, SCF/Al, and VGCNF/Al before and after hot rolling: a) Sintered pure Al; b) Sintered SCF/Al; c) Sintered VGCNF/Al; d) Local enlargement of c); e) Hot-rolled pure Al; f) Hot-rolled SCF/Al; g) Hot-rolled VGCNF/Al; h) Local enlargement of g)

The addition of SCF hurts the plastic deformability of the Al matrix, but the well interfacial bonding and the uniform dispersion give the composites higher strength. The aggregation of VGCNF causes a weaker enhancement, but the plastic deformation ability is well. After thermal deformation, the change in the arrangement of the clusters leads to a decrease in the plasticity of VGCNF/Al.

3.4 Discussion

Hot rolling will give the material a selective orientation, that is texture. In section 3.4, the mechanical properties of the composites were analyzed in terms of reinforcement size and interfacial bonding. However, different types of texture also have a direct impact on mechanical properties. Therefore, this section will analyze the texture of pure Al and composites after hot rolling and discuss the effect of the texture on the mechanical properties.

The orientation distribution function (ODF) of pure Al, SCF/Al and VGCNF/Al after hot rolling, the texture strength along the α, β orientation lines and the distribution of texture components are shown in Figure 3-10. Hot-rolled pure Al and VGCNF/Al have significant P components (φ1=70º, Φ=45º, φ2=90º); the SCF/Al has obvious rotational Gauss(Rot-Gauss) components (φ1=0º, Φ=90º, φ2=45º), as depicted in Figure 3-10 a), b) and c). On the α orientation line, the P-component content of pure Al and VGCNF/Al is similar and much higher than that of SCF/Al, and the Gauss component (φ1=0º, Φ=45º, φ2=90º) in VGCNF/Al is higher. The P component is a common recrystallized texture in the cubic crystal system, resulting from the transformation of grains in the shear band formed by the plastic deformation process[42,43]. The movement of the shear band provides energy for grain evolution[44]. Owing to the absence of reinforcement addition, the shear band has less obstruction to the movement in pure Al. It therefore has sufficient kinetic energy to drive the transformation of grains within the shear band to recrystallized grains. The VGCNF clusters are small and uniformly distributed in the Al matrix. Compared with the larger diameter SCF, the VGCNF clusters are less obstructive to the shear band motion. Consequently, more recrystallized grains are transformed by the shear band in VGCNF/Al, and the content of the P component is higher.

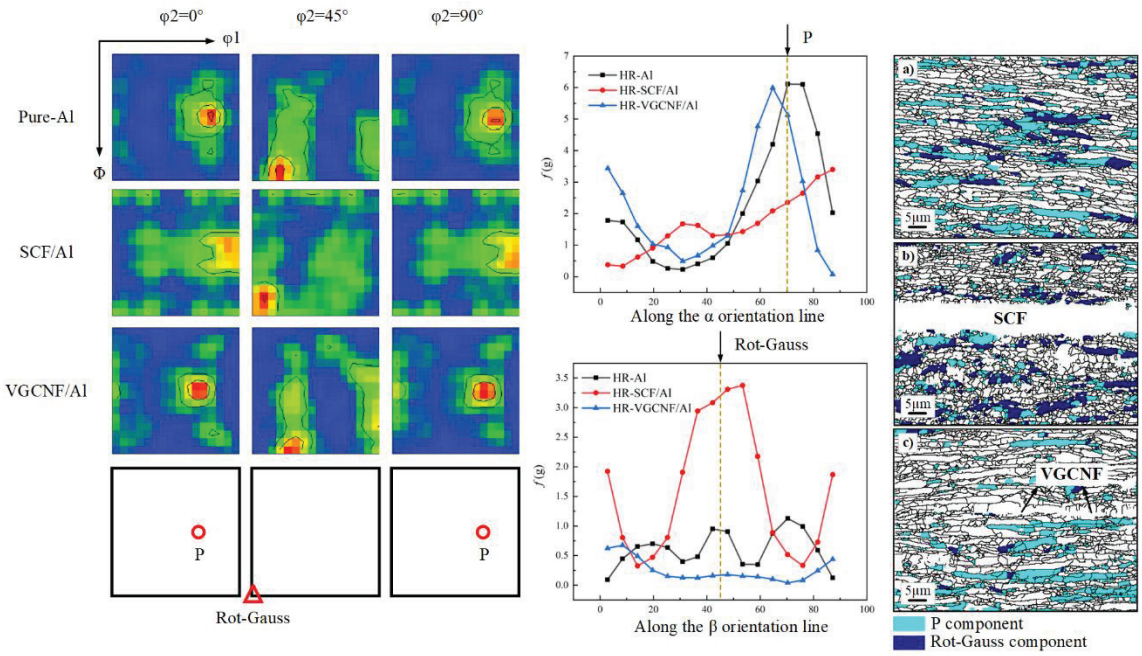

Figure 3-10 ODF distribution of pure Al and composites after hot rolling, texture strength on different orientation lines and the distribution of texture components: a) Pure Al; b) SCF/Al; c) VGCNF/Al

In the β-orientation line, the SCF/Al has higher Rot-Gauss components and Cube(φ1=0º, Φ=90º, φ2=0º) components compared with pure Al and VGCNF/Al. The research pointed out that the Rot-Gauss composition promotes the 35°-45° shear band generation along the rolling direction. The shear band in this orientation further evolves to the Cube composition, thereby generating recrystallized grains[45-47]. Owing to the larger diameter of SCF, the plastic deformation of the Al matrix of SCF/Al is greater during the hot rolling process, and the higher deformation activation energy promotes the generation of Rot-Gauss components. The Rot-Gauss component is retained for its higher resistance to plane strain compression, which promotes recrystallization grain nucleation by facilitating the formation of 35°-45° shear bands along the rolling direction[46]. Therefore, the recrystallization grain generation mode of the Al matrix of SCF/Al is the Rot-Gauss component-promoted nucleation mechanism. The small diameter reinforcement has less obstruction to the shear band movement. The primary recrystallization mechanism of VGCNF/Al is the transformation of the shear band grains into recrystallized grains mechanism.

After hot rolling, Pure Al and VGCNF/Al have a high content of P component. It

is shown that the P-component has a strong meritocratic growth characteristic, the P-component grains will grow rapidly toward the meritocratic orientation after formation[48]. As shown in Figure 3-10 a) c), the P-component grains all grow in the rolling direction after hot rolling and have a large grain size. The large grain size of P component has a negative effect on mechanical properties.

Rot-gauss components have high resistance to deformation and the ability to inhibit crack propagation[45]. It has been noted that the cracks will undergo a large deflection near the Gauss component, forming a rough fracture[49,50]. In SCF/Al, the content of Rot-Gauss component is much higher than that of Pure Al and VGCNF/Al, and the morphology of Rot-Gauss component in SCF/Al is mostly fine equiaxed crystals as shown in Figure 3-10 b), thus leading to the high yield strength of SCF/Al.

3.5 Summary

In this study, the effects of SCF and VGCNF on the microstructure, interface, thermal conductivity and mechanical properties of the composites were explored. The results demonstrate that:

(1) The SCFs are uniformly dispersed in the Al matrix and generate continuous amorphous carbides with the Al matrix at the interface. The VGCNFs are aggregated due to their small diameters and exist as agglomerates, and only a small amount of VGCNFs generate amorphous interfacial products with the Al matrix.

(2) The thermal conductivity value of SCF is lower than that of VGCNF, but has higher heat transfer efficiency. The aggregation of VGCNF negatively affects the heat transfer efficiency.

(3) The addition of SCF results in a greater degree of plastic deformation of the Al matrix during hot rolling, leading to a recrystallized mode with a Rot-Gauss component promoting nucleation mechanism. The VGCNF clusters are less obstructive to shear band motion, and the main recrystallization mechanism is the transformation of shear band grains into recrystallized grains.

(4) The meritocratic growth characteristic of P component leads to more large P

component grains in Pure Al and VGCNF/Al, which have a negative effect on mechanical properties; The strong resistance to deformation and crack extension of the Rot-Gauss component results in a high yield strength of SCF/Al.

3.6 References

[1]. LF Yi, T Yamamoto, T Onda T et al. Orientation control of carbon fibers and enhanced thermal/mechanical properties of hot-extruded carbon fibers/aluminum composites[J]. Diam Relat Mater. 2021, 116:108432.

[2]. M Wang, J She, B Chen B et al. Compressive behavior of CNT-reinforced aluminum matrix composites under various strain rates and temperatures[J]. Ceram Int. 2021, https://doi.org/10.1016/j.ceramint.2021.12.248.

[3]. R Pei, G Chen, Y Wang et al. Effect of interfacial microstructure on the thermal-mechanical properties of mesophase pitch-based carbon fiber reinforced aluminum composites[J]. J Alloy Compd. 2018, 756:8-18.

[4]. T Xu, S Zhou, X Ma et al. Significant reinforcement of mechanical properties in laser welding aluminum alloy with carbon nanotubes added[J]. Carbon. 2022, 191:36-47.

[5]. J Gayathri, R Elansezhian. Influence of dual reinforcement (nano CuO + reused spent alumina catalyst) on microstructure and mechanical properties of aluminium metal matrix composite[J]. J Alloy Compd. 2020, 829:154538.

[6]. AV Aborkin, AI Elkin, VV Reshetniak et al. Thermal expansion of aluminum matrix composites reinforced by carbon nanotubes with in-situ and ex-situ designed interfaces ceramics layers[J]. J Alloy Compd. 2021, 872:159593.

[7]. L Liu, S Li, X Zhang et al. Syntheses, microstructure evolution and performance of strength-ductility matched aluminum matrix composites reinforced by nano SiC-cladded CNTs[J]. Mater Sci Eng A. 2021, 824:141784.

[8]. C Nie, H Wang, J He. Evaluation of the effect of adding carbon nanotubes on the effective mechanical properties of ceramic particulate aluminum matrix composites[J]. Mech Mater. 2020, 142:103276.

[9]. S Lakra, TK Bandyopadhyay, S Das et al. Thermal conductivity of in-situ dual matrix aluminum composites with segregated morphology[J]. Mater Res Bull. 2021, 144:111515.

[10]. M Jagannatham, P Chandran, S Sankaran et a. Tensile properties of carbon nanotubes reinforced aluminum matrix composites: A review[J]. Carbon. 2020, 160:14-44.

[11]. X Fan, X Li, Z Zhao et al. Heterostructured rGO/MoS2 nanocomposites toward enhancing lubrication function of industrial gear oils[J]. Carbon. 2022, 191:84-97.

[12]. C Zhu, Y Su, X Wang et al. Process optimization, microstructure characterization and thermal properties of mesophase pitch-based carbon fiber reinforced aluminum matrix composites fabricated by vacuum hot pressing[J]. Compos Part B-Eng. 2021, 215:108746.

[13]. JJ Sha, ZZ LÜ, RY Sha et al. Improved wettability and mechanical properties of metal coated carbon fiber-reinforced aluminum matrix composites by squeeze melt infiltration technique[J]. T Nonferr Metal Soc. 2021, 31:317-330.

[14]. S Bahl S. Fiber reinforced metal matrix composites - a review[J]. Mater Today Proc. 2021, 39:317-323.

[15]. BS Guo, S Ni, J Yi et al. Microstructures and mechanical properties of carbon nanotubes reinforced pure aluminum composites synthesized by spark plasma sintering and hot rolling[J]. Mater Sci Eng A. 2017, 698:282-288.

[16]. L Cao, B Chen, J Wan et al. Superior high-temperature tensile properties of aluminum matrix composites reinforced with carbon nanotubes[J]. Carbon. 2022, 191:403-414.

[17]. BS Guo, S Luo, Y Wu et al. Regulating the interfacial reaction between carbon nanotubes and aluminum via copper nano decoration[J]. Mater Sci Eng A. 2021, 820:141576.

[18]. H Naji, SM Zebarjad, SA Sajjadi. The effects of volume percent and aspect ratio of carbon fiber on fracture toughness of reinforced aluminum matrix composites[J]. Mater Sci Eng A. 2008, 486:413-420.

[19]. P Wang, Z Xu, X Liu et al. Regulating the interfacial reaction of

Sc2W3O12/AgCuTi composite filler by introducing a carbon barrier layer[J]. Carbon. 2022, 191:290-300.

[20]. ZQ Shi, WL Yang, JP Wang et al. ffect of interfacial structure on the thermal conductivity of carbon nanofibers reinforced aluminum nitride composites[J]. Ceram Int. 2013, 39:3365-3370.

[21]. SI OH, JY Lim, YC Kim et al. Fabrication of carbon nanofiber reinforced aluminum alloy nanocomposites by a liquid process[J]. J Alloy Compd. 2012, 542:111-117.

[22]. BS Guo, Y Chen, Z Wang et al. Enhancement of strength and ductility by interfacial nano-decoration in carbon nanotube/aluminum matrix composites[J]. Carbon. 2020, 159:201-212.

[23]. CC Rafael, MM Bibi, GG Diego et al. High-temperature creep of carbon nanofiber-reinforced and graphene oxide-reinforced alumina composites sintered by spark plasma sintering[J]. Ceram Int. 2017, 43:7136-7141.

[24]. S Bi, ZY Liu, BL Xiao et al. Enhancing strength-ductility synergy of carbon nanotube/7055Al composite via a texture design by hot-rolling[J]. Mater Sci Eng A. 2021, 806:140830.

[25]. M Deshpande, R Gondil, S Murty et al. Studies on 7075 Aluminium Alloy MMCs with Milled Carbon Fibers as Reinforcements[J]. Trans Indian Inst Met. 2018, 71:993-1002.

[26]. JH Wu, C Zhang, QN Meng et al. Study on tensile properties of carbon fiber reinforced AA7075 composite at high temperatures[J]. Mater Sci Eng A. 2021, 825: 141931.

[27]. M Eid, S Kaytbay, A El-Assal et al. Electrical, Thermal, and Mechanical Characterization of Hot Coined Carbon Fiber Reinforced Pure Aluminium Composites[J]. Met Mater Int. 2022, https://doi.org/10.1007/s12540-022-01177-w.

[28]. ZJ Wang, SY Yang, ZH Du et al. Micromechanical Modeling of Damage Evolution and Mechanical Behaviors of CF/Al Composites under Transverse and Longitudinal Tensile Loadings[J]. Mater. 2019, 12:3133.

[29]. Y Huang, QB Ouyang, D Zhang et al. Carbon Materials Reinforced Aluminum Composites: A Review[J]. Acta Metall Sin. 2014, 27:775-786.

[30]. J Kita, H Suemasu, I Davies et al. Fabrication of silicon carbide composites with carbon nanofiber addition and their fracture toughness[J]. J Mater Sci. 2010, 45:6052-6058.

[31]. F Ogawa, C Masuda. Microstructure evolution during fabrication and microstructure-property relationships in vapour-grown carbon nanofibre-reinforced aluminium matrix composites fabricated via powder metallurgy[J]. Compos part A. 2015, 71:84-94.

[32]. V Srinivasan, S Kunjiappan, P Palanisamy. A brief review of carbon nanotube reinforced metal matrix composites for aerospace and defense applications[J]. Int Nano Lett. 2021, 11:321-345 .

[33]. A Yadav, RK Godara, G Bhardwaj et al. A Review on Fracture Analysis of CNT/Graphene Reinforced Composites for Structural Applications[J]. Arch Computat Methods Eng. 2022, 29:545-582.

[34]. AT Miranda AT. Characterization and Processing of Carbon-Based Reinforced Al-MMCs for Thermal Management Applications[J]. 2016.

[35]. DDL Chung. Comparison of submicron-diameter carbon filaments and conventional carbon fibers as fillers in composite materials[J]. Carbon. 2001, 39:1119-1125.

[36]. HB Shim, MK Seo, SJ Papk. Thermal conductivity and mechanical properties of various cross-section types carbon fiber-reinforced composites[J]. J Mater Sci. 2002, 37:1881-1885.

[37]. Y Guo, XG Liu, XS Shi et al. Investigation of Hot Workability and Microstructure Evolution of VGCNFs-Reinforced Aluminum Matrix Composites[J]. Metall Mater Trans A. 2020, 51:4100-4112.

[38]. N Li, L Wang, J Dai et al. Interfacial products and thermal conductivity of diamond/Al composites reinforced with ZrC-coated diamond particles[J]. Diamond Relat Mater. 2019, 100:107565.

[39]. N Wei, C Zhou, Z Li et al. Thermal conductivity of Aluminum/Graphene metal-

matrix composites: From the thermal boundary conductance to thermal regulation[J]. Mater Today Commun. 2022, 30:103147.

[40]. AT Miranda, L Bolzoni, N Barekar et al. Processing, structure and thermal conductivity correlation in carbon fibre reinforced aluminium metal matrix composites[J]. Mater Des. 2018, 156:329-339.

[41]. Y Guo, XG Liu, ZF Xu et al. Effect of VGCNF on high-temperature deformation performance and softening mechanism of aluminum matrix[J]. J Alloy Compd. 2020, 818:152923.

[42]. O Engler, K Lacke. Mechanism of Recrystallization Texture Formation in Aluminum Alloys[J]. Scr. Metall Mater. 1992, 27:1527-1532.

[43]. P Qu, L Zhou, VL Acoff. Deformation textures of aluminum in a multilayered Ti/Al/Nb composite severely deformed by accumulative roll bonding[J]. Mater Charact. 2015, 107:367-375.

[44]. M Hatherl, AS Malin . Shear Bands in Deformed Metals[J]. Scr Mater. 1984, 18:449-454.

[45]. Y Nguyen-Minh, JJ Sidor, RH Petrov et al. Occurrence of shear bands in rotated Goss ({110}<110>) orientations of metals with bcc crystal structure[J]. Scr Mater. 2012, 67:935-938.

[46]. M Mehdi, Y He, EG Hilinski et al. The evolution of cube ({001}<100>) texture in non-oriented electrical steel[J]. Acta Mater. 2020, 185:540-554.

[47]. S Deb, SK Panigrahi, M Weiss. The effect of annealing treatment on the evolution of the microstructure, the mechanical properties and the texture of nano SiC reinforced aluminium matrix alloys with ultrafine grained structure[J]. Mater Charact. 2019, 154:80-93.

[48]. J Xie, XP Chen, Y Cao et al. The evolution of main textures and the formation of P orientation with nanoprecipitates after friction stir processing[J]. J Manuf Process. 2022, 80:591-599.

[49]. LF Shuai, TL Huang, GL Wu et al. Development of Goss texture in Ale0.3%Cu annealed after heavy rolling[J]. J Alloy Compd. 2018, 748:399-405.

[50]. WT Wu, ZY Liu, YC Hu et al. Goss texture intensity effect on fatigue crack propagation resistance in an Al-Cu-Mg alloy[J]. J Alloy Compd. 2018, 730:318-326.

Chapter 4

Microstructure evolution, property analysis, and interface study of 3%CF-3%SiC-10%SiC functional gradient aluminum matrix composites

4.1 Introduction

In recent years, considerable attention has been paid to the development and application of aluminum (Al)-based composites because of the small density, low cost, and excellent thermal conductivity[1-3]. In our previous research, we have developed the carbon fiber (CF) reinforced Al composites with excellent thermal conductivity[4]. However, the low strength and plasticity limit the application. The current engineering field requires increasingly high material performance, and the composites reinforced with a single reinforcement are challenging to meet the increasingly complex service environment[5]. In extreme environments, materials are normally required to have both high strength and excellent electrical and thermal conductivity[6]. To resolve the conflicting performance requirements, the functional gradient material(FGM) was first proposed by Japanese scholars in 1984[7-9].

The FGM is a type of material with a gradual change in composition along one direction, resulting in different microstructures and properties in different regions to meet specific performance requirements[7,10]. The functional gradient composites(FGC) developed on this basis can fully utilize the advantage of designability by controlling the type and content of the reinforcement to give different regions different properties such as hardness, thermal conductivity, and electrical conductivity[11-16]. The FGC is prepared mainly by liquid and solid phase methods, such as centrifugal casting, powder metallurgy, ion spraying, etc.[17-21]. Among them, the spark plasma sintering (SPS) technology can remove oxides at the interface through pulse current, reducing the porosity between the reinforcement and the matrix, which has been widely applied[22,23]. The particle reinforcements, such as SiC, Al_2O_3, B_4C, etc., have high strength, and the FGC with superficial high hardness can be obtained through reasonable composition design[24-28]. Kırmızı et al.[29] prepared the 15%-30%-45%-60% SiC gradient Al matrix composites by powder metallurgy. The highest hardness was found in the 60% SiC layer. Kwon et al.[30] conducted the Al-CNT-nSiC FGC using ball milling and SPS technology. The transmission electron microscope (TEM) results demonstrated that the interlayer bonding was tight and the SiC layer with a 30% volume fraction had a hardness value

four times than that of pure Al.

There are some intractable problems in the FGC preparation in current investigations, such as excessive interface stress and low plasticity. Oza et al.[31] performed the Al-SiC-graphite gradient composites with the highest SiC volume fraction in the top layer by SPS. The results indicated that the top layer had the highest hardness value. However, the excessive SiC volume fraction led to the brittle fracture. Ferraris et al.[32] carried out gradient Al composites with 68% SiC in the surface layer for lightweight brake systems. The results claimed that excessive interfacial stresses resulted in poor interlayer bonding.

On the whole, the design of the FGC needs to consider strength-plasticity matching and the optimization of interfacial stresses. Nevertheless, few studies have conducted in-depth research on the interface structure of the FGC. The mechanism of the type and content of reinforcement affects the microstructural characteristics of each layer has also not been systematically elucidated. In this study, the FGC was designed to improve strength and ductility based on the preparation of CF reinforced Al composites with high thermal conductivity[4]. Considering strength-ductility matching and interfacial stress transition, a transition layer of 3% SiC was set between the CF reinforced layer and the 10% SiC reinforced layer. The 3% CF-3% SiC-10% SiC Al matrix FGC were prepared by the SPS. The thermal deformation behavior of the FGC was investigated comprehensively. Through the in-depth analysis of the microstructure evolution of each layer and the interlayer interface, the mechanism of the design of the gradient reinforcement was elaborated.

4.2 Experimental

The parameters of the pure Al powders, SiC particles, and CF used in this study are shown in Table 4-1. To enhance the wettability of the CF and the Al matrix and improve the interfacial thermal conductivity, the copper was coated on the CF surface by chemical method. The morphologies of pure Al powder, copper-coated CF, and SiC particles are illustrated in Figure 4-1 a) b) c), respectively. Figure 4-1 performs the

preparation process of the CF reinforced Al composites (CF/Al) and the FGC. First, the raw materials were mixed in an alcohol solution and oscillated in ultrasonic waves for 10 minutes to promote uniform dispersion. Subsequently, the mixed solution and alumina spheres of 10mm diameter were injected into the closed Al tank for ball milling. After mixing, the mixed liquid was placed in a ventilated cabinet for drying and transferred to a vacuum drying box for further drying. The obtained mixed powders were vacuum sintered using the SPS equipment (S. S. Alloy Co., Ltd.) with a mold of 30mm inner diameter, a sintering temperature of 550℃, pressure of 50MPa, and held for 30 minutes. A layer of Al foil was wrapped on the sintered composites surface to protect it. Then it was hot rolled at 450℃ with a reduction of 70%. For comparison, the pure Al blocks were prepared under identical conditions.

Table 4-1 Parameters of pure Al powder, SiC particles, and CF

Material	Diameter (μm)	Density (g/cm^3)	Thermal conductivity (W/mK)
Pure Al powder	3	2.70	237
SiC powder	2-3	3.16	270
CF	11	2.00	550

The physical phases were identified using a SmartLab-type X-ray diffractometer (XRD). The microstructure of FGC was observed adopting a JEOL-JSM-6390LA type scanning electron microscope (SEM). Electron backscatter diffraction (EBSD) analysis was performed using Oxford-ultim equipped acquisition equipment. The Helios focused ion beam (FIB) was used to cut and thin the transmission samples; the FEI Tecnai F20 transmission electron microscope (TEM) was utilized to observe the interface structure of the FGC and identify the interface products. The hardness of each layer of the Al matrix was measured by the Mitutoyo-HM-100 type Vickers hardness tester. Tensile specimens were cut along the rolling direction using Wire Electrical Discharge Machining and tested on the INSTRON 8801 hydraulic servo fatigue tester at room temperature with a strain rate of $8.3\times10^{-4}s^{-1}$. The thermal conductivity of FGC was accomplished in the axial and horizontal directions, respectively.

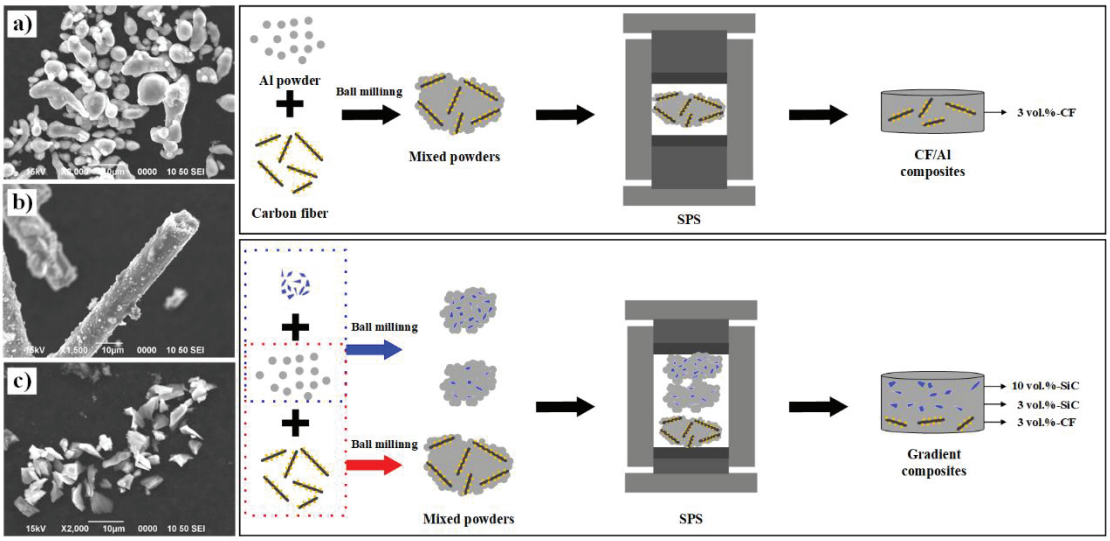

Figure 4-1 The SEM morphologies of the Pure Al powder, SiC powder, and CF, as well as the schematic illustration of the preparation of the CF/Al and the FGC

4.3 Results

4.3.1 Microstructure

Figure 4-2 a)-j) show the SEM morphologies of the different layers and interfaces of the FGC. The XRD diffraction patterns of the FGC before and after hot rolling and the Vickers hardness values from the 3% CF layer to the 10% SiC layer are proposed in the right side of Figure 4-2. The SiC particle content is gradually increasing from bottom to top, and the SiC particles are uniformly distributed in each layer, as performed in Figure 4-2 a), c), e), g), and i). The CF and the SiC particles are well bonded to the Al matrix, as indicated in Figure 4-2 g). After hot rolling, the CF is aligned along the hot rolling direction, as pointed out in Figure 4-2 h) and j). As seen in Figure 4-2 b) and f), the arrangement of SiC particles in the 3% SiC layer and the 10% SiC layer has not changed significantly after hot rolling, but the aggregation of SiC particles appeared at the interface of 3% SiC and 10% SiC, as concluded in Figure 4-2 d). No defects, such as cracks and holes, are observed at the interface of the layers before and after hot rolling, indicating good bonding between the layers.

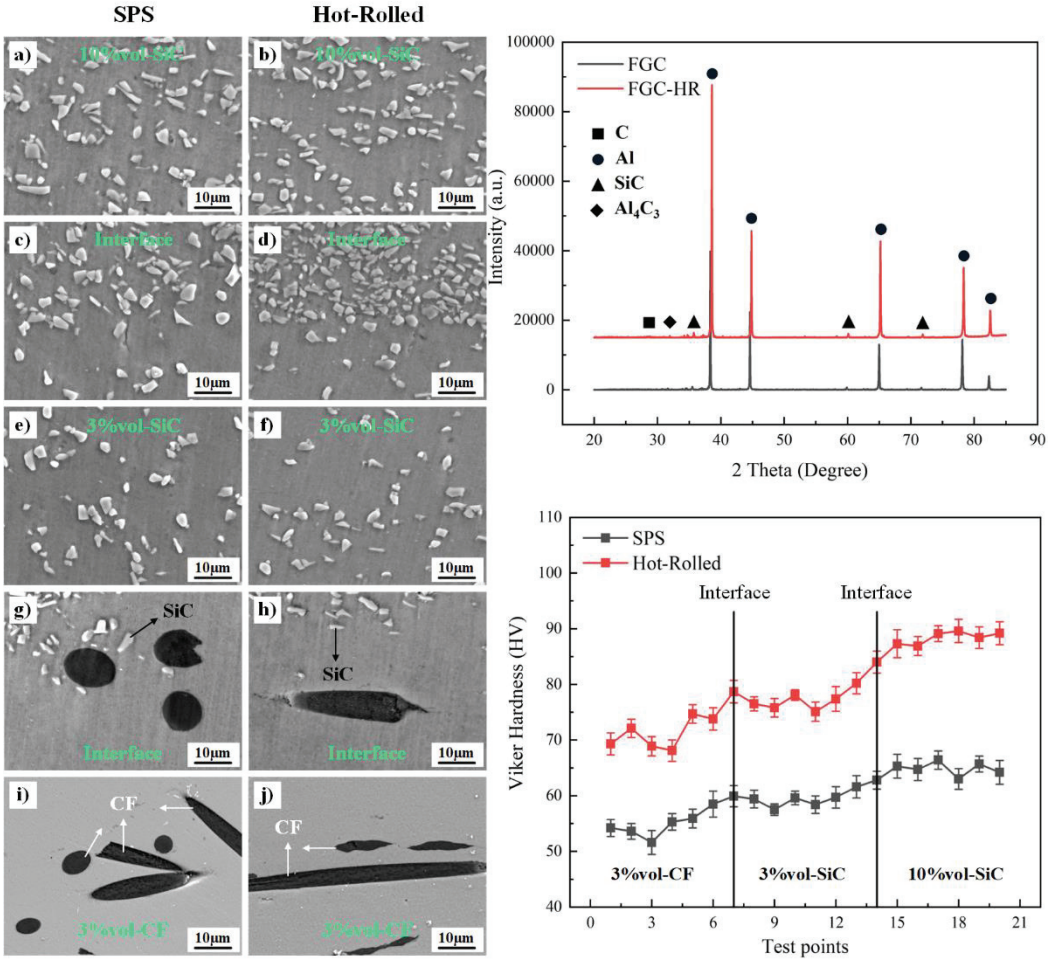

Figure 4-2 The SEM morphologies, XRD diffraction patterns, and Vickers hardness values of the various layers and interfaces of the FGC

In the X-ray diffraction pattern, the Al phase, C phase, SiC phase, and a small amount of Al_4C_3 phase were labeled by the peak-seeking process. The Vickers hardness results show that the hardness values gradually increase from the 3% CF layer to the 3% SiC layer to the 10% SiC layer, which is applicable for both before and after hot rolling. In addition, higher hardness values are observed at both interfaces, indicating higher stress values or specificity of the microstructure at the interface. The increase in the hardness values of the layers after hot rolling is attributed to the evolution of the microstructure during thermal deformation and the residual deformation stresses.

To investigate the microstructural characteristics of each layer, the EBSD analysis was performed on the FGC before and after hot rolling. The Inverse Pole Figure (IPF), grain boundary distribution, local stress distribution (KAM map), and the grain size and grain boundary distribution of each layer of the FGC before hot rolling are

demonstrated in Figure 4-3. Figure 4-3 a) and b) show that there is no obvious pattern in the grain orientation from the 3% CF layer to the 10% SiC layer. The grain boundary distribution in Figure 4-3 d) illustrates a greater degree of grain boundary deformation in the 10% SiC layer, and the KAM map in Figure 4-3 f) also displays a greater value of intragrain stress in this layer, indicating that the higher content of SiC particles during the sintering process leads to greater stress on the nearby Al matrix. Furthermore, the grain size decreases gradually from the 3% CF layer to the 10% SiC layer, suggesting that the SiC particles have a hindering effect on the grain boundary movement and grain growth.

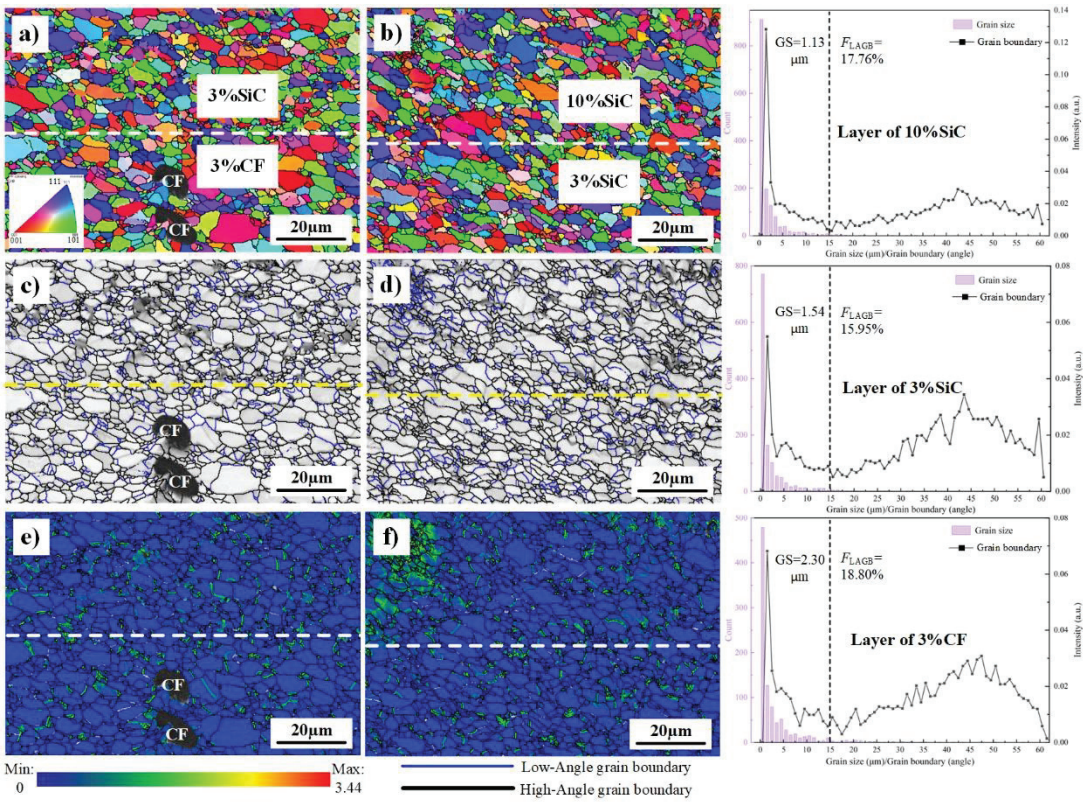

Figure 4-3 The IPF map, grain boundary distribution map, KAM map, and the grain size and grain boundary distribution of each layer of the FGC before hot rolling

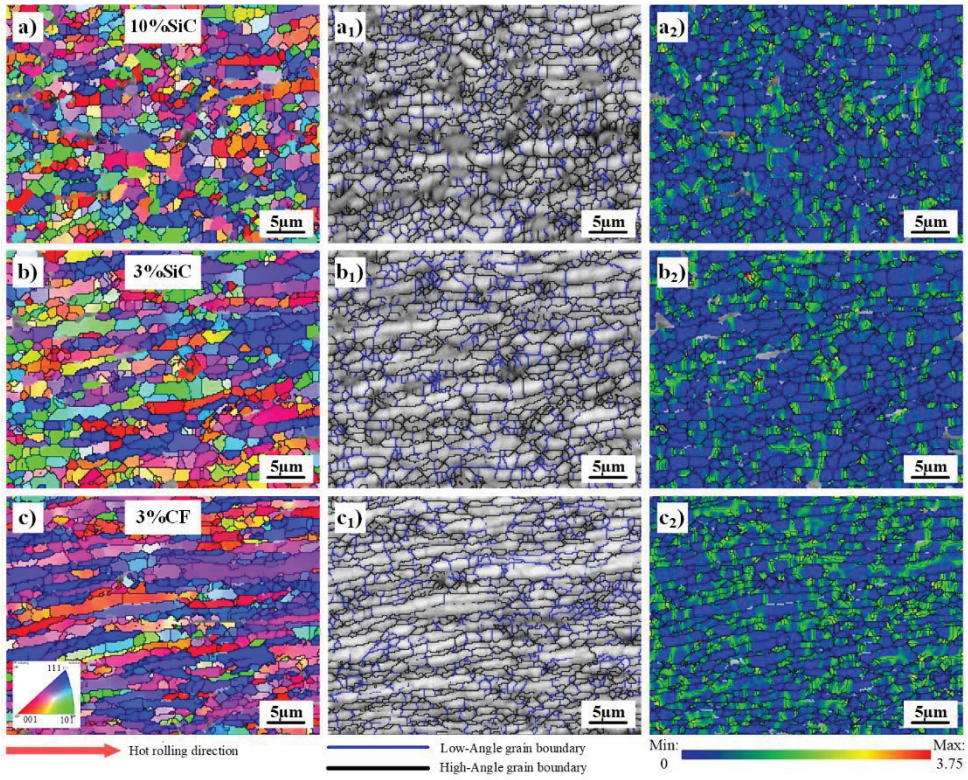

Figure 4-4 The IPF map, grain boundary distribution map, and KAM map of each layer of the FGC after hot rolling

The microstructure of each layer of the FGC after hot rolling is illustrated in Figure 4-4. The shape and orientation of the grains in each layer are clearly different after hot rolling: the grains of the 3%CF layer is extended along the rolling direction, and most of the grains are <111>//RD orientation, as described in Figure 4-4 c) and c_1). While in the 3% SiC layer, some of the grains are fibrous-shaped, and considerable equiaxed grains are found at the grain boundaries, as illustrated in Figure 4-4 b) and b_1). There are enormous equiaxed, fine grains with random grain orientation in the 10% SiC layer, as depicted in Figure 4-4 a) and a_1). Additionally, the grain size of the 3% CF, 3% SiC, and 10% SiC layers are 1.76μm, 1.54μm, and 0.92μm, respectively. The percentage of high angle grain boundaries (HAGBs) are 55.75%, 60.47%, and 65.80%, respectively. The smallest grain size and the highest percentage of HAGBs can be seen in the 10% SiC layer. Combined with the continuous dynamic recrystallization mechanism of Al, it is known that the dynamic recrystallization percentage is the highest in the 10% SiC layer. As shown in Figure 4-4 a_2), b_2), c_2), the residual stress in the 3% CF layer after hot rolling is higher than that in the 3% SiC layer and the 10% SiC layer. It is attributed

to the particle stimulated nucleation (PSN) generated by the SiC particles promotes the generation of recrystallized grains and consumes numerous dislocations and low-angle grain boundaries, resulting in lower residual stress values.

4.3.2 Mechanical properties

The mechanical parameters, stress-strain curves, and corresponding fracture morphology of the Al, CF/Al, and the FGC before and after hot rolling are displayed in Table 4-2 and Figure 4-5. According to the data in Table 4-2 and the stress-strain curves in Figure 4-5, although the CF/Al has a slightly higher yield strength than pure Al, its plasticity is worse. The yield strength of the FGC before hot rolling is 167.12% higher than the Al and 149.65% higher than the CF/Al; after hot rolling, it is 132.11% higher than the Al and 62.46% higher than the CF/Al. In terms of plasticity, the elongation of FGC is slightly higher than that of pure Al before hot rolling and similar to that of pure Al after hot rolling. Therefore, the FGC has both high yield strength and excellent plastic deformation ability.

Table 4-2 The mechanical parameters of Al, CF/Al, and FGC

Material	Modulus (GPa)	Yield strength (MPa)	Elongation (%)
Al-SPS	44.25±0.73	70.19±2.96	3.64±0.54
Al-HR	45.17±1.25	127.64±3.71	6.07±0.27
CF/Al-SPS	42.04±1.16	75.10±2.93	0.46±0.12
CF/Al-HR	45.12±2.15	182.37±2.20	1.87±0.36
FGC-SPS	62.19±2.76	187.49±3.12	4.39±0.28
FGC-HR	66.43±1.93	296.27±5.27	6.46±0.19

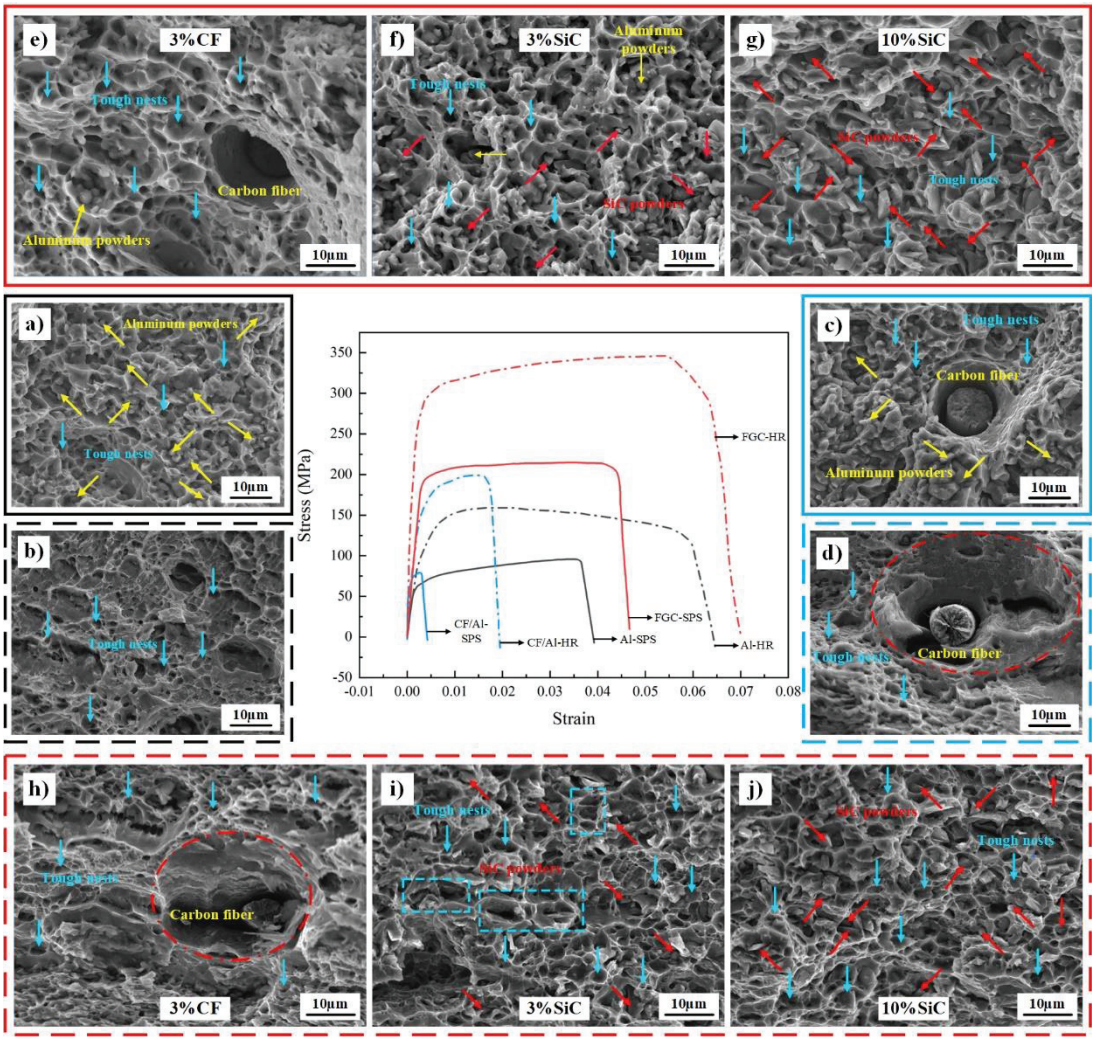

Figure 4-5 The stress-strain curves and tensile fracture morphologies of Al, CF/Al, and FGC are as follows: Pure Al's fracture morphology: a) before HR b) after HR; CF/Al's fracture morphology: c) before HR d) after HR; FGC's fracture morphology before hot rolling: e) 3%CF layer f) 3%SiC layer g) 10%SiC layer; FGC's fracture morphology after hot rolling: h) 3%CF layer i) 3%SiC layer j) 10%SiC layer

The fracture morphology of Al, CF/Al, and FGC are presented in Figure 4-5. For a more visual presentation, the fractures are highlighted using boxes with the same color and style as the stress-strain curves. Tough nests are observed in Figure 4-5 a) and b), as shown by the blue arrows. In the pure Al before hot rolling, poorly bound Al particles can still be observed, as displayed by the yellow arrows in Figure 4-5a). The poor bonding of Al particles also has a negative impact on plasticity. Only a few tough nests are observed in Figure 4-5c), and numerous Al particles are distributed on the fracture, indicating that the addition of CF results in a less dense Al matrix, which in turn leads

to poor plasticity. The number of tough nests increases in CF/Al after hot rolling, as provided in Figure 4-5 d). However, the area of the brittle fracture zone caused by the failure of the CF and the Al matrix interface has enlarged, as illustrated by the red dotted frame in Figure 4-5 d).

Before hot rolling, each layer in the FGC has different fracture characteristics, as shown in Figure 4-5 e), f), and g). Tough nests and a few Al particles are observed in the 3% CF layer, and the CF is pulled off due to tensile load. In the 3% SiC and 10% SiC layers, uniformly distributed SiC particles can be observed in the tough nests, as performed by the red arrows in Figure 4-5 f) and g). The two SiC layers have more and smaller tough nests, which confer a higher plastic deformation capacity to the FGC. After hot rolling, the interface between CF and the Al matrix in the 3% CF fails and causes a local brittle fracture, as pointed out by the red dotted line in Figure 4-5 h). Smaller tough nests are observed in the fractures of the 3% SiC and 10% SiC layers. As concluded in Figure 4-5 i), the blue dotted line box presents the tough nests elongated along the horizontal direction in the 3% SiC layer, while the tough nests in Figure 4-5 j) are mostly equiaxed, which is attributed to the higher recrystallization percentage of the 10% SiC layer after hot rolling.

Therefore, the local brittle fracture result from the failure of the interface between CF and the Al matrix is the main factor causing the low plasticity. In contrast, SiC particles do not lead to local failure over large areas due to their smaller size and uniform distribution.

4.3.3 Thermal conductivity

The thermal conductivity of Al, CF/Al, and FGC before and after hot rolling was tested along the axial and horizontal directions (along the rolling direction after hot rolling). The test schematic and the thermal conductivity results are shown in Figure 4-6. Before hot rolling, the difference in thermal conductivity between the axial and horizontal directions of each material is not significant, which is in view of the equiaxed shape of most grains after sintering. The thermal conductivity values of Al and CF/Al

before hot rolling are higher than that of the FGC. On the one hand, this is attributed to the addition of SiC particles introducing more interfaces, the heat losses through the interfaces. On the other hand, due to the small grain size of the SiC layer in FGC, the smaller the grain size, the more grain boundaries, and the numerous grain boundaries also cause heat loss.

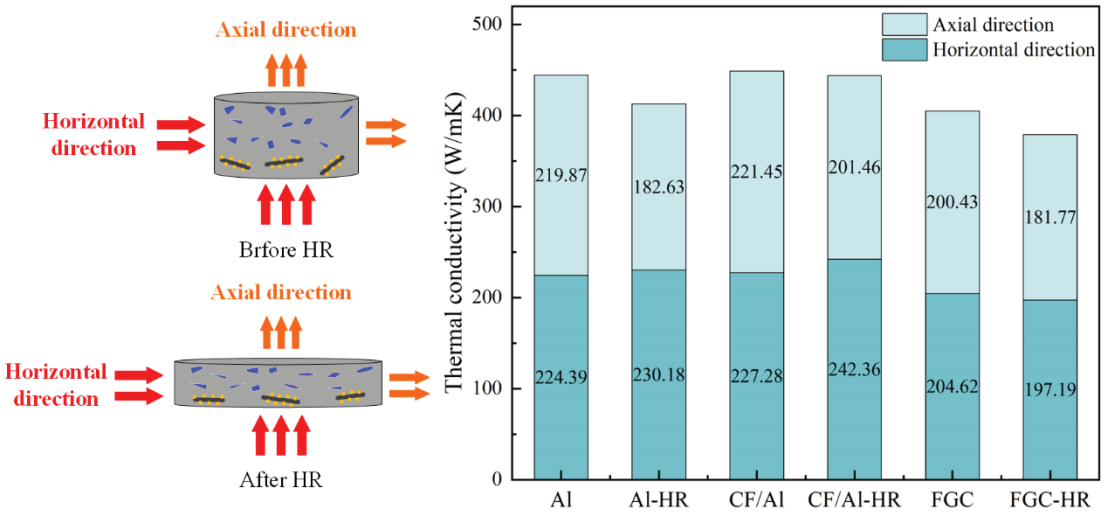

Figure 4-6 Schematic diagram and test results of thermal conductivity of Al, CF/Al, and FGC before and after hot rolling

After hot rolling, the thermal conductivity of each material in the axial direction is lower than that in the horizontal direction. This is because the grains elongate in the rolling direction after hot rolling, and heat conduction in the axial direction will pass through more grain boundaries, resulting in greater heat loss. Furthermore, the thermal conductivity of Al and CF/Al along the hot rolling direction increased after hot rolling. This is attributed to the increase in the dense density of the Al matrix and the alignment of CF in CF/Al along the rolling direction, the phenomenon explained in detail in our previous study[4]. After hot rolling, the thermal conductivity of the FGC along the hot rolling direction decreased. The CF in the 3%CF layer is mainly arranged along the rolling direction, and the high thermal conductivity in the CF axial direction is favorable to more efficient heat transfer. In the SiC layer, the hot rolling does not provide higher heat transfer efficiency because the thermal conductivity of SiC particles is essentially the same in all directions[33,34]. Moreover, the fine grain size after hot rolling leads to a higher density of grain boundaries, and the higher density of dislocations caused by hot

rolling, resulting in a higher heat loss in the SiC layer, ultimately leading to a lower overall thermal conductivity value of the FGC.

4.4 Discussion

4.4.1 The interlayer interface and microscopic interface of FGC

The different reinforcement distribution and microstructure characteristics of each layer directly impact the overall properties of the FGC. The microstructure of the interface also play an essential role as the transition area connecting the layers. In this section, the microstructure of the interlayer interface and the microscopic interface between the reinforcement and the Al matrix after hot rolling will be investigated in depth.

Figure 4-7 shows the microstructure of 3% CF-3% SiC and 3% SiC-10% SiC interfaces. Figure 4-7 a) and d) demonstrate the variation of grain orientation in each layer. Compared with the 3%CF layer, the random orientation grains of the 3%SiC layer and the 10%SiC layer gradually increase. Figure 4-7 b) and e) show the distribution rendered according to grain size, where red color indicates large size grains and blue color indicates small size grains. Figure 4-7 b) and e) again reveal the pattern of gradual increase of fine equiaxed crystals from 3% CF layer to 10% SiC layer. And the change in grain orientation and grain size on both sides of the interface inevitably leads to more significant intergranular stresses. Figure 4-7 c) and Figure 4-7 f) are calculated by using Grain components in Channel 5 data analysis software. This component highlights the areas of stress concentration by calculating the misorientation in the grains. In Figure 4-7 c) and f), the red area indicates the stress concentration area, it can be seen that there are apparent stress concentrations at each layer interface.

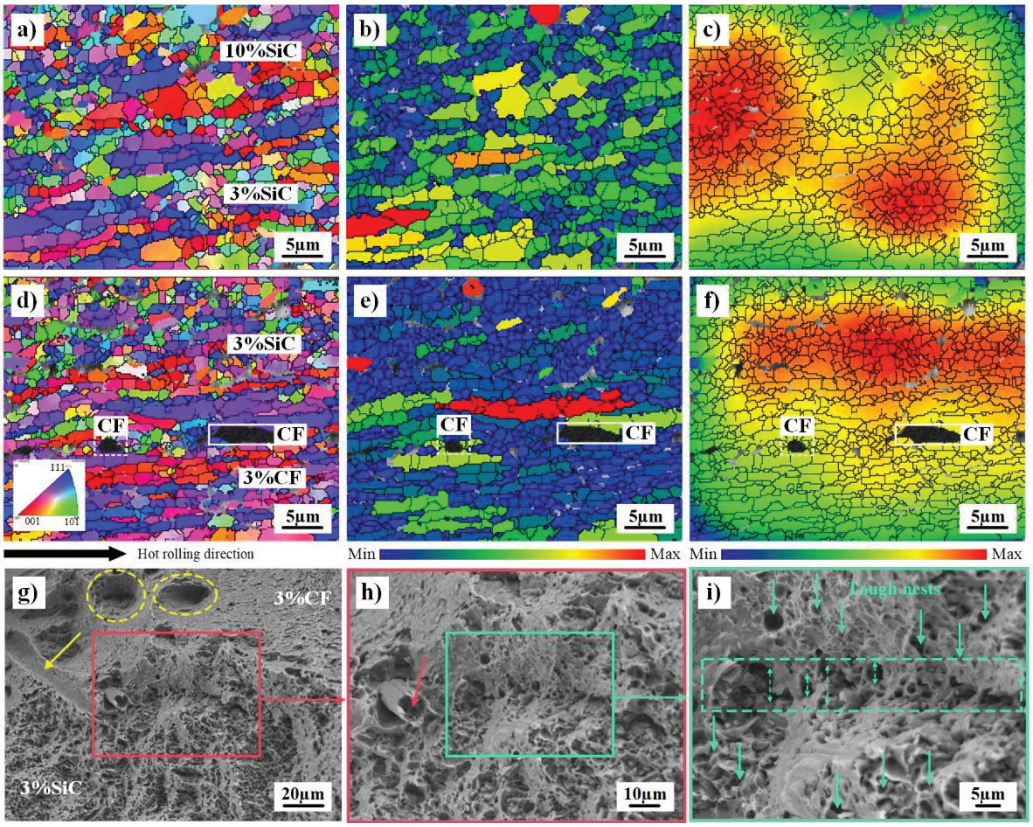

Figure 4-7 EBSD map at each layer interface and fracture morphology at the CF-SiC interface: a) and d) IPF map of the FGC interface; b) and e) Grain size distribution; c) and f) Stress distribution; g), h) and i) fracture morphology at the interface

To explore the interface stress effect on the mechanical properties, the tensile fracture morphology at the interface was observed. Figure 4-7 g), h), and i) demonstrate the fracture morphology at the 3% CF-3% SiC interface and its local enlargement. Macroscopically, the fracture in the CF layer is relatively flat and fractures at an angle to the tensile direction, indicating that shear stress is the main cause of failure, as described in Figure 4-7 g). Failure zones caused by the CF pullout and fracture are also observed, as depicted by the yellow dotted line and arrow in Figure 4-7 g). Considerable small-sized tough nests perpendicular to the tensile direction are observed in the SiC layer in Figure 4-7 g). This indicates that the interface is also the dividing line between microstructure and plastic deformability. As seen in Figure 4-7 h) and i), the interface failure extends along the vertical direction with fine tough nests on both sides of the interface, as illustrated by the green arrows in the figure.

The different grain orientation and grain boundary distribution on both sides of the interface have a hindering effect on dislocation movement and crack extension[35]. On the one hand, high interfacial energy storage will promote recrystallization grain nucleation; on the other hand, it will lead to high interfacial stress. The recrystallized grain nucleation improves the plasticity of the interface to some extent, as evidenced by the production of fine tough nests in Figure 4-7 i). However, cracking failure occurs at the interface when high interfacial stresses cannot be counteracted.

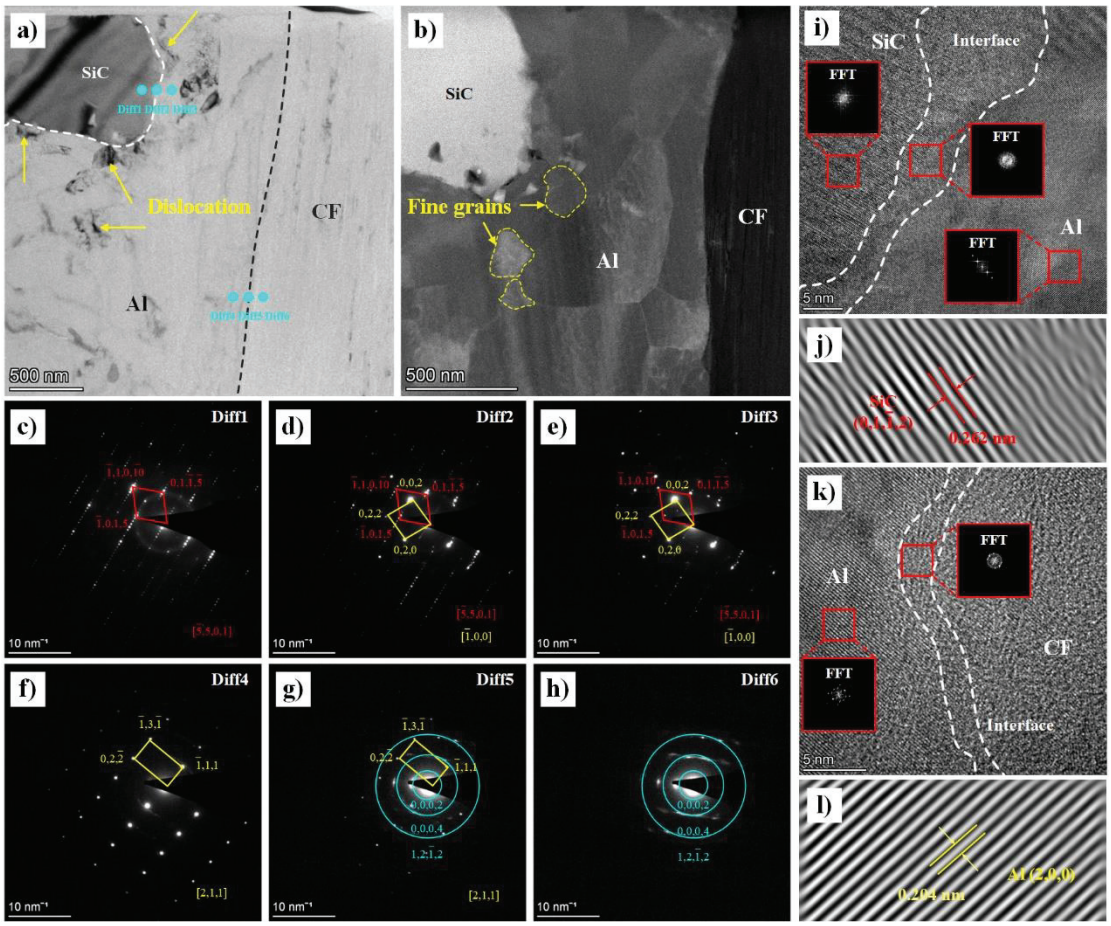

Figure 4-8 The TEM images of the SiC-Al interface and CF-Al interface: a) bright field TEM image; b) dark field TEM image; c)-h) diffraction spots; i)-l) High-resolution images at the interface and FFT and IFFT conversion

The TEM morphology, high-resolution images, and diffraction spots at the SiC-Al interface and CF-Al interface are presented in Figure 4-8. Figure 4-8 a) shows the bright field TEM image at the interface, no cracks or pores at the interface between SiC particles and Al and between CF and Al are observed at the nanoscale, indicating that

the interface between SiC and CF and the Al matrix is well bonded. Affected by strong plastic deformation, the distortion inside the SiC particles is large. The dislocations marked by the yellow arrows in Figure 4-8 a) also confirm that the SiC particles are more effective in blocking the dislocation motion than CF. Figure 4-8 b) shows the dark field TEM image at the interface, as seen by the yellow dashed box in the figure, the size of the grains near the SiC particles is smaller compared with the CF.

Figure 4-8 c), d), and e) display the diffraction spots at the interface of SiC, SiC-Al interface, and the Al matrix near the interface, respectively. As presented in Figure 4-8 d), there is a semi-coherent interface between SiC and Al, which gives SiC and Al a close interface bond[36]. The SiC diffraction spots can still be observed at the Al matrix near the interface, as provided in Figure 4-8 e). Figure 4-8 f), g), and h) show the diffraction spots at the Al matrix near the interface, the interface between Al and CF, and the CF, respectively. There is also a semi-coherent interface between CF and Al with tight bonding, as performed in Figure 4-8 g). As shown in Figure 4-8 f), no diffraction rings of CF are observed in the Al matrix near the interface. In comparison with Figure 4-8 e), the SiC and the Al matrix have larger interfacial reaction region. This is also confirmed by the high-resolution diagrams at the interface, as pointed out in Figure 4-8 i) and l), where the interfacial region between SiC and Al is wider. The interfacial bond between SiC and the Al matrix is tighter than that of CF, which is one of the reasons for the greater hindrance of dislocation motion by SiC. As concluded in Figure 4-8 i), j), k) and l), the interplanar spacing of SiC is 0.262nm, and the interplanar spacing of Al is 0.204nm by IFFT conversion, and tight amorphous compounds have been generated between SiC-Al and CF-Al. The interface structure of the semi-coherent interface and the generation of non-crystalline compounds provides a bridge for the load transmission and heat transmission between the enhanced body and the Al matrix, which positively improves the intensity and thermal performance of the FGC.

4.4.2 High mechanical property mechanism

According to Section 4.3.2, the FGC has both high yield strength and high plastic deformation capacity. Combined with the fracture morphology, EBSD maps, and TEM images, the reason why the FGC has high strength can be explained as follows: On the one hand, the PSN effect induced by SiC particles and its hindering effect on the grain boundary motion results in a smaller grain size of the Al matrix, causing the fine-grain strengthening; on the other hand, the addition of the SiC introduces more dislocations into the Al matrix and further increases the dislocation density after hot rolling, giving the FGC higher strength.

Based on the discussion of interlayer interface structure and dislocation morphology in Section 4.4.1, it can be inferred that the mechanism that endows FGC with high plastic deformation capacity is mainly due to the dislocation formation promoted by the SiC and the hindrance of cracking by the gradient structure. The KAM map shown in Figure 4-3 suggests that the addition of SiC causes lattice distortion in the Al matrix, leading to more dislocation sources. The multiplication of dislocations is promoted by plastic deformation, and more dislocations are induced in the SiC layer. There are significantly more dislocations near SiC than CF, as presented in Figure 4-8 a). Under external loading, considerable dislocations in the SiC layer slip, ensuring the crystal can undergo slip and thus enhancing the plastic deformation capability.

In addition, the design of the gradient structure gives the FGC a gradient microstructure, which means that the grain size gradually decreases from the 3% CF layer to the 3% SiC layer to the 10% SiC layer, resulting in a noticeable interface between the SiC layer and the CF layer. As provided in Figure 4-7 g), there is a significant difference in the fracture morphology of the SiC layer and the CF layer on both sides of the interface. Cracks will either stop propagating or deflect at the interface, resulting in a large amount of energy consumption. Therefore, the gradient structure has the effect of impeding the propagation of cracks between layers, which has a positive effect on the overall plastic deformation capability of the FGC.

4.4.3 Texture evolution and recrystallization mechanism

Section 4.3.1 revealed the different microstructure of the FGC layers, and the differences in grain size and reinforcement will further affect the evolution of microstructure during the thermal deformation process, including grain nucleation and growth orientation and recrystallization mechanisms. Clarifying the microstructure evolution of the FGC layers not only explains the mechanical behavior but also provides guidance for designing and optimizing FGCs. As shown in the Orientation Distribution Function (ODF) diagram in Figure 4-9, the type and strength of the texture of each layer after hot rolling have significant differences. The 3% CF layer has a strong Copper component and Brass component, while the 3% SiC layer and the 10% SiC layer have a high R component. The texture orientation strength graph reveals that the 3%CF layer has the highest orientation intensity among these four textures. The most apparent contrast is the Brass component, where the 3% CF layer has a much higher orientation intensity than the two SiC layers. The brass component and Copper component are typical rolled texture[37,38], indicating that the 3% CF layer is in the rolling orientation grain growth stage, which is also confirmed by the coarse grain morphology of the Copper and Brass components in Figure 4-9 a).

Furthermore, the comparison demonstrates that the strength of the Copper component decreases from the 3% CF layer to the 3% SiC layer to the 10% SiC layer, indicating that the SiC layer undergoes faster recrystallization at the same deformation. The PSN effect, caused by SiC particles, promotes the nucleation of recrystallization grains during plastic deformation. Compared with CF, the smaller size and aspect ratio of SiC particles leads to a wider range of nucleation orientations, which produces a weaker recrystallization texture. As a result, the texture orientation strength of the 3% SiC and 10% SiC layers is lower than that of the 3% CF layer.

The Goss components and the R components are typical recrystallized texture[39,40]; there are two main types of R components nucleation[40,41]. The first is nucleation by reversion in the rolling texture, which means nucleation by continuous recrystallization or in situ recrystallization within the grain of the rolling component. When nucleated

by in situ recrystallization, the orientation of recrystallization does not change significantly because it does not involve the movement of large angle grain boundaries, allowing the rolling texture to be preserved. Therefore, it is often adjacent to the rolling texture. The second is the formation of R-oriented nuclei within the S-oriented grains between the deformation zones, and this type of nucleation leads to a change in orientation. As seen in Figure 4-9 a) b), the R components in the 3% CF layer are ordinarily adjacent to the Copper and Brass components. In contrast, in Fig. 9 c), d) and e), most of the R components are randomly distributed and independent of the Copper and Brass components.

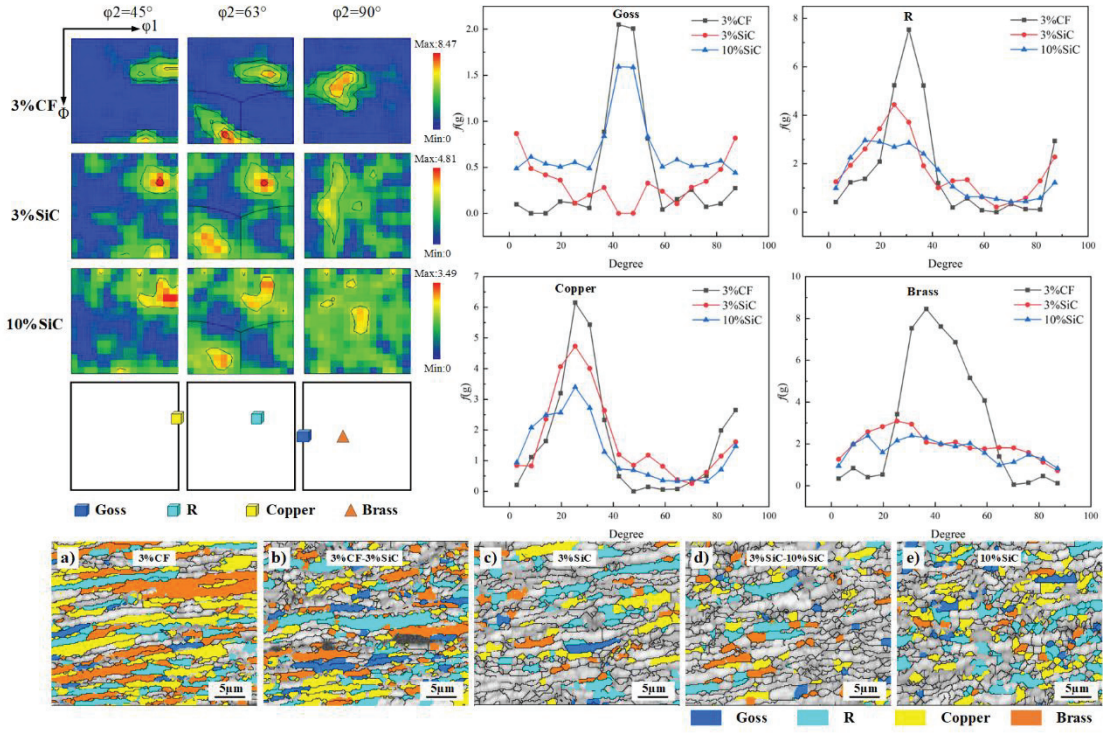

Figure 4-9 ODF diagram, texture orientation strength diagram, and texture distribution of each layer of FGC after hot rolling

The differences in local plastic deformation between CF and SiC layers result in different recrystallization nucleation mechanisms. Compared with CF, the smaller SiC particles lead to larger local plastic deformation within the Al matrix during hot rolling. The uniform deformation promotes the generation of shear bands, then the deformation further facilitates the nucleation of S-oriented grains within the shear bands, promoting

the growth of R-oriented grain nucleation. Generally, the growth of selectively oriented grains competes with grain nucleation. However, when the local plastic deformation energy of the CF layer fails to break the energy barrier, the growth of selectively oriented grains consumes significant energy, leaving insufficient energy to promote grain nucleation. In such cases, the rolling texture recrystallizes in situ by reverting to nucleation.

The difference between the two modes of in situ recrystallization and nucleation-growth recrystallization is the fundamental reason for the different microstructural characteristics of the FGC layers after hot rolling. The in-situ recrystallized grains produced in the rolling texture are characterized by large grain size and dependence on the rolling texture grains, as provided in Fig. 9 a). The recrystallized grains of this morphology do not contribute to enhancing mechanical properties. In contrast, the recrystallized grains of nucleation-growth mode are small and equiaxed, giving the SiC layers higher strength and better plastic deformability, as displayed in Fig. 9 c), d), e).

4.5 Summary

In this study, 3% CF-3% SiC-10% SiC Al matrix FGC were prepared by SPS. Through the microstructure characterization and property testing of FGC, the mechanism of reinforcement type and content on the microstructure evolution and mechanical behavior were investigated in depth. The following conclusions can be drawn:

(1) The reinforcement in the FGC layers is uniformly distributed. The FGC has good bonding interfaces between the 3% CF-3% SiC and 3% SiC-10% SiC layers.The difference in reinforcement type and volume fraction leads to different microstructure characteristics of the FGC layers.

(2) FGC simultaneously has high yield strength and plastic deformation ability. The fine grain strengthening effect due to SiC gives the high strength of FGC. The promotion of dislocation formation by SiC and the crack hindrance by gradient structure are the main reasons for the high plastic deformability.

(3) The changes of grain orientation and grain size at the interlayer interface lead to high interlayer stress, which further causes interface failure and cracking. The semi-coherent interface between SiC-Al and CF-Al promotes good interfacial bonding.

(4) As the addition of SiC particles introduces more interfaces and leads to smaller grain size and higher grain boundary density, the thermal conductivity values of FGC in the axial and horizontal directions are lower than those of Al and CF/Al.

(5) The difference in grain size and content between CF and SiC leads to in situ recrystallization for the 3% CF layer, while the 3% SiC and 10% SiC layers are mainly nucleation-growth recrystallization mechanisms. The different recrystallization mechanisms result in the different mechanical properties of CF and SiC layers in FGC to a certain degree.

4.6 References

[1]. R Ekici, MK Apalak, M Yildirim. Indentation behavior of functionally graded Al-SiC metal matrix composites with random particle dispersion[J]. COMPOS PART B-ENG. 2011, 42:1497-1507.

[2]. P Li, Y Tong, X Wang, YS Sato, H Dong. Microstructures and mechanical properties of AlCoCrFeNi2.1/6061-T6 aluminum-matrix composites prepared by friction stir processing[J]. MAT SCI ENG A-STRUCT. 2023, 863:144544.

[3]. K Zhong, J Zhou, C Zhao, K Yun, L Qi. Effect of interfacial transition layer with CNTs on fracture toughness and failure mode of carbon fiber reinforced aluminum matrix composites[J]. COMPOS PART A-APPL S. 2022, 163:107201.

[4]. Y Guo, WQ Li, XG Liu, K Sugio, YJ Ke, KY Wang, WC Liu, G Sasaki. Effect of copper coating on interfacial properties, interfacial thermal resistance, microstructure evolution and mechanical properties of aluminum matrix composites[J]. J ALLOY COMPD. 2022, 917:165376.

[5]. M Tayyebi, M Alizadeh. Thermal and wear properties of Al/Cu functionally graded metal matrix composite produced by severe plastic deformation method[J]. J MANUF PROCESS. 2023, 85:515-526.

[6]. AG Arsha, E Jayakumar, TPD Rajan, V Antony, BC Pai. Design and fabrication of functionally graded in-situ aluminium composites for automotive pistons[J]. MATER DESIGN. 2015, 88:1201-1209.

[7]. M Yamanouchi, M Koizumi, T Hirai, I Shiota. Proceedings of the First International Symposium on Functionally Gradient Materials. Japan. 1990.

[8]. M Koizumi. The concept of FGM, ceramic transactions[J]. FUNCT GRADIENT MATER. 1993, 34:3-10.

[9]. M Koizumi. FGM activities in Japan[J]. COMPOS PART B-ENG. 1997, 28B:1-4.

[10]. D Muniraj, VM Sreehari. Damage assessment of sandwich structures with Al/SiC functionally graded plasma sprayed faceplates subjected to single and repeated impacts[J]. COMPOS STRUCT. 2022, 287:115369.

[11]. A Sharma, Y Morisada, H Fujii. Bending induced mechanical exfoliation of graphene interlayers in a through thickness Al-GNP functionally graded composite fabricated via novel single-step FSP approach[J]. CARBON. 2022, 186:475-491.

[12]. HX Zhu, R Abbaschian. Microstructures and properties of in-situ NiAl-Al2O3 functionally gradient composites[J]. COMPOS PART B-ENG. 2000, 31:383-390.

[13]. T Fujii, K Tohgo, M Iwao, Y Shimamura. Fracture toughness distribution of alumina-titanium functionally graded materials fabricated by spark plasma sintering[J]. J ALLOY COMPD. 2018, 766:1-11.

[14]. R Jojith, M Sam, N Radhika. Recent advances in tribological behavior of functionally graded composites: A review[J]. ENG SCI TECHNOL. 2022, 25:100999.

[15]. A Strojny-Nędza, K Pietrzak, W Węglewski. The Influence of Al2O3 Powder Morphology on the Properties of Cu-Al_2O_3 Composites Designed for Functionally Graded Materials (FGM)[J]. J MATER ENG PERFORM. 2016, 25:3173-3184.

[16]. EI Salama, SS Morad, AMK Esawi. Fabrication and mechanical properties of aluminum-carbon nanotube functionally-graded cylinders[J]. MATERIALIA. 2019, 7:100351.

[17]. R Duan, S Li, B Cai, Z Tao, W Zhu, F Ren, MM Attallah. In situ alloying based laser powder bed fusion processing of β Ti-Mo alloy to fabricate functionally graded composites[J]. COMPOS PART B-ENG. 2021, 222:109059.

[18]. J Zygmuntowicz, A Miazga, P Wiecinska, W Kaszuwara, K Konopka, M Szafran. Combined centrifugal-slip casting method used for preparation the Al2O3-Ni functionally graded composites[J]. COMPOS PART B-ENG. 2018, 141:158-163.

[19]. F Erdemir, A Canakci, T Varol, S Ozkaya. Corrosion and wear behavior of functionally graded Al2024/SiC composites produced by hot pressing and consolidation[J]. J ALLOY COMPD. 2015, 644:589-596.

[20]. V Bikkina, SR Talasila, K Adepu. Characterization of aluminum based functionally graded composites developed via friction stir processing[J]. T NONFERR METAL SOC. 2020, 30:1743-1755.

[21]. M Saadatmand, JA Mohandesi. Comparison Between Wear Resistance of Functionally Graded And Homogenous Al-SiC Nanocomposite Produced by Friction Stir Processing (FSP)[J]. J MATER ENG PERFORM. 2013, 23:736-742.

[22]. RS Parihar, SG Setti, RK Sahu. Recent advances in the manufacturing processes of functionally graded materials: a review[J]. SCI ENG COMPOS MATER. 2018, 25:309-336.

[23]. M Naebe, K Shirvanimoghaddam. Functionally graded materials: A review of fabrication and properties[J]. APPL MATER TODAY. 2016, 5:223-245.

[24]. N Radhika, J Sasikumar, JL Sylesh, R Kishore. Dry reciprocating wear and frictional behaviour of B4C reinforced functionally graded and homogenous aluminium matrix composites[J]. J MATER RES TECHNOL. 2020, 9:1578-1592.

[25]. CA León-Patiño, EA Aguilar-Reyes, E Bedolla-Becerril, A Bedolla-Jacuinde, S Méndez-Díaz. Dry sliding wear of gradient Al-Ni/SiC composites[J]. WEAR. 2013, 301:688-694.

[26]. C Huang, A List, L Wiehler, M Schulze, F Gärtner, T Klassen. Cold spray deposition of graded Al-SiC composites[J]. ADDIT MANUF. 2022, 59:103116.

[27]. T Wu, Y Hu, Y Leng, M Zhang, N Naerkezha, M Wang. In situ observation of fracture in homogeneous and functionally graded 6061Al/SiCp composites[J]. MAT SCI ENG A-STRUCT. 2022, 830:142279.

[28]. ZL Chao, ZW Wang, LT Jiang, SP Chen, BJ Pang, RW Zhang, SQ Du, GQ Chen, Q Zhang, GH Wu. Microstructure and mechanical properties of B4C/2024Al functionally gradient composites[J]. MATER DESIGN. 2022, 215:110449.

[29]. G Kırmızı, H Arık, H Çinici. Experimental study on mechanical and ballistic behaviours of silicon carbide reinforced functionally graded aluminum foam composites[J]. COMPOS PART B-ENG. 2019, 164:345-357.

[30]. H Kwon, M Leparoux, A Kawasaki. Functionally Graded Dual-nanoparticulate-reinforced Aluminium Matrix Bulk Materials Fabricated by Spark Plasma Sintering[J]. J MATER SCI TECHNOL. 2014, 30:736-742.

[31]. MJ Oza, KG Schell, EC Bucharsky, T Laha, S Roy. Developing a hybrid Al-SiC-graphite functionally graded composite material for optimum composition and mechanical properties[J]. MAT SCI ENG A-STRUCT. 2021, 805:140625.

[32]. M Ferraris, F Gili, X Lizarralde, A Igartua, G Mendoza, G Blugan, L Gorjan, V Casalegno. SiC particle reinforced Al matrix composites brazed on aluminum body for lightweight wear resistant brakes[J]. CERAM INT. 2022, 48:10941-10951.

[33]. W Węglewski, P Pitchai, M Chmielewski, PJ Guruprasad, M Basista. Thermal conductivity of Cu-matrix composites reinforced with coated SiC particles: Numerical modeling and experimental verification[J]. INT J HEAT MASS TRAN. 2022, 188:122633.

[34]. T Schubert, B Trindade, T Weißgärber, B Kieback. Interfacial design of Cu-based composites prepared by powder metallurgy for heat sink applications[J]. MAT SCI ENG A-STRUCT. 2008, 475:39-44.

[35]. FM Xu, SJ Zhu, J Zhao, M Qi, FG Wang, SX Li, ZG Wang. Fatigue crack growth in SiC particulates reinforced Al matrix graded composite[J]. MAT SCI ENG A-STRUCT. 2003, 360:191-196.

[36]. Y Xie, Y Huang, F Wang, X Meng, J Li, Z Dong, J Cao. Deformation-driven metallurgy of SiC nanoparticle reinforced aluminum matrix nanocomposites[J]. J ALLOY COMPD. 2020, 823:153741.

[37]. S Wang, A Xiao, Y Lin, X Cui, X Sun. Effect of induced pulse current on mechanical properties and microstructure of rolled 5052 aluminum alloy[J]. MATER CHARACT. 2022, 185:111757.

[38]. JX Zhang, C Liu, WC Liu, CS Man. Effect of precipitation state on texture evolution in cold-rolled continuous cast AA 2037 aluminum alloy[J]. J ALLOY COMPD. 2017, 728:1199-1208.

[39]. LF Shuai, TL Huang, GL Wu, X Huang, OV Mishin. Development of Goss texture in Al-0.3%Cu annealed after heavy rolling[J]. J ALLOY COMPD. 2018, 749:399-405.

[40]. JX Zhang, M Ma, WC Liu. Effect of initial grain size on the recrystallization and recrystallization texture of cold-rolled AA 5182 aluminum alloy[J]. MAT SCI ENG A-STRUCT. 2017, 690:233-243.

[41]. O Engler, HE Vatne, E Nes. The roles of oriented nucleation and oriented growth on recrystallization textures in commercial purity aluminium[J]. MAT SCI ENG A-STRUCT. 1996, 205:187-198.

Chapter 5

Conclusions

The rapid development of science and technology has gradually increased the demand for high-performance Al matrix composites. In the design of high-performance aluminum matrix composites, the type and size of the reinforcement, interfacial modifications, and subsequent thermal processing parameters can directly affect the performance of the composite. In order to solve the common problems in the design of current aluminum matrix composites, such as poor wettability of reinforcement and aluminum matrix, poor plasticity of composites, less than ideal thermal properties and lower strength, this paper presents an in-depth study and analysis from three aspects of interface modification, reinforcement size and reinforcement of composites, respectively.

1. Interface modification: Effect of copper coating on interfacial properties, interfacial thermal resistance, microstructure evolution and mechanical properties of aluminum matrix composites

In order to promote the interfacial bonding between the reinforcement and the Al matrix and to improve the interfacial bonding strength while reducing the interfacial reaction, interfacial modification is usually used. Among the various interface modification methods, copper coating is widely used because of both its economy and effectiveness. In this study, copper was coated on the surface of short carbon fibers by ultrasonic-assisted chemical plating, and two composites were prepared by SPS technique using uncoated and coated short carbon fibers with 3% volume fraction as the reinforcement, respectively. The microstructural characteristics, interfacial structure and interfacial products, mechanical properties and thermal conductivity of the copper-coated and uncoated composites were compared. The mechanism of copper coating on microstructure evolution, interfacial reaction, mechanical properties and thermal properties was analyzed in depth. In addition to this, the copper-coated and uncoated

composites were hot rolled to investigate the effect of copper coating on the heat deformation properties. The mechanism of the effect of the change of carbon fiber arrangement on the thermal conductivity of the composites due to the hot rolling process was also analyzed. The following conclusions were obtained:

(1). The copper coating improves the wettability of short carbon fiber and Al matrix, resulting in better electrical conductivity of the mixed powder of copper-coated carbon fiber and Al powder. This leads to the full effect of the pulse current during the sintering process, which better removes the oxide film on the surface of the Al powder and results in good metallurgical bonding of the copper-coated composites. In contrast, the poor electrical conductivity of the mixture of uncoated copper carbon fiber and Al powder results in poor metallurgical bonding of the uncoated copper composites. The oxide film on the surface of the Al powder is not completely removed by the pulsed current, leading to the presence of obvious oxide bands in SEM observations and EDS analysis.

(2). EDS analysis results indicated that, after ball milling and sintering, the copper coating on short carbon fibers partially exfoliated and diffused into the Al matrix, with only a small amount remaining adhered to the short carbon fibers.

(3). Both composites underwent strong plastic deformation after hot rolling. EBSD results revealed that the uncoated copper composites experienced cracking at the interface due to stress concentration, and the oxide bands from sintering remained present in the Al matrix. In contrast, the copper-coated composites exhibited well-bonded interfaces, and no interfacial cracking was observed even in stress-concentrated areas. These findings suggest that interface modification improves interfacial coherence, enhancing the plastic deformation ability of the composites.

(4). The XRD results showed that only elemental C and Al were present in both composites. It is difficult to be detected due to the low content of other elements. The TEM results at the interface showed that the interfacial product of the uncoated short carbon fiber and the Al matrix in the sintered state was amorphous carbide, while the harmful product Al_4C_3 was generated at the interface after hot rolling. Amorphous

carbides were also generated between the copper coated short carbon fibers and the Al matrix, but the thickness was less than that of the uncoated copper composites, and no harmful crystalline products were observed at the interface after hot rolling. Therefore, it is known that the copper coating has the effect of inhibiting the interfacial reaction.

(5). Nano-hardness measurements at the interface revealed that the hardness values of uncoated carbon fibers decreased sharply after hot rolling, while the hardness values at the interface increased substantially. In contrast, the hardness of copper-coated carbon fibers did not change significantly before and after hot rolling. These results suggest that uncoated carbon fibers reacted violently with the Al matrix during hot rolling, leading to the production of crystalline products and higher interfacial hardness values. During this process, carbon atoms diffused into the Al matrix, causing damage to the structure of carbon fibers and a decrease in their strength. In contrast, the copper coating protected the structure of carbon fibers from damage during thermal deformation by inhibiting the violent interfacial reaction, resulting in improved mechanical properties of the composites.

(6). Room temperature tensile tests revealed that the copper-coated composites exhibited slightly higher yield strength and plasticity than the uncoated composites. This is attributed to the good metallurgical bonding of the copper-coated composites and the protection of the carbon fiber structure. However, the plasticity of both composites is much lower than that of pure Al. SEM observations of the tensile fracture indicate that the larger diameter of short carbon fibers results in cutting effects on the Al matrix, leading to reduced plasticity of the composites.

(7). Thermal conductivity tests revealed that the copper-coated composites had higher thermal conductivity than the uncoated composites, both before and after hot rolling. This is attributed to the good metallurgical bonding of the copper-coated composites and the modification of the interface by the copper coating. Calculations of the interfacial product thickness and interfacial thermal conductivity indicate that the thickness of the interfacial product is inversely proportional to the interfacial thermal conductivity for interfacial products with lower thermal conductivity. After hot rolling, the short carbon fibers in both composites were aligned in the rolling direction, resulting

in higher thermal conductivity in that direction due to the higher thermal conductivity of the short carbon fibers in the axial direction.

(8). Texture analysis revealed that the coated and uncoated composites exhibited different texture strengths. The recrystallization grain mechanisms were traced based on the type of texture, and the results indicated that the dynamic recrystallization mechanisms of SCF/Al and Cu-SCF/Al involved continuous dynamic recrystallization mechanisms transitioning from low-angle grain boundaries to high-angle grain boundaries, shear band grain nucleation, and the Rot-Gauss texture promoting recrystallized grain nucleation.

2. Reinforcement size: Effect of short carbon fiber and nano carbon fiber as reinforcement on microstructure and properties of hot-rolled aluminum matrix composites

The first part of the study demonstrated that the larger diameter of short carbon fibers negatively affects the plasticity of composites. Thus, this part of the study investigates the effect of reinforcement size on composites. Two composites were prepared using short carbon fibers and vapor phase grown carbon nanofibers (VGCNFs) as reinforcement at the same volume fraction (3% vol.). The study investigated the effects of reinforcement size on the microstructure, interfacial structure, mechanical properties, and thermal properties of the composites. Both short carbon fiber and carbon nanofiber reinforced composites were hot-rolled to investigate the mechanism of the influence of reinforcement size on the thermal deformation of the composites. The main conclusions are as follows:

(1). SEM results revealed that agglomeration occurred in the Al matrix due to the smaller diameter and larger aspect ratio of VGCNFs. In contrast, short carbon fibers did not agglomerate at the same volume fraction due to their larger size, and were uniformly distributed in the Al matrix.

(2). EBSD results indicated that short carbon fiber reinforced composites have smaller grain size and higher grain boundary density compared to carbon nanofiber reinforced composites. This is attributed to the hindering effect of short carbon fibers

on grain boundary motion and the stimulation of nucleation. KAM results revealed that the addition of short carbon fibers resulted in higher residual stresses in the Al matrix, while the addition of carbon nanofibers did not introduce excessive stresses into the Al matrix.

(3). After hot rolling, short carbon fiber reinforced composites exhibit more equiaxed fine grains, while the grains in carbon nanofiber reinforced composites mainly take the form of fibers along the rolling direction. The dynamic recrystallization process of short carbon fiber reinforced composites is faster for the same amount of deformation, which is attributed to the obstruction of dislocation and grain boundary motion by short carbon fibers, providing an energy drive for recrystallization.

(4). SEM results revealed that short carbon fibers were tightly bonded to the Al matrix, while VGCNFs had pores at the interface with the Al matrix due to agglomeration. TEM results showed that the interface between short carbon fibers and the Al matrix was well bonded, with continuous and thick interface products. In contrast, obvious pores were observed at the interface between VGCNFs and the Al matrix. Further amplification of the interface revealed the generation of amorphous carbides at the bond between VGCNFs and the Al matrix.

(5). Nano-hardness measurements at the interface revealed that interfacial hardness values of short carbon fibers and the Al matrix were higher than those of VGCNFs and the Al matrix, both before and after hot rolling. This is attributed to the good interfacial bonding of short carbon fibers with the Al matrix.

(6). Tensile stress-strain curves at room temperature revealed that carbon nanofiber-reinforced composites in the sintered state had plasticity comparable to that of pure Al and yield strength slightly higher than that of pure Al. This is attributed to the smaller size and lower strength of carbon nanofiber clusters. However, after hot rolling, the plasticity of carbon nanofiber-reinforced composites was reduced, and the yield strength values were lower than those of pure Al. Observation and analysis of the tensile fracture showed that the carbon nanofiber clusters changed from equiaxed to elongated along the rolling direction with sharp ends, which could easily become a source of cracks and lead to failure due to stress concentration. Moreover, mutual

agglomeration between VGCNFs made it difficult to play a good reinforcement role, resulting in low strength of carbon nanofiber-reinforced composites.

(7). Before and after hot rolling, short carbon fiber reinforced composites exhibit higher yield strength than both pure Al and carbon nanofiber reinforced composites, but lower plasticity. This is attributed to the homogeneous dispersion of carbon fibers in the Al matrix, the pinning effect on grain boundaries and dislocations, the load transfer mechanism, and the fine grain reinforcement resulting in high strength of the composite. However, as shown in the first part of the study, the large diameter of short carbon fibers has a negative effect on the plasticity of the composites, resulting in lower plasticity.

(8). Thermal conductivity results of both composites before and after hot rolling revealed that carbon nanofiber reinforced composites had higher thermal conductivity than short carbon fiber reinforced composites, both before and after hot rolling. This is mainly due to the higher thermal conductivity of VGCNF compared to short carbon fibers. However, calculations of the thermal conductivity efficiency of the two reinforced materials showed that, although VGCNF reinforced composites have higher thermal conductivity under the same volume fraction, the thermal conductivity efficiency of VGCNF is lower than that of short carbon fiber. This is because VGCNF is agglomerated and exists in the form of clusters in the Al matrix, generating more heat loss in the heat conduction process, resulting in low heat conduction efficiency. In contrast, short carbon fibers are well combined with the Al matrix and produce only a small amount of heat loss at the interface, resulting in high thermal conductivity efficiency.

3. Reinforcement of composites: Microstructure evolution, property analysis, and interface study of 3%CF-3%SiC-10%SiC functional gradient aluminum matrix composites

The addition of reinforcement to the Al matrix inevitably affects the integrity of the Al matrix and has a negative impact on its plastic deformability. Previous studies have shown that the larger diameter of short carbon fibers leads to lower plasticity of

the composites, and although carbon nanofibers do not have an overly negative effect on the plasticity of the composite, the agglomeration of carbon nanofibers leads to lower strength of the composites. Therefore, achieving the synergistic enhancement of strength and plasticity of composites is a difficult problem in current research. The design of heterogeneous structure and the preparation of gradient structure are effective means to solve the strength-plasticity problem. In this part of the study, short carbon fiber reinforced Al matrix composites were used to achieve the synergistic enhancement of strength and plasticity of composites through the design of a gradient structure. The 3% CF-3% SiC-10% SiC gradient-reinforced Al matrix composites were prepared using the SPS technique, and the microstructure characteristics, mechanical properties, interfacial structure, and thermal conductivity of the gradient composites were investigated. The mechanism of the design of the gradient structure on tissue evolution and mechanical properties was analyzed, and the heat deformation properties of the gradient composites were investigated by hot rolling. The following conclusions were obtained:

(1). SEM observations of the layers of the gradient composites revealed that no defects such as pore cracks were observed. The morphological differences between different layers were relatively obvious, and the distribution of reinforcement in each layer was uniform, with the reinforcement well bonded to the Al matrix. After hot rolling, short carbon fibers were distributed along the hot rolling direction, while the distribution of silicon carbide particles did not change significantly.

(2). Peak-seeking XRD results of the gradient composites before and after hot rolling detected the presence of C-phase, Al-phase, SiC-phase, and Al_4C_3-phase.

(3). Microhardness measurements of each layer of the gradient composites and at the interface revealed that hardness values gradually increased from the 3% CF layer to the 3% SiC layer to the 10% SiC layer, and the interfacial hardness of each layer was significantly higher than the hardness value of the previous layer. This indicates that the gradient composites have more complex microstructure characteristics at the interface of each layer.

(4). EBSD results revealed that for the gradient composites in the sintered state,

the grain size of the 3% CF layer was larger than that of the 3% SiC layer and the 10% SiC layer. Correspondingly, the residual stress and the percentage of low-angle grain boundaries in the 3% CF layer were lower than those in the SiC layer. This is attributed to the fact that the addition of SiC particles has a stronger effect on grain boundary and dislocation motion compared to short carbon fibers, resulting in smaller grain size and higher stress values in the composites.

(5). After hot rolling, the grain size of all layers of the gradient composites substantially reduced, but the 10% SiC layer had the smallest grain size while the 3% CF layer had the largest grain size. The SiC layer had more equiaxed fine grains in terms of grain morphology, and more randomly oriented grains in terms of grain orientation. This indicates that the two SiC layers had a faster dynamic recrystallization process than the CF layer for the same amount of deformation. This is mainly attributed to the stronger grain boundary and dislocation pegging of SiC particles, as well as stimulated nucleation.

(6). Tensile stress-strain curves at room temperature showed that the gradient composites had both higher yield strength and plasticity compared to pure Al and single short carbon fiber reinforced composites. Observation of the tensile fracture revealed that the 3% SiC layer had a large number of small-sized tough nests, along with the 10% SiC layer before and after hot rolling. Therefore, the fine grain strengthening effect due to SiC contributed to the high strength of the gradient composites. The promotion of dislocation formation by SiC and the hindrance of cracks by the gradient structure were the main reasons for the high plastic deformability.

(7). Thermal conductivity measurements in horizontal and axial directions revealed that the thermal conductivity of the gradient composites was lower than that of pure Al and short carbon fiber reinforced composites. This was attributed to the addition of SiC particles, which led to more interfaces in the composites, resulting in heat loss when passing through the interfaces. As the number of interfaces increased, the heat loss also increased, leading to lower thermal conductivity. Additionally, for the gradient composites, the thermal conductivity in the axial direction after hot rolling was

lower than that in the horizontal direction. This was mainly due to the higher density of grain boundaries in the axial direction after hot rolling, resulting in more heat loss.

(8). Characterization and analysis of the interlayer interface of the gradient composites revealed that residual stresses at the interlayer interface were high, and the interface was the dividing line between plasticity and grain orientation. The higher stresses made the interlayer interface prone to be the first to fail during the deformation process.

(9). TEM observations at the interface between the short carbon fiber and the Al matrix and the interface between the SiC and the Al matrix showed that both reinforcements were well bonded to the Al matrix, and no defects such as cracks or holes were observed at the interface in the bright-field TEM photographs. A higher density of dislocations was observed near the SiC particles, indicating that SiC particles have a greater pegging effect on dislocations than short carbon fibers. Analysis of diffraction spots at the interface showed that SiC has a semi-coherent interface with both the short carbon fiber and the Al matrix, indicating that both reinforcements were tightly bonded to the Al matrix. FFT of the interfacial products showed that both SiC particles and short carbon fibers generated amorphous carbides with the Al matrix, and the generation of interfacial products also indicated good interfacial bonding.

(10). After hot rolling, the gradient Al matrix composite layers have different textures. The 3% CF layer has more Copper and Brass textures, i.e., rolled textures, while the SiC layer has more R texture, i.e., recrystallization texture. The SiC layer has a higher recrystallization percentage, which is supported by the side effects. Judging from the distribution and morphology of the texture, the recrystallization mechanism of the CF layer is mainly in situ recrystallization, while the SiC layer mainly forms recrystallized grains through the nucleation-growth mechanism. The different recrystallization mechanisms lead to different recrystallized grain morphologies, which in turn affect the microstructure and mechanical properties of the different layers.

Acknowledgments

I have received a lot of help and guidance from many people during my doctoral studies. I would like to express my sincere gratitude to all the people who have helped me.

First of all, I would like to express my sincere gratitude to Professor Sasaki for his great support and guidance, including establishing the Ph.D. project, experiment plan guidance, thesis writing, and scholarship application. I also thank Professor Sugio for his guidance and assistance in the experiments. And express my thanks to Professor Matsuki and Professor Choi for their continuous help. I am deeply appreciative of Professor Xingang Liu of Yanshan University for his tremendous support in experiments, analysis, and writing.

I also want to thank my husband, Dr. Wenquan Li, for his support and encouragement throughout my Ph.D. studies. He not only provided me with ample support in my personal life but also helped me significantly with my experiments. I am also thankful to Dr. Wenchuang Liu, Dr. Zixiang Qiu, Dr. Di Wu, Dr. Jia Zhao, and Dr. Xiao Yan for their kindly help. Special thanks to Kaiyao Wang of Yanshan University for her great support in the experiment. Thanks to Tang Yuan, my cat, for being my companion for three years.

And sincerely thanks to the China Scholarship Council for supporting my life for the past three years.

Finally, I want to thank my family for their support and love over the years. During the six years from graduate school to doctoral study, I appreciate their understanding of my busy scientific research life.

As I graduate from this PhD program, I will embark on my next journey with a grateful heart to all of you.

Published Papers in Regard to This Thesis

1. Ying Guo, Wen-quan Li, Xin-gang Liu, Kenjiro Sugio, Yu-jiao Ke, Kai-yao Wang, Wen-chuang Liu, Gen Sasaki. Effect of copper coating on interfacial properties, interfacial thermal resistance, microstructure evolution and mechanical properties of aluminum matrix composites, Journal of Alloys and Compounds, 917, 2022, 165376. (Chapter 2)

2. Ying Guo, Wen-quan Li, Xin-gang Liu, Kenjiro Sugio, Yu-jiao Ke, Kai-yao Wang, Wen-chuang Liu, Gen Sasaki. Effect of short-carbon fiber and nano-carbon fiber as reinforcement on microstructure and properties of hot-rolled aluminum matrix composites, Journal of Materials Science, 57, 2022, 20197-20209. (Chapter 3)

3. Ying Guo, Wen-quan Li, Xin-gang Liu, Kenjiro Sugio, Wen-chuang Liu, Ayako S. Suzuki, Gen Sasaki. Microstructure evolution, property analysis, and interface study of 3%CF-3%SiC-10%SiC functional gradient aluminum matrix composites, Materials Science & Engineering A, 872, 2023, 145010. (Chapter 4)

Presentations

1. Preparation of Copper-coated Short Carbon Fiber Reinforced Aluminum Matrix Composites and Improvement of Carbon Fiber Distribution by Hot Rolling. Proceedings of JSME International Conference on Materials and Processing 2022. Okinawa, Japan.